THREE-DIMENSIONAL PHOTOELASTIC ANALYSIS OF THE SURFACE STRESS DISTRIBUTION IN THE PIN OF A LAP JOINT

By

Max Marlin Spencer

Bachelor of Science
Oklahoma State University
Stillwater, Oklahoma
1956

Master of Science
Oklahoma State University
Stillwater, Oklahoma
1957

Submitted to the Faculty of the Graduate School of
the Oklahoma State University
in partial fulfillment of the requirements
for the degree of
DOCTOR OF PHILOSOPHY
May, 1960

THREE-DIMENSIONAL PHOTOELASTIC ANALYSIS OF THE SURFACE STRESS DISTRIBUTION IN THE PIN OF A LAP JOINT

Thesis Approved:

Ladislaus J. Fila
Thesis Adviser

W. H. Easton
Thesis Adviser

O. H. Hamilton

John B. Wyatt

Dean of the Graduate School

ACKNOWLEDGEMENT

The writer wishes to acknowledge the grant from the National Science Foundation which aided the investigator through a portion of the period of study.

The continued support of the School of Mechanical Engineering through Dr. James H. Boggs and of the Division of Engineering Research through Dr. Clark A. Dunn was greatly appreciated.

The writer is indebted to his co-advisers, Professor L. J. Fila and Professor W. H. Easton, for their useful suggestions and guidance during this investigation.

Recognition should also be given to Professor John Wiebelt, Professor Bert S. Davenport, George Cooper, John McCandless and Preston Wilson for assistance during various phases of the project.

The writer again wishes to express gratitude to his family for the sacrifices made in order that this thesis might be completed.

TABLE OF CONTENTS

LIST OF TABLES

LIST OF FIGURES

LIST OF FIGURES (Continued)

LIST OF FIGURES (Continued)

LIST OF PLATES

CHAPTER I

INTRODUCTION

Three-dimensional photoelasticity is a tool for experimental stress analysis which will facilitate the solution of many heretofore unsolved problems. (1). Like all experimental methods it is not intended to replace the theory, but simply to supplement the theory in an area of great utility. Many complex three-dimensional objects are almost impossible to simulate with a mathematical model. Three-dimensional photoelasticity, strain gages, stress coat and similar methods are the only feasible means available to solve these complex problems. (2). Of these experimental methods only photoelasticity can actually expose what takes place beneath the surface of an experimental model. Any shape which can be cast or formed from stock photoelastic material can be investigated to determine the stresses at points of interest.

The particular problem dealt with in this thesis is a good example of what can be done with three-dimensional photoelasticity. A pin in a lap joint cannot readily be simulated with a mathematical model and the use of the other experimental tools is precluded by a basic limitation in each case. Stress coat cannot be used because the bearing of the plates upon the pin would distort or eliminate any information that might be obtained. Strain gages also would be

affected by the bearing of the various members, probably crushing the gage, so that again no useful information could be obtained. Neither of these methods can give information about the internal stresses which exist in a part of complex shape.

The manner in which the pin of a joint carries the applied load has been of interest for quite some time. (3). To date,however, no one has purported to state with confidence just what is the actual stress distribution. This information is of great value to aircraft and missile design and construction where a high degree of structural integrity is desired. By structural integrity it is meant that every component should carry its share of the load or that every component should be stressed to within a given percentage of its strength. This is necessary in order to obtain the highest strength-weight ratio for a given margin of safety, which in turn means greater cargo capacity, greater maneuverability, higher speed or longer range.

A two-dimensional photoelastic study of the pin in a lap joint has been accomplished. (4). This study indicates that much can be gained by making a three-dimensional photoelastic stress analysis. This thesis describes the method of three-dimensional photoelasticity as applied to the actual problem of determining the stress distribution in the surface of the pin of a lap joint.

CHAPTER II

MECHANICS OF THREE-DIMENSIONAL PHOTOELASTICITY

Not many complicated problems have been solved using three-dimensional photoelasticity to date because it is a difficult method of analysis. (1). One of the difficulties that must be overcome is the simulation of the object to be investigated by a material that has properties such that it will behave as does the original object. There are materials, now available, which aid the investigator through this first phase of the investigation. The material used in this investigation is Hysol 6000-OP, an epoxy resin having the necessary properties. (5).

The second difficulty which must be overcome is the loading of the model of the object of investigation. The model must be loaded in a manner which causes the same reactions in the model as those which occur in the actual part.

The third problem which faces the investigator is how to get the information from the model, assuming it is contained therein. This is actually a multifold problem in itself. In any photoelastic analysis, the stresses which exist in a model are indirectly indicated by fringes. These fringes have a definite relationship to the load which is applied to the model. In two-dimensional photoelasticity it is usually necessary to examine the model in a polariscope set-up while the model is

loaded. This, of course, is possible only for systems which have geometrical shapes and variations in one plane. This precludes examining a complex geometrical part by this method.

A method exists by which the fringes can be "frozen" into a model. This is one of the fundamental processes in three-dimensional photoelasticity. This "freezing" is accomplished by heating the model to a temperature known as the critical temperature and then cooling the model while it is subjected to the load. This phenomenon of permanent deformation and frozen stress patterns has been explained by assuming that photoelastic materials consist of two interwoven molecular structures which are alike in all respects except in their fusibility when heated. At room temperature both are solid, but at the critical temperature one of these molecular networks retains its solid form whereas the other becomes liquid and solidifies again when the temperature returns to ambient. (1)(6). Once the stresses are frozen into the model there are two general methods of solution. These methods are known as the plate method and the scattering light method.

The plate method involves slicing the model into thin plates which can then be examined using a standard polariscope. If the slicing operation is carefully controlled, in order that the model is not reheated, then no slicing effects are noted. (7). The plate method is the general method used in this investigation and the slicing procedure is illustrated and discussed in Appendix D. The scattered light method was first demonstrated by Weller (8) in 1939.

Since that time several investigators have utilized the scattered light method for the analysis of stresses produced by simple types of loads. (9)(10)(11). This method requires special equipment and, at present, appears to be quite limited in its application. Therefore, it is not readily applicable to a complex shape.

There are some auxiliary methods which may be used to supplement either of the two general methods. One of these methods is known as the oblique incidence method. This method has been used with success by some investigators. (12)(13). The method involves the passage of light through the model at various prescribed angles of incidence and subsequent correlation of the differences in the fringe patterns which occur at these angles. The accuracy associated with this method may be low for some cases; therefore, it is not used for quantitative evaluation in this investigation. (14). A second auxiliary method which may be used to supplement or replace the plate method is known as the compensator method. This method will be discussed later in this chapter.

The model slice is placed into the field of a standard polariscope and analyzed similarly to the two-dimensional case when the plate method is used. If the slice is originally parallel to and in a plane of geometrical and load symmetry in the three-dimensional object, then the principal stresses lie in the plane of the slice. Two-dimensional methods in this case apply directly with few, if any, corrections. If the slice is such that it does not conform to the above special case then corrections must be made to take into account the location of the

slice. The information obtained from the general slice will be accurate insofar as that particular plane is concerned. However, when integrating this information with the information from other slices to obtain the total result, some corrections will probably be necessary.

The modern two-dimensional method of analysis is based upon the determination of the fringe order at all points in a model as well as the determination of the isoclinic pattern for the model. As stated previously the fringe order at a point in a model is an indication of the stress system at the point. The relationship which expresses this statement is

$$n\lambda = Ct(p-q) \qquad \text{(II-1)}$$

from which $(p-q)/2 = n\lambda/2Ct$,

where p and q are the algebraic maximum and minimum stresses respectively, n is the fringe order, t is the model thickness, λ is the wave length of the light and C is a constant known as the stress-optic coefficient. (1).

Hence $$\tau_{max} = nF, \qquad \text{(II-2)}$$

in which τ_{max} is the maximum shear stress and F is a constant for any particular model and light source. This constant F is defined as the model fringe value and is given by

$$F = \lambda/2Ct = f/t \qquad \text{(II-3)}$$

where f is another constant equal to $\lambda/2C$ and is known as the material fringe value. Material fringe values for all photoelastic materials can be found readily by using a tension calibration model and determining the fringe order corresponding to various stress

magnitudes. The expression for the difference between principal stresses is

$$(p-q)/2 = nf/t, \qquad \text{(II-4)}$$

so that $(p-q) = 2nf/t$.

To determine the magnitude and direction of either p or q more information is necessary. This information is obtained from the isoclinics. An isoclinic is the locus of points along which the principal stresses have parallel directions. The isoclinics for a model are obtained by using the plane polariscope and rotating the polarizer and analyzer together through 90°. The isoclinics furnish basic data, which, when combined with the values of (p-q) from a photoelastic stress pattern, provide the necessary and sufficient information for the complete solution of a two-dimensional stress problem. (1).

The manner in which the isoclinics furnish the necessary information has been given by Frocht (1) in equation form as

$$p_i = p_o - \int_o^i (p-q)ds_1/\rho_2 , \qquad \text{(II-5)}$$

where p_o is the algebraic maximum principal stress at some reference point, p_i is the algebraic maximum principal stress at a general point, (p-q) is obtained from equation (II-4) and ds_1 and ρ_2 are shown in Figure 1.

In Figure 1 S_1 is the curve the tangent to which represents the direction of the maximum principal stress at the point of tangency and S_2 is the curve the tangent to which represents the direction of the minimum principal stress at the point of tangency. These two curves

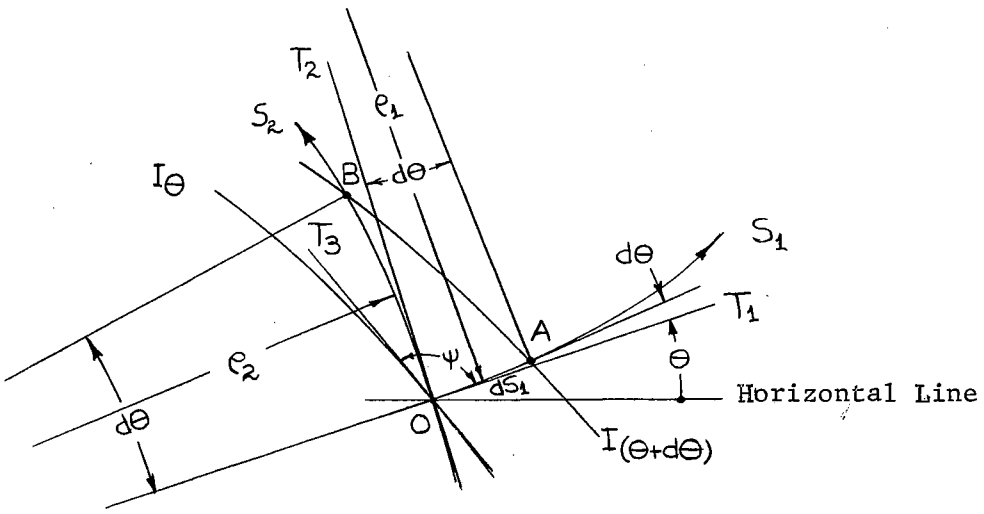

Figure 1. Sketch Showing Filon's General Transformation of the Lame-Maxwell Equation, from Frocht (1)

are known as stress trajectories. Also in Figure 1 T_1, T_2 and T_3 are tangents to the curves S_1, S_2 and I_θ respectively, where I_θ and $I_{(\theta+d\theta)}$ are the isoclinics which pass through points O and A respectively. The angle between T_1 and T_3 measured counterclockwise is ψ and ρ_1 and ρ_2 are the radii of curvatures of S_1 and S_2 respectively.

In Figure 1 in the limit the angle OAB is $(180°-\psi)$, so that

$$OB/OA = \tan(180°-\psi) = -\tan\psi \quad .$$

Upon inversion this may be written as

$$OA/OB = -\cot\psi \quad . \qquad \text{(II-6)}$$

From Figure 1 $\quad OB = \rho_2 d\theta \ ,$

so that $\quad 1/\rho_2 = d\theta/OB \ .$

After multiplication of both sides by OA this may be written as

$$OA/\rho_2 = d\theta \ OA/OB \ .$$

Since OA is ds_1 and since OA/OB is equal to $(-\cot\Psi)$ this equation may be written as

$$ds_1/\rho_2 = -\cot\Psi\, d\theta \ . \qquad \text{(II-7)}$$

Upon substitution of this expression for ds_1/ρ_2 in equation (II-5) the transformed equation is

$$p_i = p_o + \int_o^i (p-q)\cot\Psi\, d\theta \ , \qquad \text{(II-8)}$$

which may be written for graphical integration as

$$p_i = p_o + \sum_o^i [(p-q)\cot\Psi]\Delta\theta \qquad \text{(II-9)}$$

Another method which is available to determine the normal stresses across a straight line is known as the shear difference method. (1). This method is based upon the equations of equilibrium for a two dimensional element. These equations are

$$\frac{\partial\sigma_x}{\partial x} + \frac{\partial\tau_{xy}}{\partial y} = 0 \qquad \text{(II-10)}$$

and

$$\frac{\partial\sigma_y}{\partial y} + \frac{\partial\tau_{xy}}{\partial x} = 0 \qquad \text{(II-11)}$$

From equation (II-10) it follows that

$$(\sigma_x)_i = (\sigma_x)_o - \int_o^i \frac{\partial\tau_{xy}}{\partial y}\, dx \ , \qquad \text{(II-12)}$$

in which $(\sigma_x)_i$ and $(\sigma_x)_o$ denote respectively the stresses at points i and o, Figure 2.

If a section Y'-Y' parallel to the Y axis is passed through point i and a curve of the shear stresses $\tau_{xy} = f(y)$ is plotted for that section then $\left(\frac{\partial\tau_{xy}}{\partial y}\right)$ at the point i represents the slope of the τ_{xy} curve at i' with respect to the Y axis. This statement can be expressed as

$$\frac{\partial\tau_{xy}}{\partial y} = \tan\alpha.$$

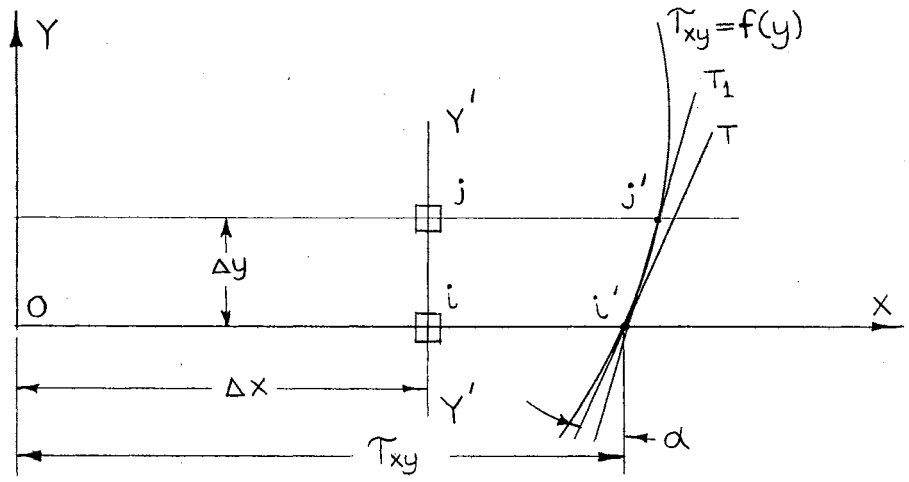

Figure 2. Sketch Showing an Approximation to the True Slope of the Shear Function

An approximation to the required slope at i' is obtained by calculating the horizontal shear stress at i and at a nearby point j lying on a vertical line through i and dividing the difference between these stresses $\Delta\tau_{xy}$ by Δy, the distance between i and j. Thus

$$\tan\alpha = \frac{[(\tau_{xy})_j - (\tau_{xy})_i]}{\Delta y} = \frac{\Delta\tau_{xy}}{\Delta y}\text{, approximately,} \qquad \text{(II-13)}$$

in which $(\tau_{xy})_j$ and $(\tau_{xy})_i$ denote the shear stresses τ_{xy} at j and i, respectively. Equation (II-12) can now be written as

$$(\sigma_x)_i = (\sigma_x)_o - \sum_o^i \frac{\Delta\tau_{xy}}{\Delta y}\,\Delta x\,. \qquad \text{(II-14)}$$

In these equations the shear stresses at points i and j can be calculated from the relation

$$\tau_{xy} = \left(\frac{p-q}{2}\right)\sin 2\theta,$$

where θ is the angle between the directions of (σ_x) and the greater principal stress, p.

A specific method, previously mentioned, which may be used to supplement or to take the place of the modern method, is known as compensation. This method utilizes the basic principle upon which rests the foundation of photoelasticity in general. This principle is the ability of a photoelastic material to impart directional characteristics to incident light. Light, upon passing through a stressed photoelastic medium, is retarded in a manner dependent upon the stresses which are present in that medium. It has been found that the retardation of the light at a point in a plane perpendicular to the light is a function of the shear stress which exists at that point. Compensation is achieved by using white light as a source and superimposing over the point under inspection a uniform tensile or compressive load which is adjusted both in magnitude and direction until a dark zone forms. From the fringe order or stress in the compensator strip at compensation the fringe order in the model at that stress can be readily found. (14). The above statements have been expressed in equation form by Frocht. (1).

The retardation in general is given as

$$R = Ct(p-q) \ , \qquad \text{(II-15)}$$

in which R is the retardation and the other variables have been defined previously. If quantities pertaining to the model are denoted by the subscript (m) and those pertaining to the compensator by (c), then the retardations R_m and R_c are given by

$$R_m = (p-q)_m C_m t_m \qquad \text{(II-16)}$$

and

$$R_c = (p-q)_c C_c t_c \ .$$

Since the compensator will be either in tension or compression

$$(p-q)_c = \sigma_c \qquad \text{(II-17)}$$

and $R_c = \sigma_c C_c t_c$.

Compensation is effected and extinction takes place when

$$R_m = R_c ,$$

so that $(p-q)_m C_m t_m = \sigma_c C_c t_c ,$

whence $(p-q)_m = \sigma_c C_c t_c / C_m t_m$. (II-18)

From equation (II-3)

$$f = \lambda/2C \text{ or } C = \lambda/2f ; \qquad \text{(II-19)}$$

that is, the constant C in the stress-optic-law equation (II-1) is inversely proportional to the shear fringe value of the material. Hence

$$C_c/C_m = f_m/f_c \text{ .} \qquad \text{(II-20)}$$

Substituting in equation (II-18)

$$(p-q)_m = \sigma_c t_c f_m / t_m f_c , \qquad \text{(II-21)}$$

from which (p-q) can be calculated from a compensator of arbitrary material and thickness. It should be noted that extinction or compensation is achieved only when the compensator stress system is exactly opposed to the model stress system or when the stresses in the model plus the stress in the compensator combine to produce an isotropic point. An isotropic point is a point at which the normal stresses are equal in all directions. This fact is useful in determining the sign of the stress on a free boundary.

On a free boundary one of the principal stresses vanishes and the remaining principal stress is tangent to the boundary. By varying the

load on the compensator and aligning it so that it is either parallel to or perpendicular to the boundary the sign and magnitude of the model stress can readily be determined. If the boundary is in tension, a tension compensator will cause extinction of the light when it is perpendicular to the boundary while containing the same fringe order as that fringe order which exists in the model. If the boundary is in compression, extinction will be achieved when the tension compensator is parallel to the boundary while containing the same fringe order as that fringe order which exists in the model.

CHAPTER III

EXPERIMENTAL APPARATUS

The Loading Frame

The loading frame is basically a four-bar linkage with a safety bar to prevent oven damage in the event that the model breaks. This is shown in Plate I. The load is applied to the pin in the lap joint through a series of three-bar linkages. This enables the lap joint to be self-aligning. The loads on each outside plate are equal in magnitude, and the directions are parallel. The load on each plate is also one-half of the load on the center plate so that an ideal system of loading is achieved. The loading frame operates satisfactorily, as can be seen by observing the symmetry which occurs in the resulting plate stress patterns. This is shown in Plates VIII and IX.

In the loading frame design, no undesirable translations occur, and a sufficient load can be applied to the lap joint to cause the "freezing" of many fringes into each of the components of the lap joint. The detail drawings of the loading frame components are shown in Appendix E. There is no sensible leakage from the air cylinder, and except for a small portion of the load required to overcome friction in the various joints, the lap joint load can be determined indirectly from the air pressure, (p) psi. The air cylinder cross-sectional area equals πin^2. The ratio of the load applied by the air cylinder to the load applied to the joint is

PLATE I

LOADING FRAME AND IAP JOINT

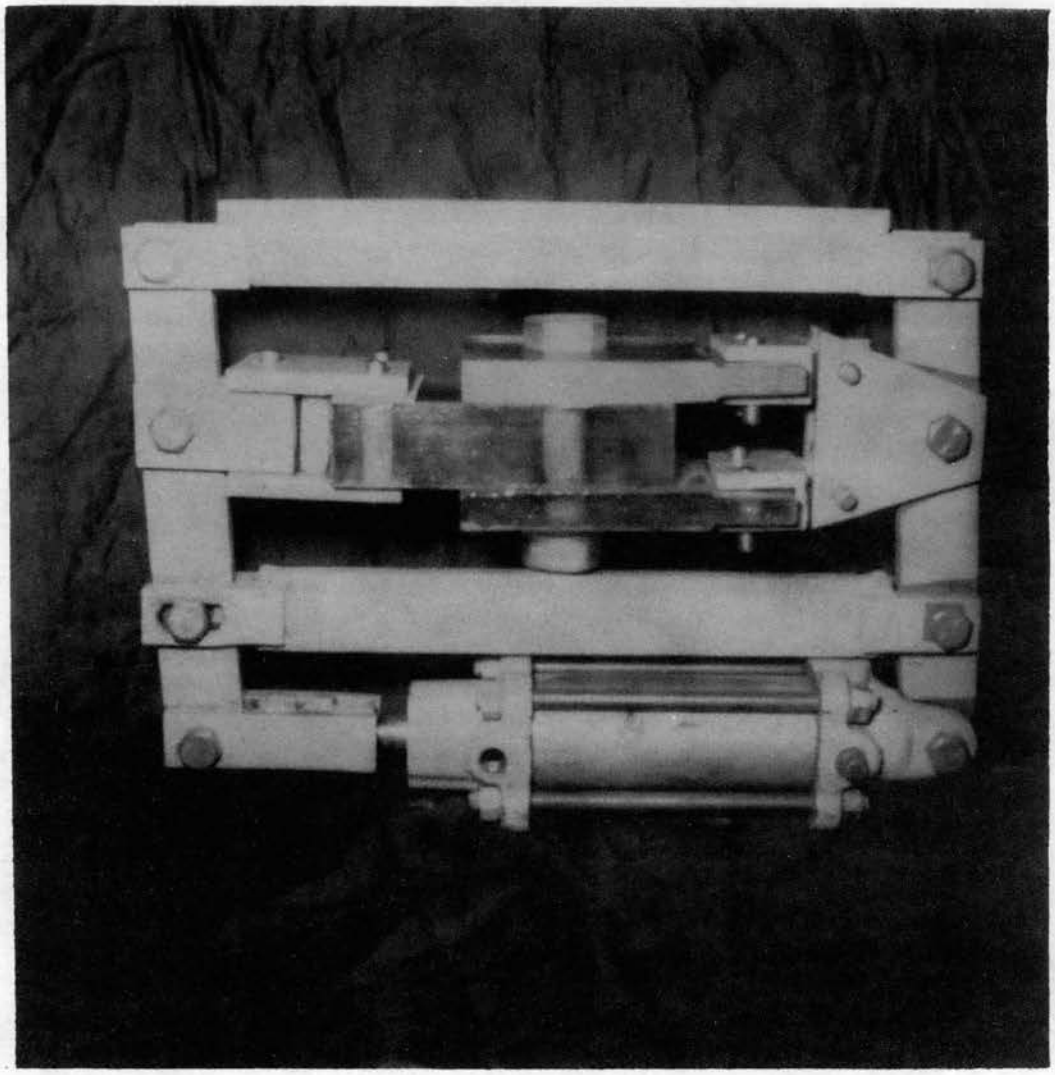

one-third. Therefore the lap joint load is $\pi(3)(p)$ or 9.42p lb.

The Oven

The main criterion for designing and building the oven is that the ensuing cooling rate be no greater than $2^{\circ}F/hr$. A large mass is concentrated in the central portion of the oven in order to increase the heat capacity. This mass is insulated and heated as shown in Figure 3. The natural cooling rate of this oven decreases with decreasing temperatures, and at the critical temperature it is too great. The model cooling rate, however, should be linear. Therefore it is necessary that the oven cooling rate be controlled in some manner. This is achieved by the use of a variac to decrease the voltage applied to the heating element as the temperature decreases.

The controlled oven cools in a linear manner and at a rate less than $2^{\circ}F/hr$ as shown in Figure 47. The effect of departing from the recommended cooling rate is to possibly introduce extraneous fringes into the model as a result of thermal stresses. It requires a great deal of time for the oven to come to equilibrium with its surroundings. That the oven comes to equilibrium is important, however, since the cooling rate is a function of the quantity of energy stored in the oven. To insure that the oven comes to equilibrium, it is necessary to soak it at a given variac voltage and observe the temperature variation. The oven is calibrated by determining the voltage settings which are necessary to obtain the desired temperatures at oven equilibrium.

A natural circulation of air is achieved by locating pairs of holes

in the top of the cavity liner and pairs of holes in the bottom of the cavity liner. The oven cavity is sealed by a tight fitting lid and by fiberglas strips which are inserted into the juncture of the lid and oven body. The model is shielded by the cavity liner from coil heat radiation.

PLATE II

OVEN AND AIR COMPRESSOR

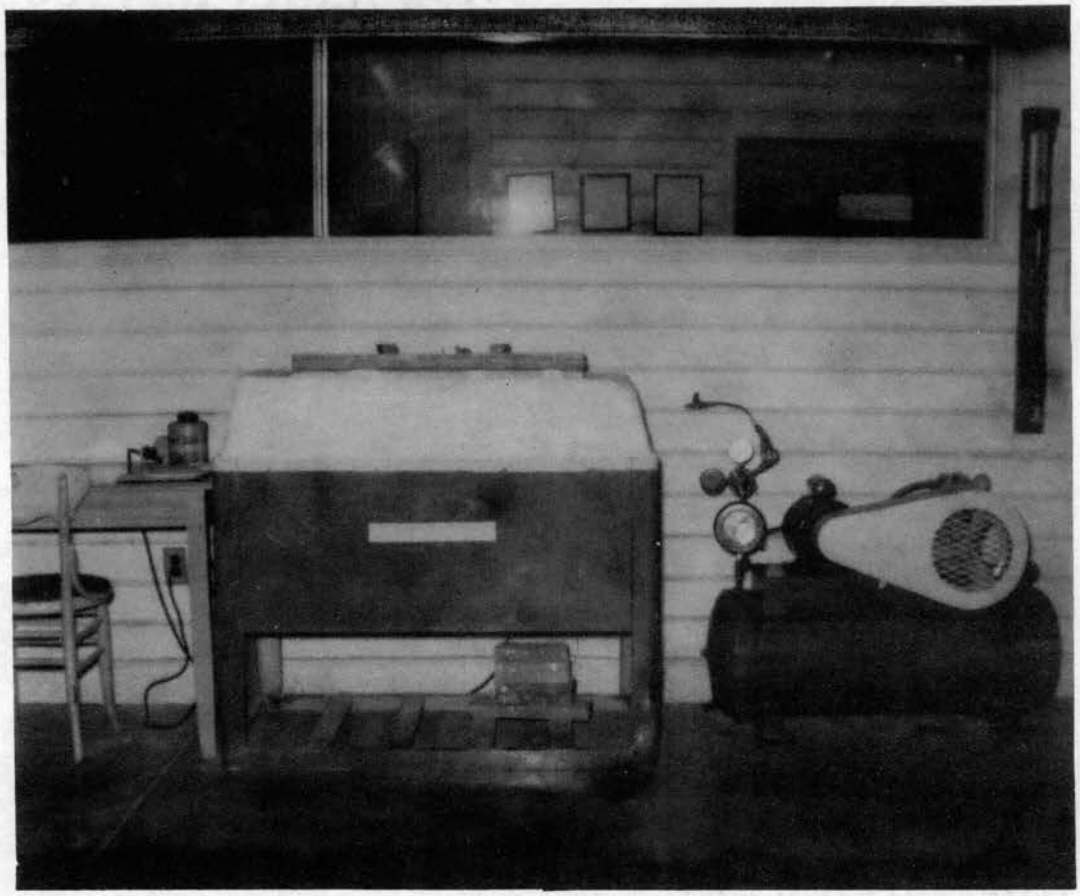

PLATE III

OVEN COMPONENTS

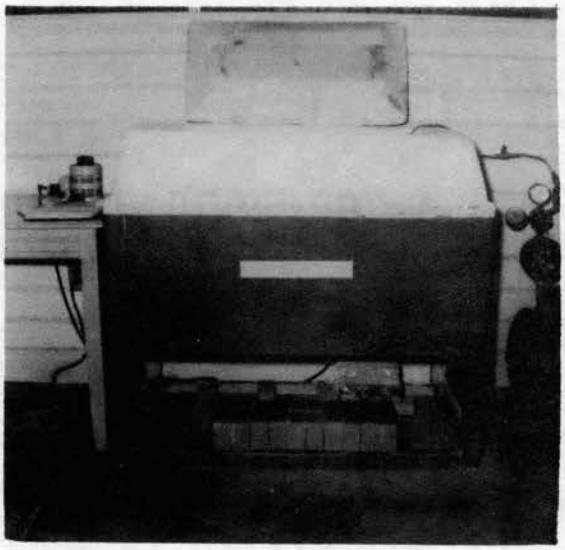

1. Oven Lid, Body and Bricks

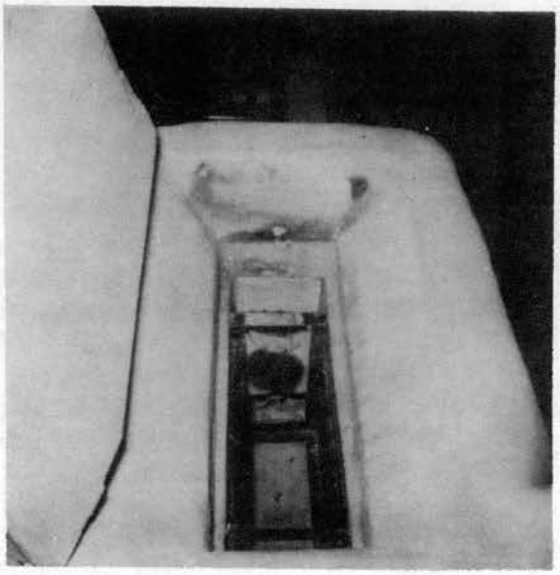

2. Oven Cavity Liner and Heating Coils

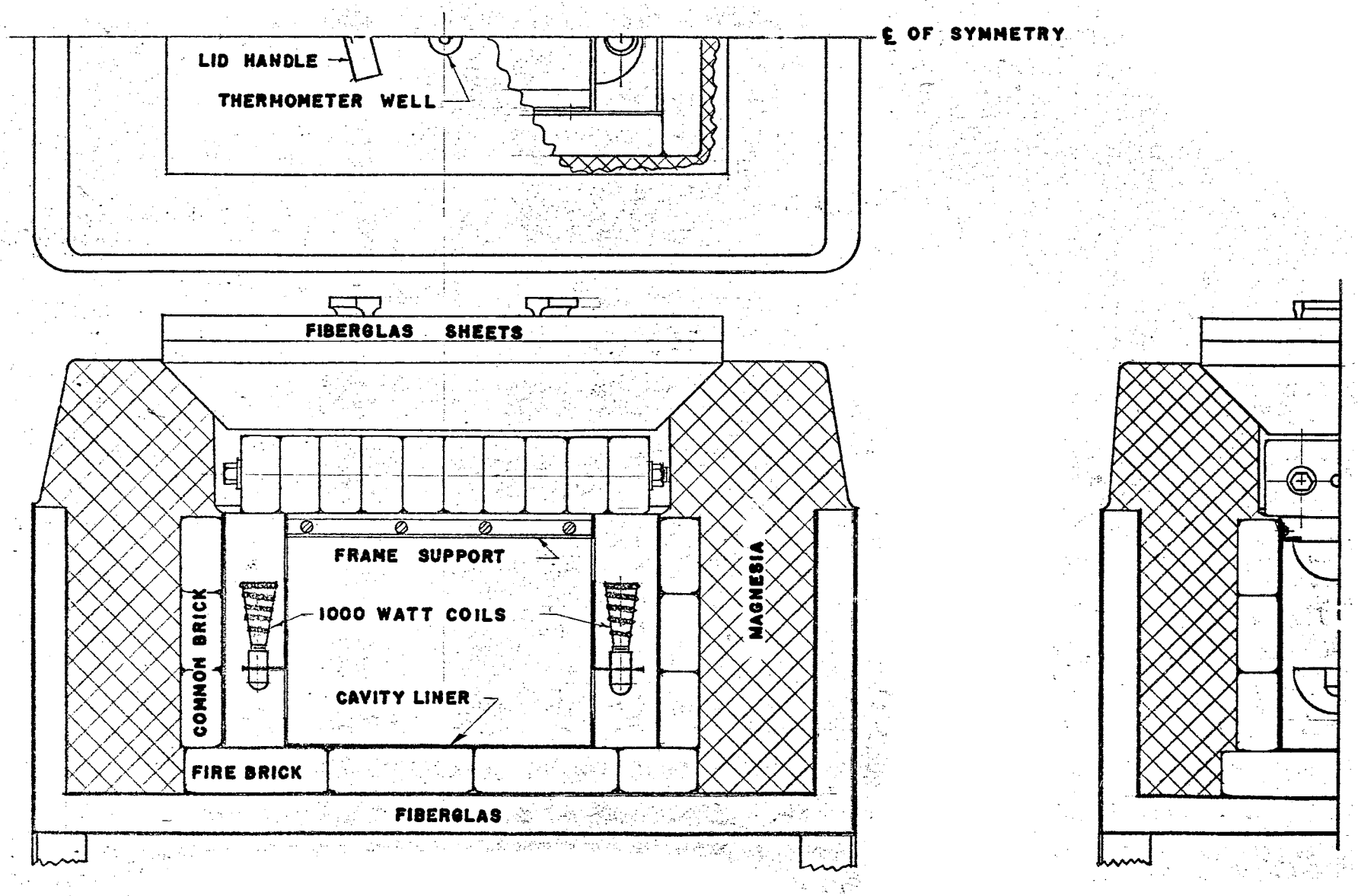

Figure 3. Oven Components

The Lap Joint

The lap joint design corresponds closely to practice followed in the aircraft industry at present. (3). The assembled joint is shown in Plate I. The lap joint components are made from Hysol 6000-OP standard stock material. The 1½-inch center lap joint plate is made from a 1½ x 24 x 18-inch plate. The 3/4 lap joint plates are made from a 3/4 x 24 x 18-inch stock plate and the lap joint pin is made from a 1½-inch diameter rod. The mechanical and photoelastic properties of Hysol 6000-OP are given in Appendix A.

The lap joint plates are essentially three sets of three-bar linkages which insure that an ideal system of loads is applied to the lap joint pin. The material of the plates is the same as the material of the pin in order that harmful surface effects are eliminated from the photoelastic investigation.

The deformation of the pin occurs in a direction parallel to the applied load and symmetrical patterns are produced in the lap joint pin which indicates that the lap joint design and construction are satisfactory. Some difficulty is encountered in the machining of Hysol 6000-OP. The procedure followed in machining the lap joint is essentially the same as that described in Appendix D.

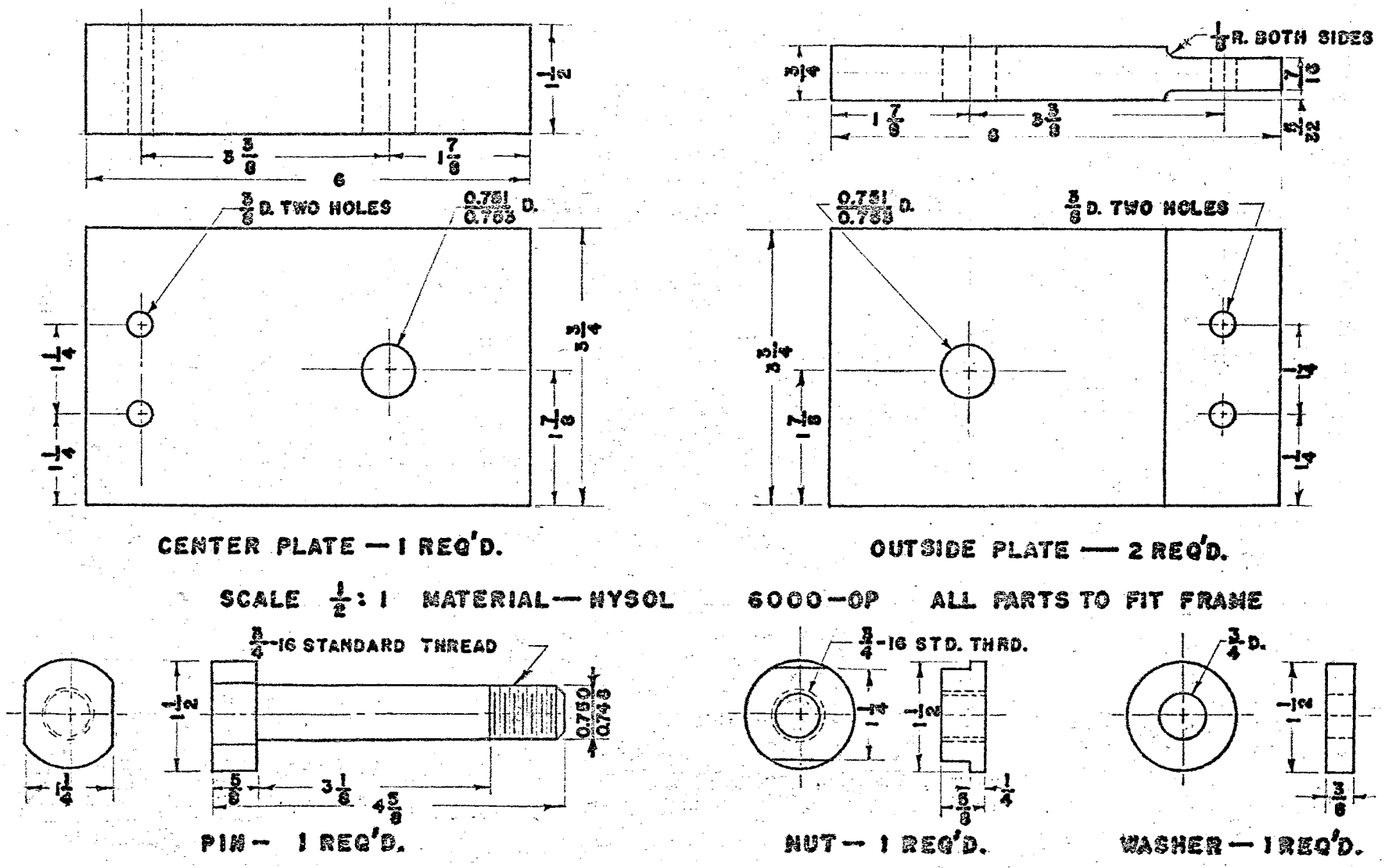

Figure 4. Details of Lap Joint Components

The Photoelastic Equipment

The polariscope is a standard transmission type. The monochromatic light is produced by a mercury-vapor lamp isolated by a Wratten 77 filter. This light source is used for fringe examination and fringe photographing. A white light source is used to locate isotropic points and to determine partial fringe orders. The general polariscope set-up for visual examination is shown in Plate IV. The fringe pattern from the photoelastic component is projected through the telescope onto a white paper which serves as a viewing screen. All components of the polariscope are clamped to a supporting bar. This bar is shown in Plate IV. Location of the components on the supporting bar permits each part to be correctly aligned and oriented.

A tracing box can be placed into the system for the purpose of examining isoclinics and subsequently stress trajectories. This is shown in Plate V. This procedure facilitates the tracing of isoclinics by causing the light rays to be reflected through 45 degrees from a mirror onto a horizontal tracing glass. Plane polarized light is desired for this procedure; therefore, the quarter wave plates are not utilized. The various isoclinics are obtained by rotating the polarizer and analyzer through 90 degrees in desired increments.

In order to produce a permanent record of the fringe pattern in each pin slice, and in order to provide a convenient pattern from which the analysis can be accomplished, photographs are invaluable. Photographing in the polariscope is accomplished by placing a camera into the light path as shown in Plate V. Care must be taken to insure that the axis of the camera lens is parallel to the light path. The focal plane of the camera

lens must be perpendicular to the direction of the light path. This is achieved by using a camera stand and by inspecting the pattern produced by a standard photoelastic member on the camera ground glass. The lens shutter must be open and set with an f stop of 6.3 to achieve satisfactory results. A bright spot is produced in the center of the light field if some filtering is not introduced between the mercury lamp and the photoelastic specimen. The bright spot is caused by the mercury lamp. To eliminate the spot a ground glass is placed directly in front of the mercury lamp. This eliminates the bright spot and produces a more uniform intensity across the polarizing field. The actual procedure used to take the photographs is described in Appendix B.

PLATE IV

GENERAL POLARISCOPE SET-UP

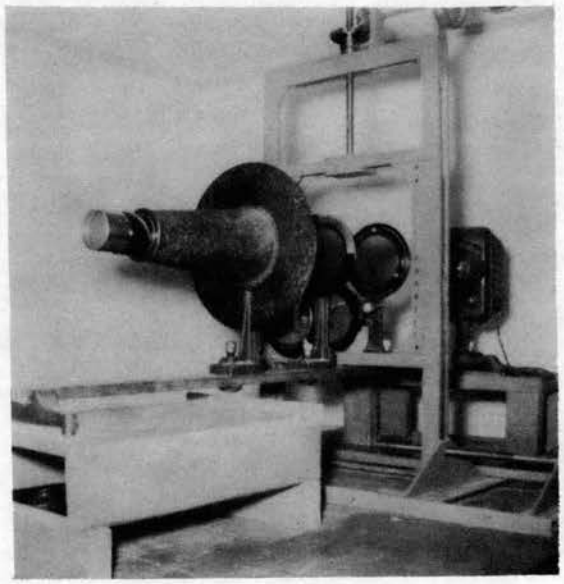

Reading from left to right the elements are

1. Supporting Bar
2. Telescope
3. Analyzer
4. Quarter Wave Plate
5. Loading Frame
6. Quarter Wave Plate
7. Polarizer
8. Mercury Lamp

PLATE V

SPECIAL POLARISCOPE SET-UPS

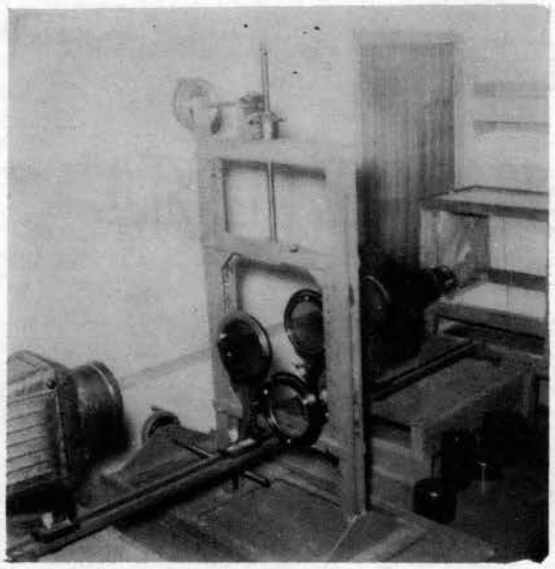

1. Tracing Box Included

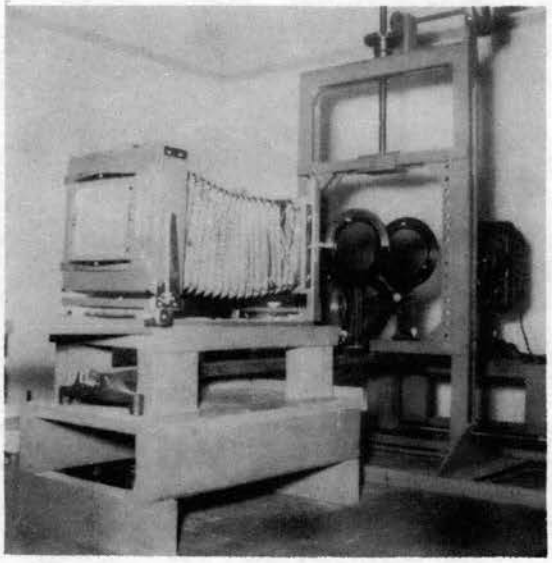

2. Camera Included

CHAPTER IV

EXPERIMENTAL PROCEDURE

One annealing run and six stress "freezing" runs were made. The annealing run was made in order to relieve the pins of any residual stresses which might be present. The first stress "freezing" run was made with an air pressure of 46 psi which caused a tensile failure in the outside joint plates. The second run was made with an air pressure of 26 psi. Run three was made with an air pressure of 16 psi. Run four was made with an air pressure of 6 psi and run five was made with an air pressure of 3 psi. Runs two through five were sliced longitudinally and distinct fringe patterns were obtained. Plates VI through XIII illustrate these fringe patterns. Run six was made with an air pressure of 6 psi, and transverse slices were cut from the pin. The particular procedures followed during each of the three phases of annealing and stress freezing, slicing and examination, and photographing follow.

Annealing and Stress Freezing

Mr. M. M. Leven of the Westinghouse Corporation suggested that Hysol 6000-OP be used to facilitate this investigation. This is a new photoelastic material manufactured specifically for three-dimensional investigations. (5). The lap joint components were made of Hysol 6000-OP accord-

ing to the specifications shown in Figure 4. The lap joint pin was annealed prior to investigation in order to relieve any stresses which might be present in the standard stock. (1)(14). This was done by heating the oven to the annealing temperature (280°F) and soaking the oven until equilibrium was reached. This required approximately forty-eight hours depending upon the voltage applied to the heating coils and the room temperature. Upon reaching equilibrium the oven lid and the top row of bricks were removed in order that the lap joint pins could be placed into the oven cavity. Care was taken to insure that the lap joint pins rested on a flat surface, and that the pin was not exposed to direct heat conduction through the cavity liner. These two precautions were taken by resting the pin on a sheet of asbestos board. The sheet was of the same width as the oven cavity width and rested upon the supports which are shown in Figure 3.

After insertion of the lap joint pins into the oven, the top layer of bricks and the lid were replaced. The small gap which occurred at the juncture of the lid and the oven body was sealed with fiberglas strips. The oven was then reheated to the annealing temperature and allowed to reach thermal equilibrium. This required approximately twelve hours depending upon the amount of time the lid was removed and the room temperature. After coming to equilibrium the oven was soaked at the required voltage to insure that the model was at a uniform temperature. The model should be soaked at 280°F for approximately four hours per inch of model thickness. (5).

The oven was then forced to cool in a linear manner and at a rate no greater than 2°F per hour. A typical cooling curve is shown in Figure 47. After the oven had come to approximately room temperature the pins were

removed and examined in the polariscope system to determine the annealing effectiveness. One cycle of annealing rendered the pins essentially stress-free and ready for a stress freezing run.

The actual stress freezing runs were made in the same manner as the annealing runs except that the oven maximum temperature was 270°F rather than 280°F. The lap joint was made up with no tension on the lap joint pin and placed into the loading frame. Air pressure was then applied to the loading frame air cylinder in order to align the lap joint plates. Then the lap joint pin was subjected to approximately five pound-inches torque, and the head of the pin was scribed with lines parallel to the directions of the applied joint tensile forces. The oven was sealed and the temperature was raised to 270°F. The air cylinder pressure during oven heating was maintained at a value equal to, or less than, the desired stress freezing pressure. Upon reaching the critical temperature the pressure regulator was set at the pressure corresponding to the load for each particular test. After setting the pressure regulator the oven was soaked at the critical temperature for twelve hours in order that the model temperature would be uniform. The oven temperature was then allowed to decrease in the manner indicated in Figure 47. The load during cooling was constant as indicated by the pressure gage. Upon cooling to approximately room temperature, the loading frame and the lap joint were removed. The lap joint pin was then sliced following the procedure described in Appendix D.

Slicing

The longitudinal slices were cut from the pins in the manner indicated in the following figure. It should be noted that the terms upper boundary and lower boundary refer to the orientation of the pin with respect to the load.

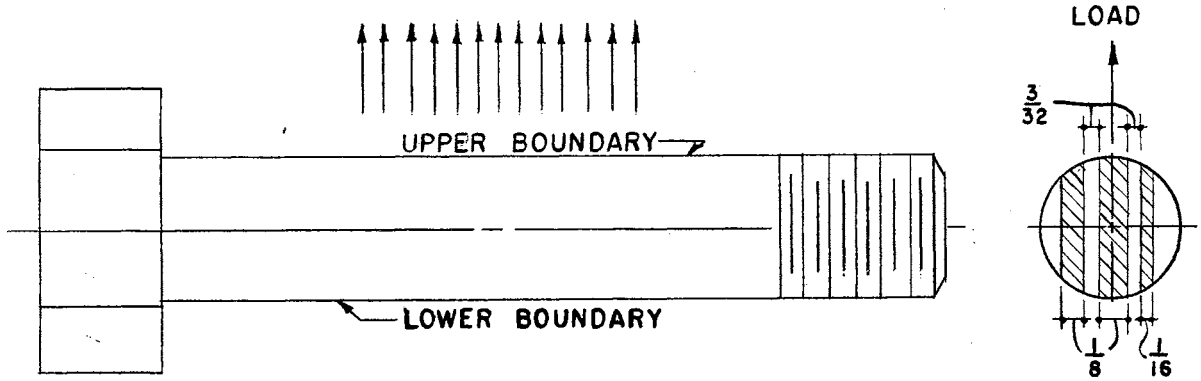

Figure 5. Longitudinal Slicing Details

The transverse slices were cut from the pins in the manner indicated in the following figure.

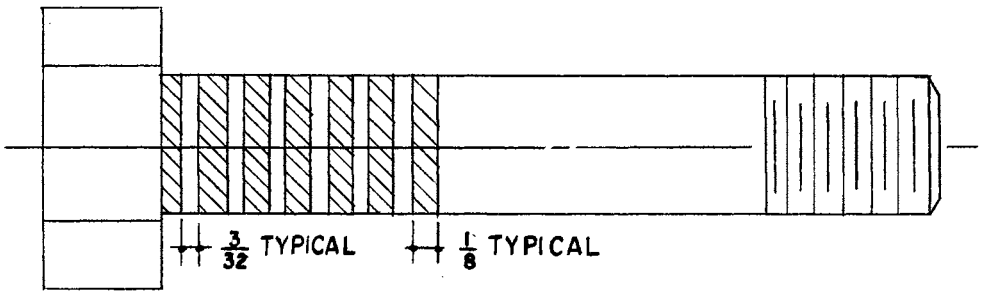

Figure 6. Transverse Slicing Details

Examination and Photographing

The lap joint plates were examined in the polariscope after each stress freezing run to determine if the lap joint pin had been loaded correctly. No quantitative information was desired from this procedure but a useful purpose was served by indicating the number of fringes to be expected in the lap joint pins as well as indicating the symmetry of the applied loads. This is shown in Plates VIII and IX.

The lap joint slices were examined with the polariscope and photographs were taken of each slice after a sufficient time had elapsed to remove the "time stresses." (15). The polariscope set-up for photographing is shown in Plate V. Monochromatic light was used to take the photographs and the photographic procedure is described in Appendix B. All photographs were taken with the pin slices in a plane perpendicular to the light source. The resulting photographs are shown in Plates Vi, VII, X, XI, XII and XIII. The slices were supported for photographing by small clamps attached to the general loading frame shown in Plate IV. Care was taken to insure that the clamping force exerted upon the pin slices was small so that extraneous fringes would not be introduced into the model slices.

The lap joint pin slices and lap joint plates were coated with a thin film of Halowax oil which made unnecessary the sanding and rouge polishing normally used in two-dimensional photoelasticity. (8). The index of refraction of Halowax oil is approximately the same as the index of refraction of Hysol 6000-OP. The procedure of oil coating rather than sanding and polishing was used to avoid rounding the edges of the pin slices and consequently distorting the true boundary pattern.

CHAPTER V

RESULTS

Photographs and sketches provide the information which is necessary to solve equation (II-9). This equation is presented again for convenience as

$$P_i = P_o + \sum_{o}^{i} [(p-q)\cot\Psi]\Delta\theta \ . \qquad \text{(II-9)}$$

In this equation (p-q) is determined from equation (II-4) to be equal to 2nf/t. The material fringe value f is given in Table XI. The thickness of the model, t, is measured and the fringe order n can be determined from the photograph. The fringe order, however, can be more accurately determined from compensation, as described in Chapter II; therefore compensation is used to supplement the photographs in this respect. The black lines in the following Plates are the fringes; however, since the photographs were taken with a bright background, the fringes appear in half order increments; that is, the first black line between a region of zero stress and a region of high stress is of the half order, n = ½. The second black line in the same direction is of the one and one-half order, n = 1½, etc. Thus, in effect, the white bands in the photographs can be treated for discussion as fringes of the first order; that is, the white band in an area of zero stress is of order, n = 0. The next white band which appears between zero and a stressed region is of the first order n = 1, etc. This can be seen by referring to Plate VI. The fringe order results are given in Figures 11 and 13-28.

In order that the graphical integration can be carried out, p_o must be known at one point in the model. There are many points at which p_o is known and two such points are used in the analysis in Chapter VI. The other variables which appear in equation (II-9) are obtained from the isoclinic sketches, Figures 7-10 and 12. The notation for these variables is the same as the notation shown in Figure 1.

The photographic results of run two verify that the load was applied to the lap joint components in a satisfactory manner. Evidence of this is shown in Plates VIII and IX. The run two lap joint top plate and bottom plate fringe patterns are symmetrical and have the same fringe distribution. The run two lap joint center plate also has a symmetrical fringe pattern. The lap joint outside plate ends, shown in Plate IX, are each symmetrical and in both cases the hole fringe patterns are similar. The lap joint fringe patterns for all of the stress freezing runs were similar to those obtained for run two.

The transverse slices gave no photographic results but they did provide valuable information. Upon examining the slices in the polariscope it was found that no full fringe orders appeared. This means that the stress parallel to the axis is approximately constant for each particular slice. This was verified by an examination of the plates which applied the load to the pin and is illustrated in Figure 34. The transverse slices were also examined in the polariscope with a white light source. This examination revealed that there was some stress variation, corresponding to the variation shown in Figure 34, but not enough to be quantitatively evaluated by using only the transverse slices.

The second major equation which is utilized in the analysis is equation (II-14) which is presented again for reference as

$$(\sigma x)_i = (\sigma x)_o - \sum_o^i \Delta\tau xy \frac{\Delta x}{\Delta y}. \qquad \text{(II-14)}$$

This equation applies to cases in which the stress variations along straight lines are desired. The upper and lower boundaries of the pin are very close approximations to straight lines and as such provide a direct case for the application of this formula. The unknown quantities in equation (II-14) can be determined from sketches or photographs which show (p-q) at points along and near the boundary, which indicate the direction of the principal stress, (p), at corresponding points and which give the starting value $(\sigma x)_o$. The magnitudes of the starting values $(\sigma x)_o$ for one point on the lower boundary and for one point on the upper boundary were obtained from the pin fringe patterns, and the sign of each starting value was determined by compensation as described in Chapter II. The final information needed for the solution of equation (II-14) is shown in Figures 7-28. The curves in Figures 14, 16, 18, 20, 22, 24, 26 and 28 were obtained by determining the fringe order at points on the net which is shown in Figure 29 when this net was applied to the pin fringe patterns.

PLATE VI

PIN FRINGE PATTERNS FOR RUN TWO

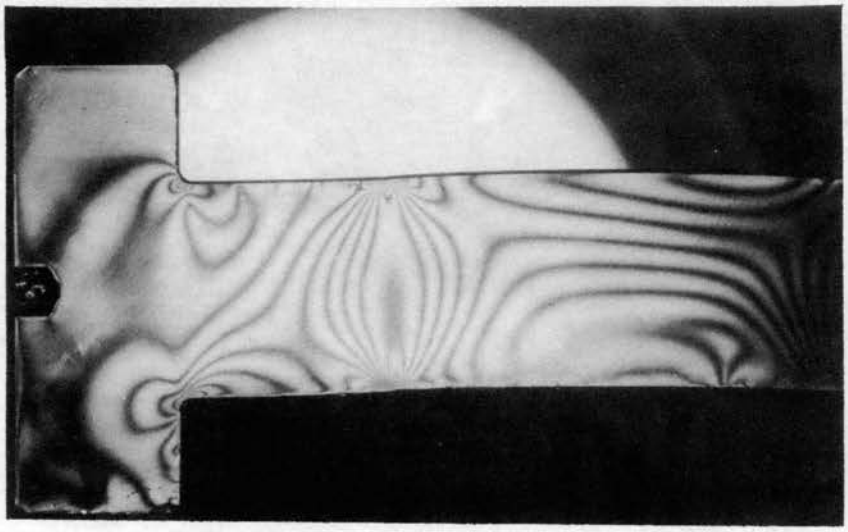

1. Center Slice - Head

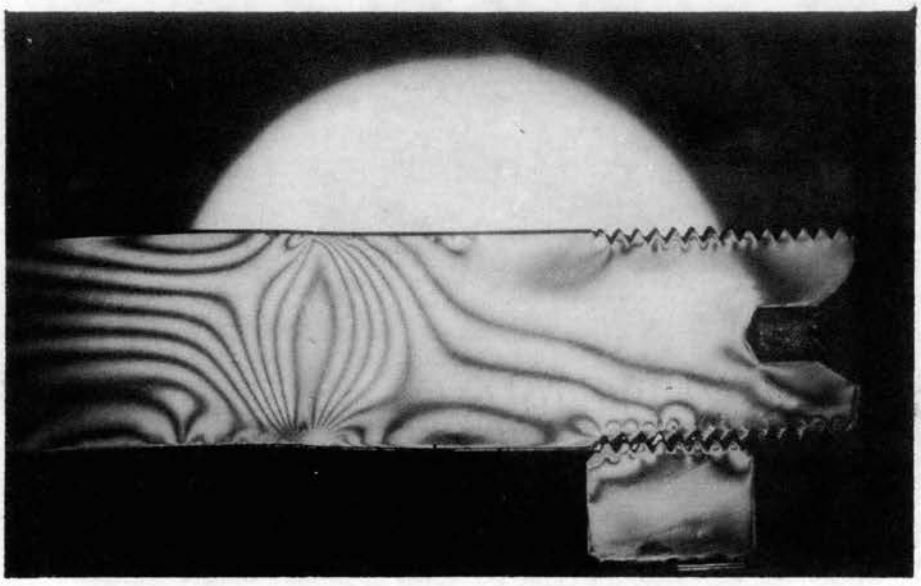

2. Center Slice - End

PLATE VII

PIN FRINGE PATTERNS FOR RUN TWO

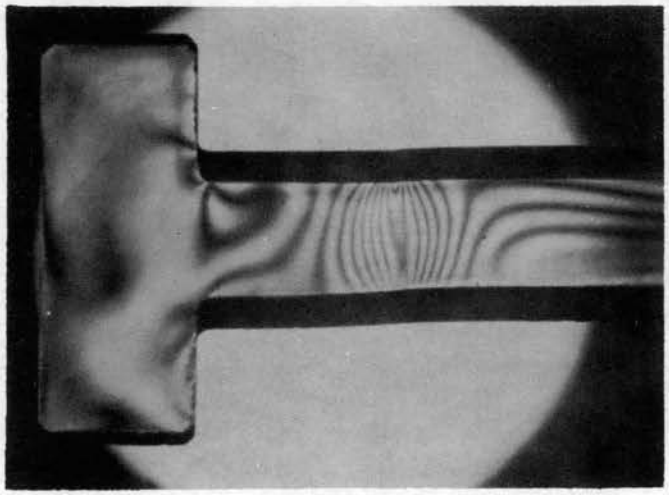

1. Side Slice - Head

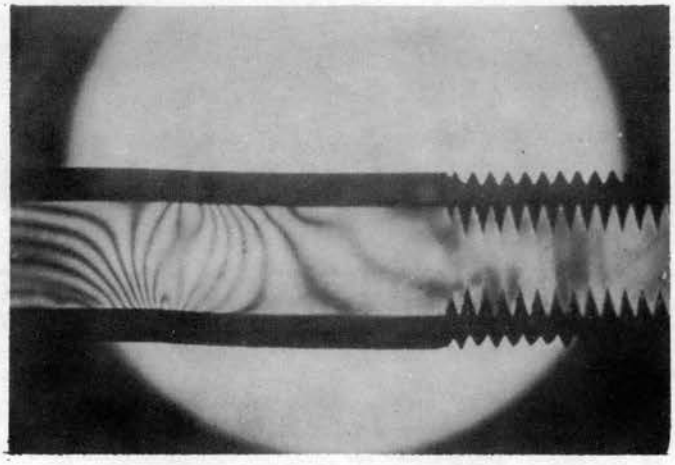

2. Side Slice - End

PLATE VIII

LAP JOINT PLATE FRINGE PATTERNS FOR RUN TWO

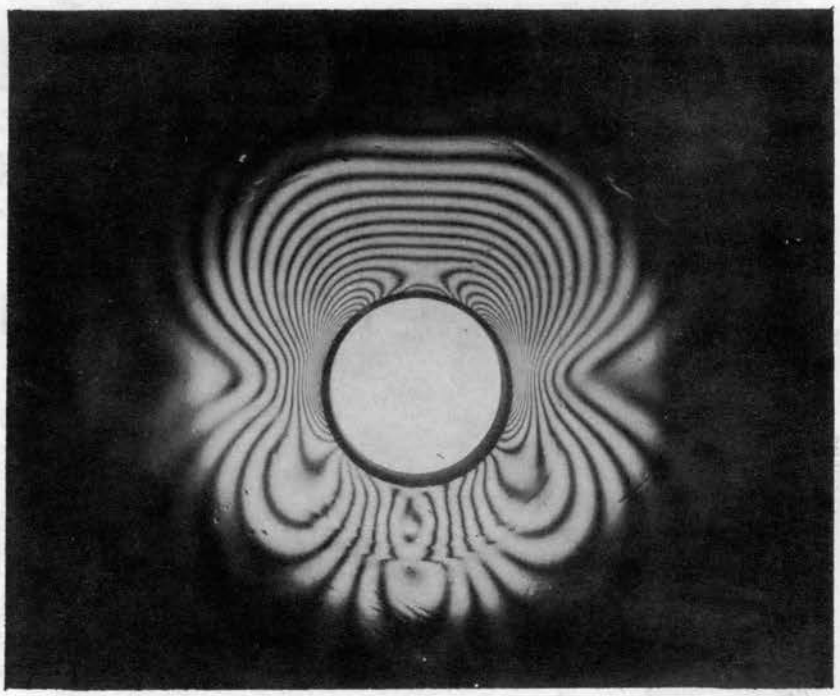

1. Top Plate

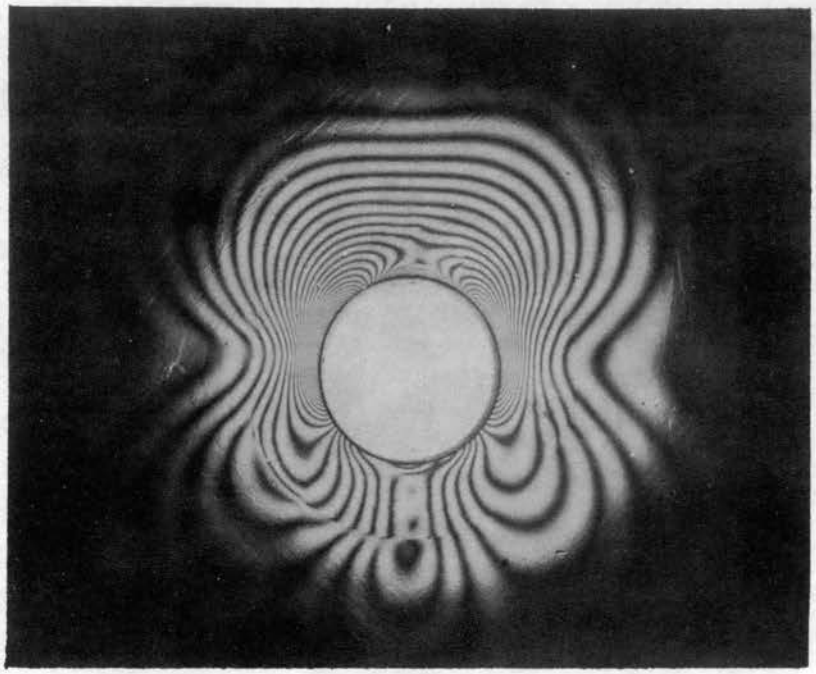

2. Bottom Plate

PLATE IX

LAP JOINT PLATE FRINGE PATTERNS FOR RUN TWO

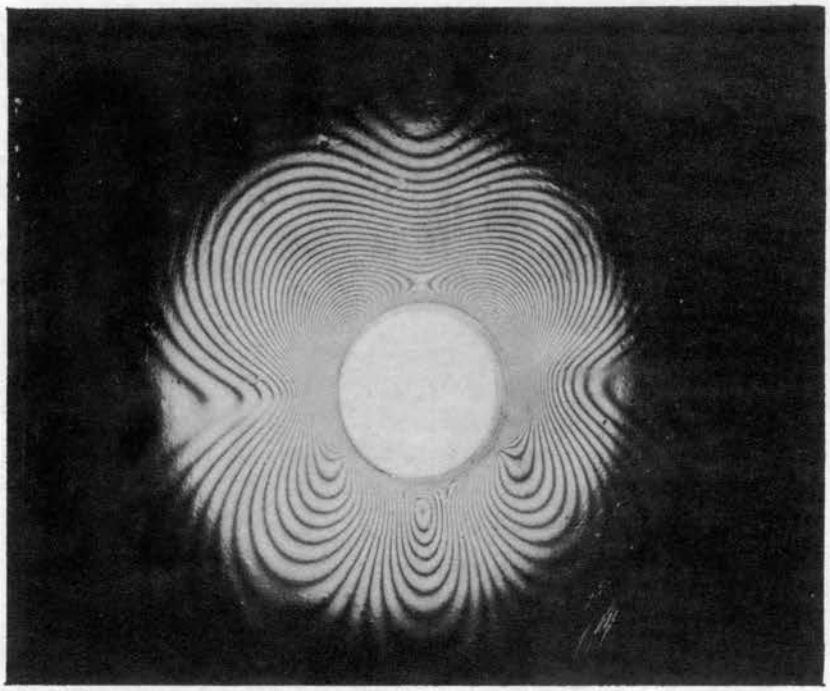

1. Center Plate

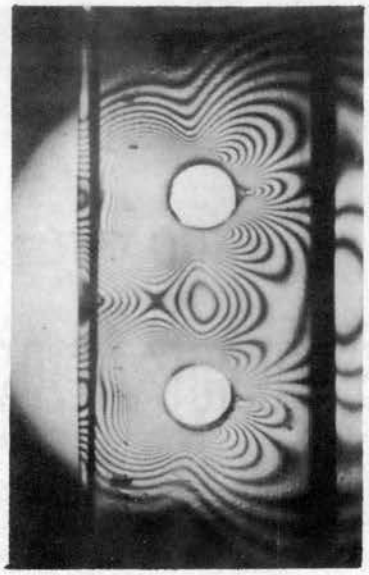

2. Bottom Plate End

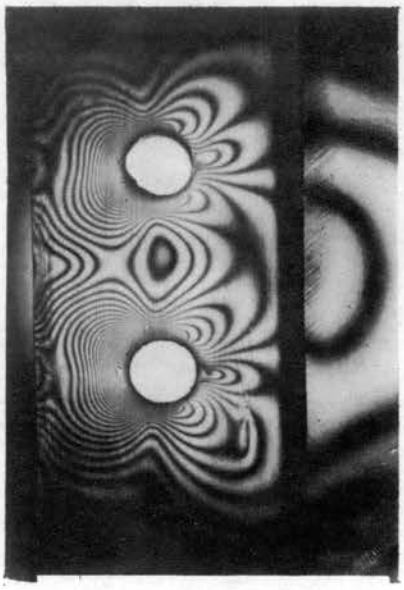

3. Top Plate End

PLATE X

PIN FRINGE PATTERNS FOR RUN THREE

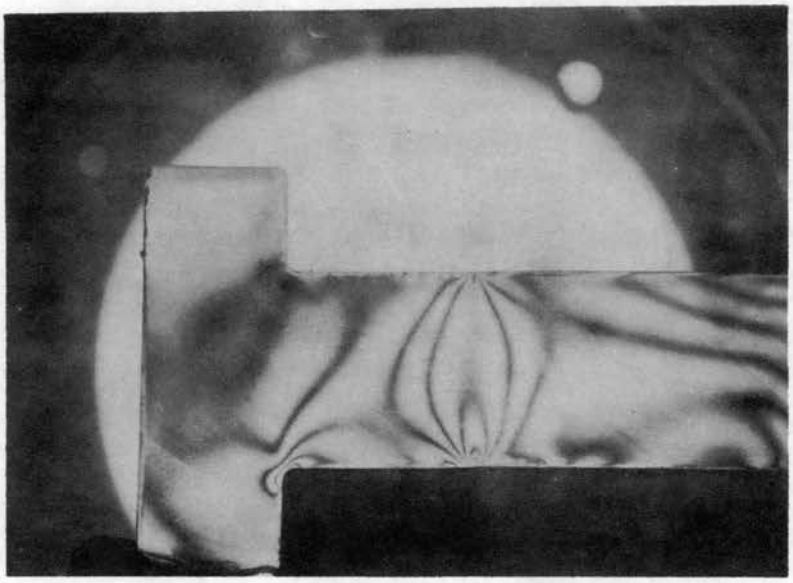

1. Center Slice

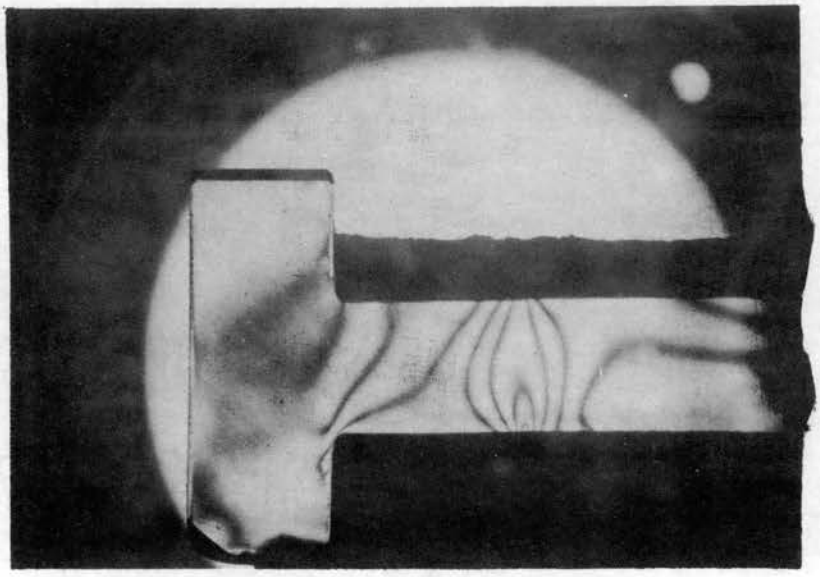

2. Side Slice

PLATE XI

PIN FRINGE PATTERNS FOR RUN FOUR

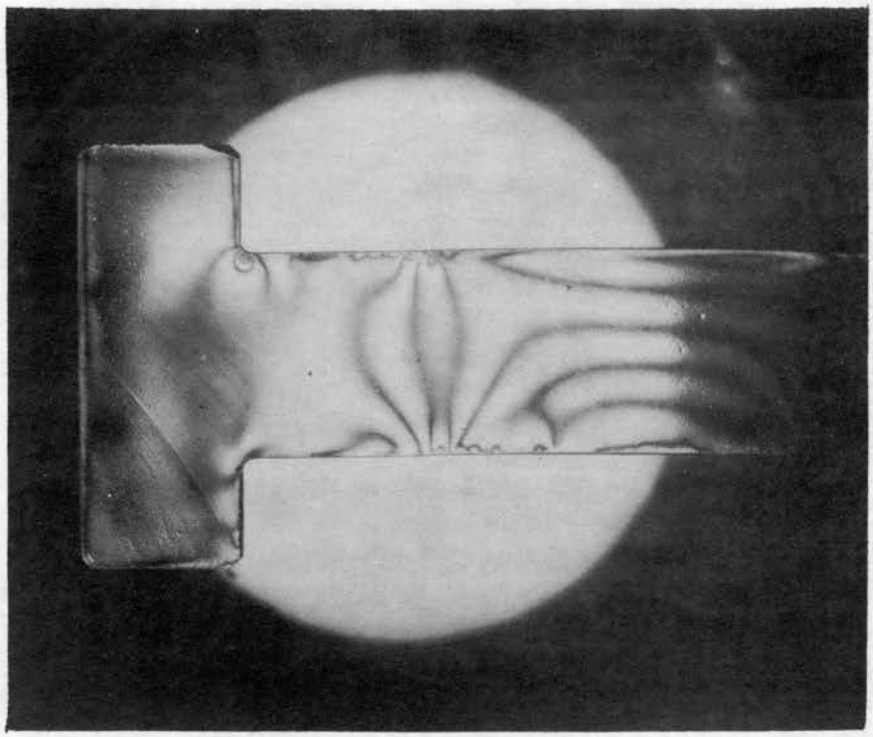

1. Center Slice

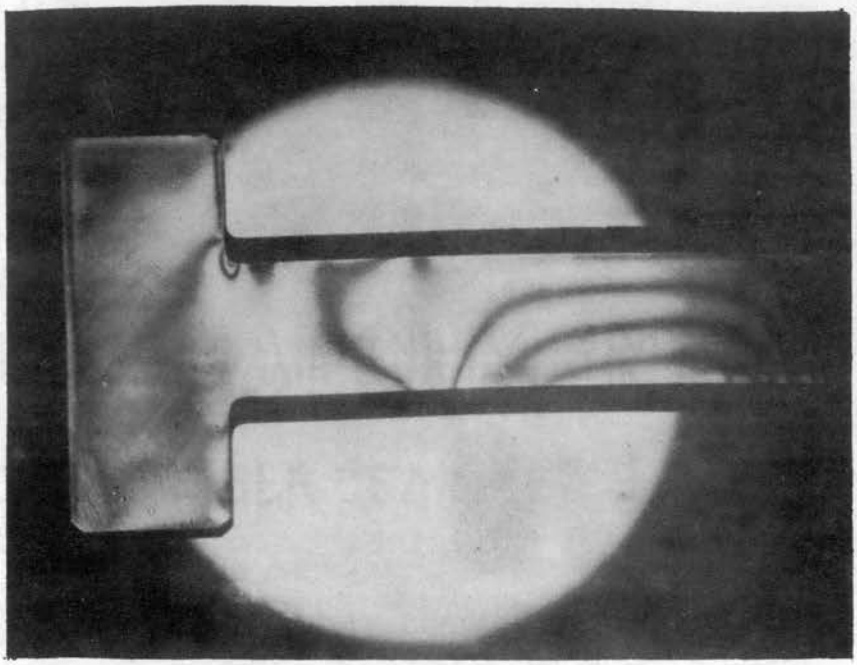

2. One-Eighth Inch Side Slice

PLATE XII

PIN FRINGE PATTERN FOR RUN FOUR

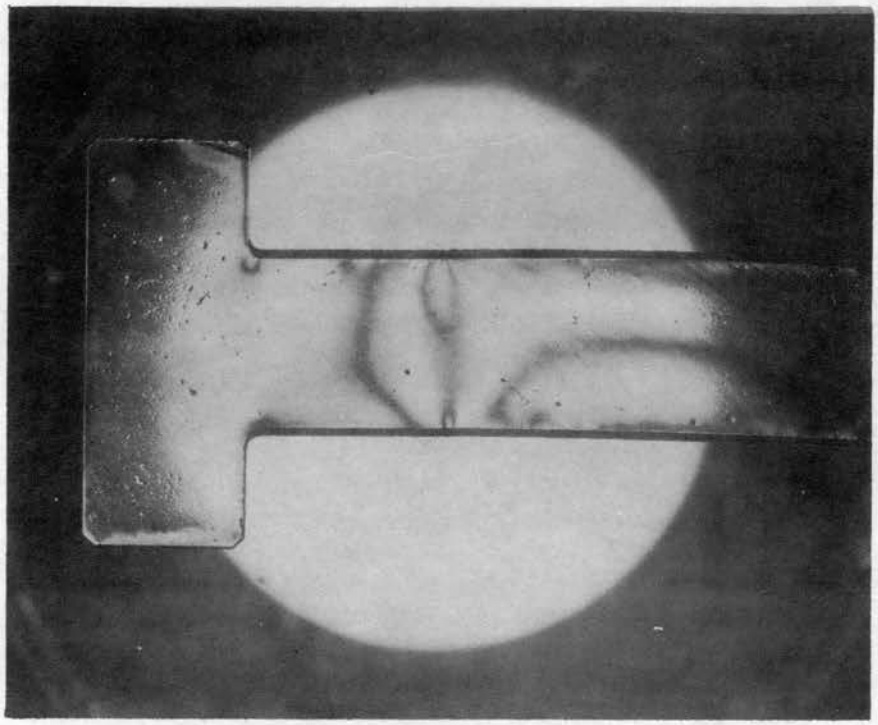

One-Sixteenth Inch Side Slice

PLATE XIII

PIN FRINGE PATTERNS FOR RUN FIVE

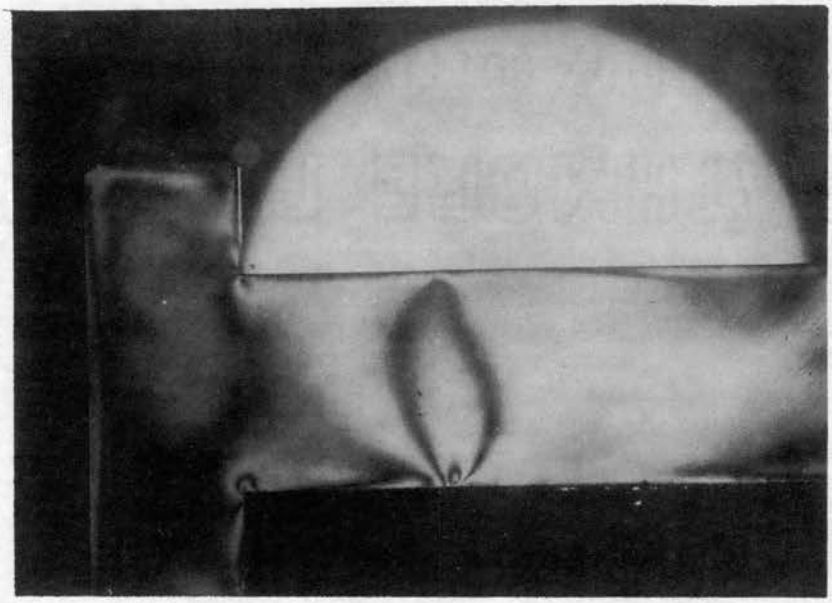

1. Center Slice

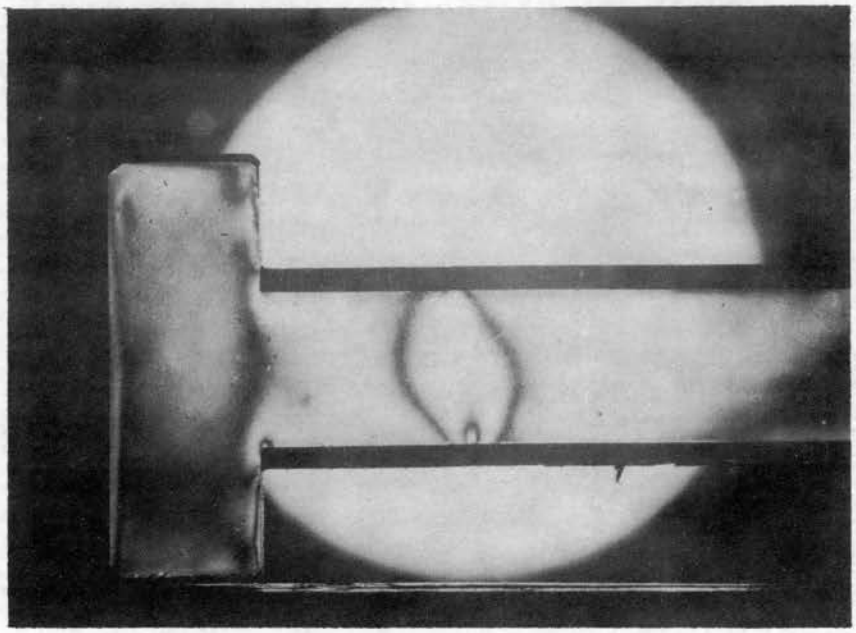

2. Side Slice

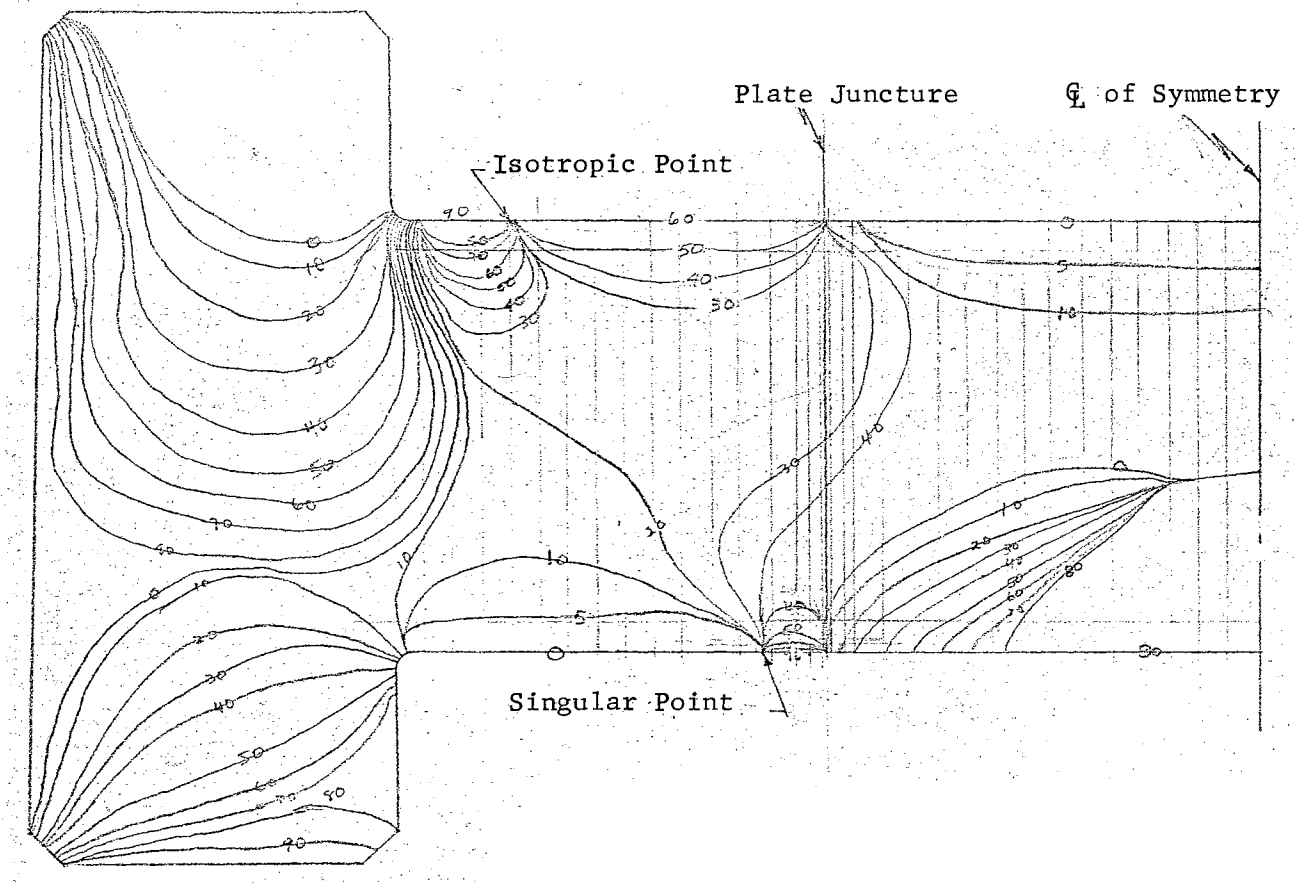

Figure 7. Sketch of the Run Two Pin Isoclinics

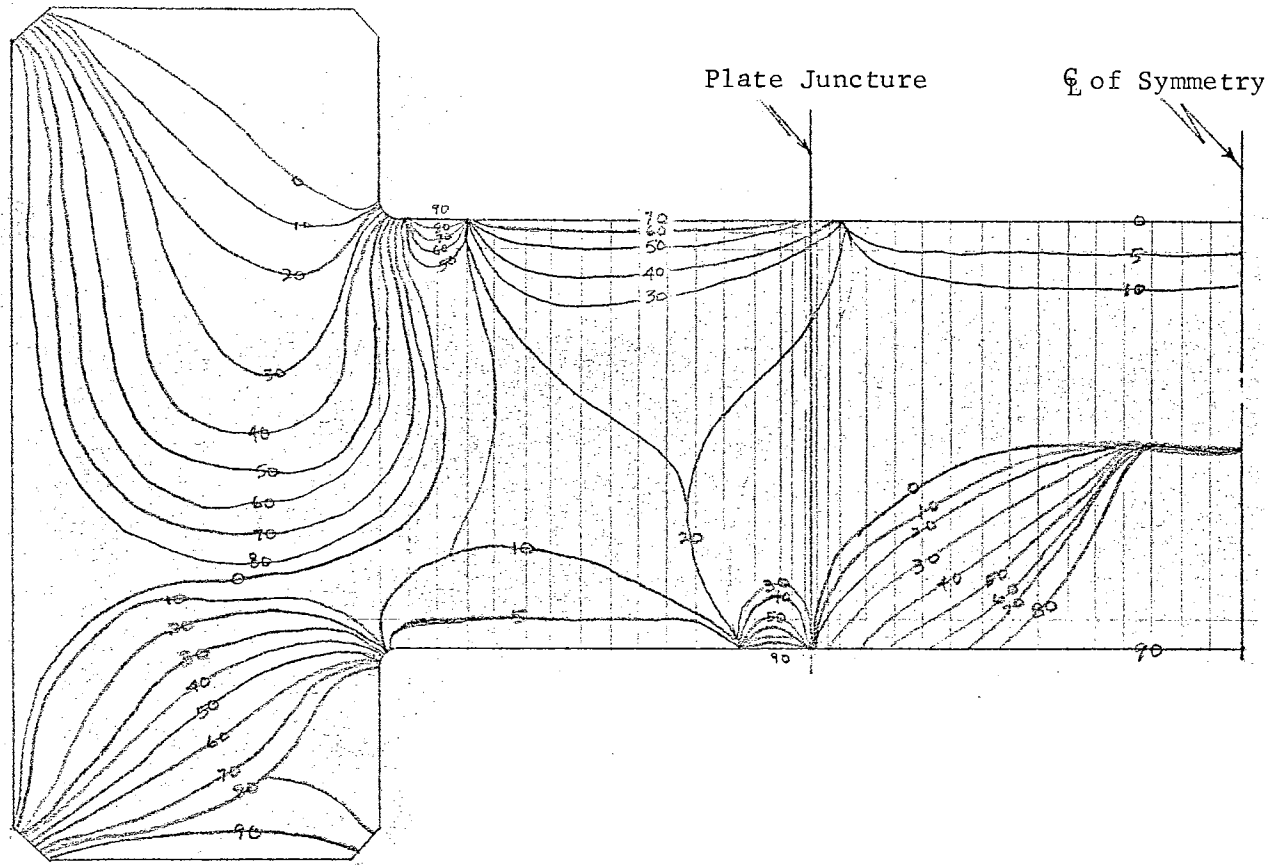

Figure 8. Sketch of the Run Three Pin Isoclinics

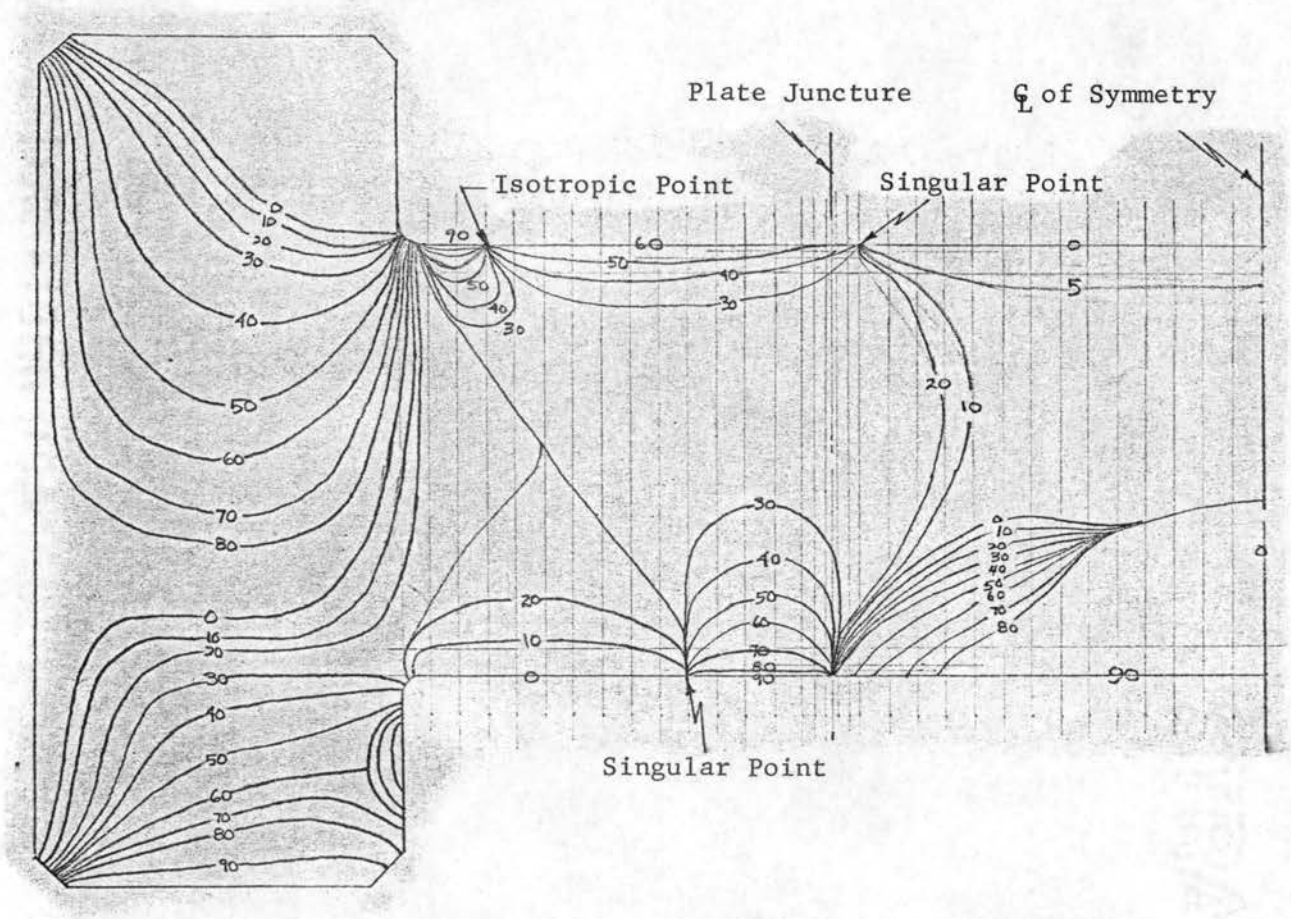

Figure 9. Sketch of the Run Four Pin Isoclinics

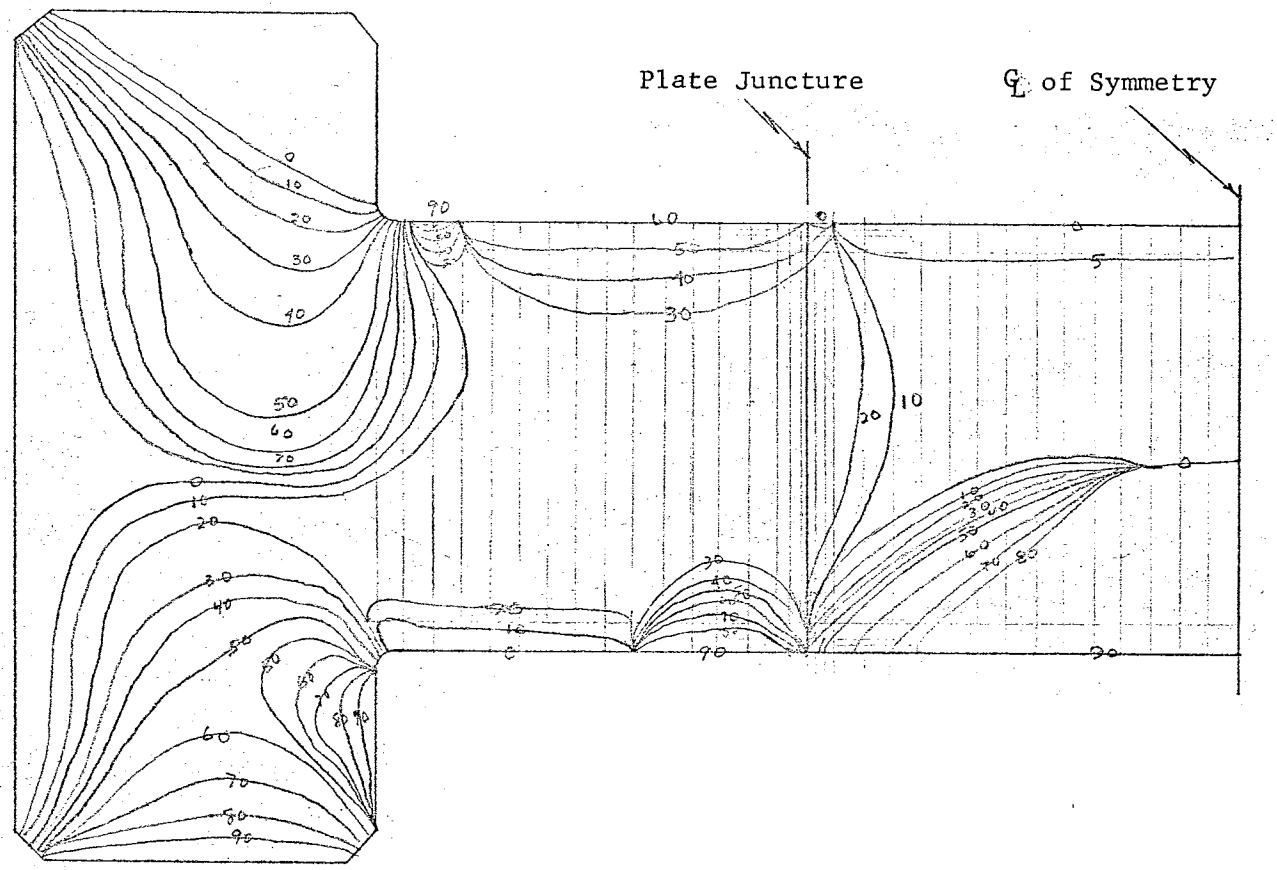

Figure 10. Sketch of the Run Five Pin Isoclinics

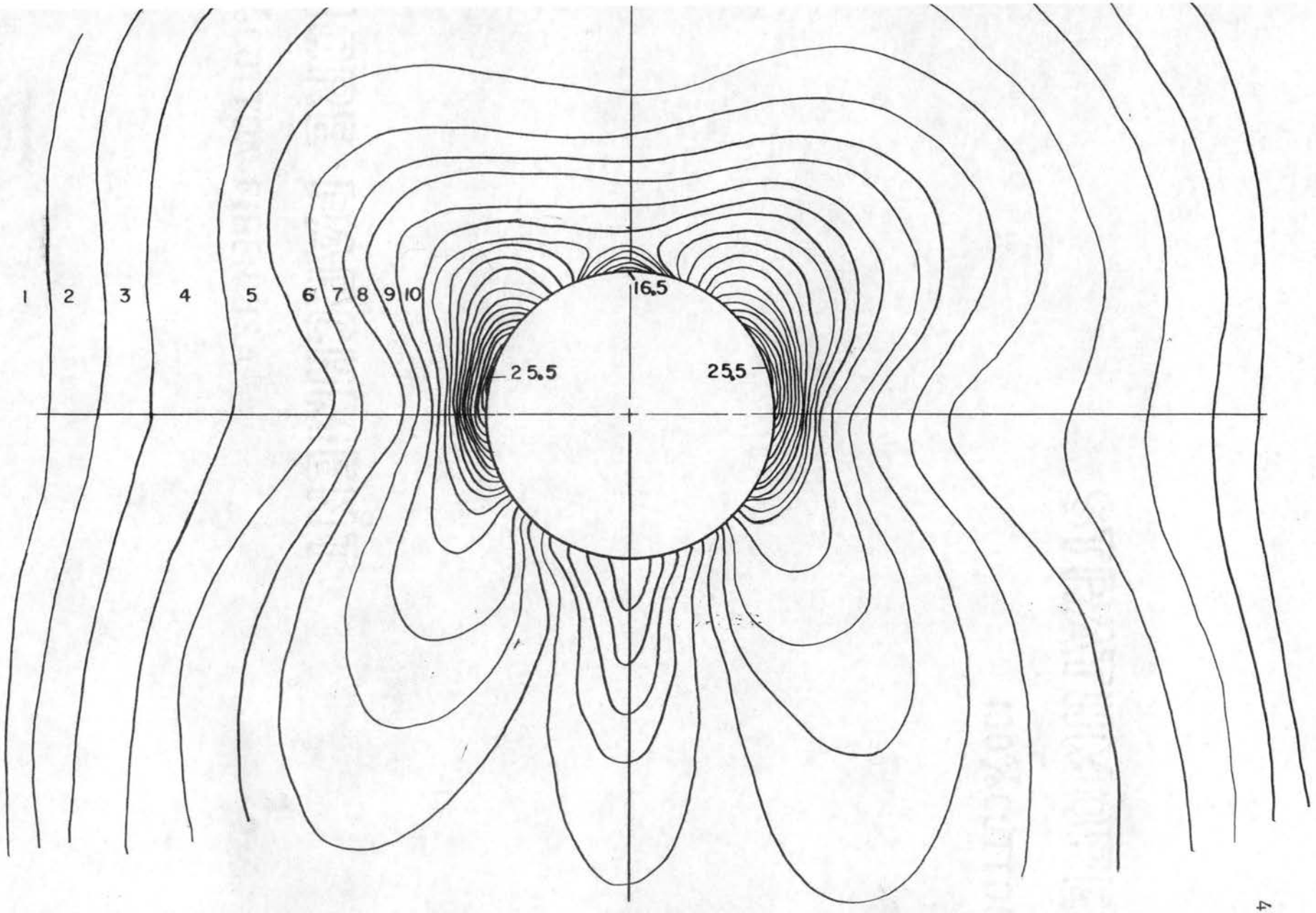

Figure 11. Sketch of the Run Four Center Plate Fringe Pattern

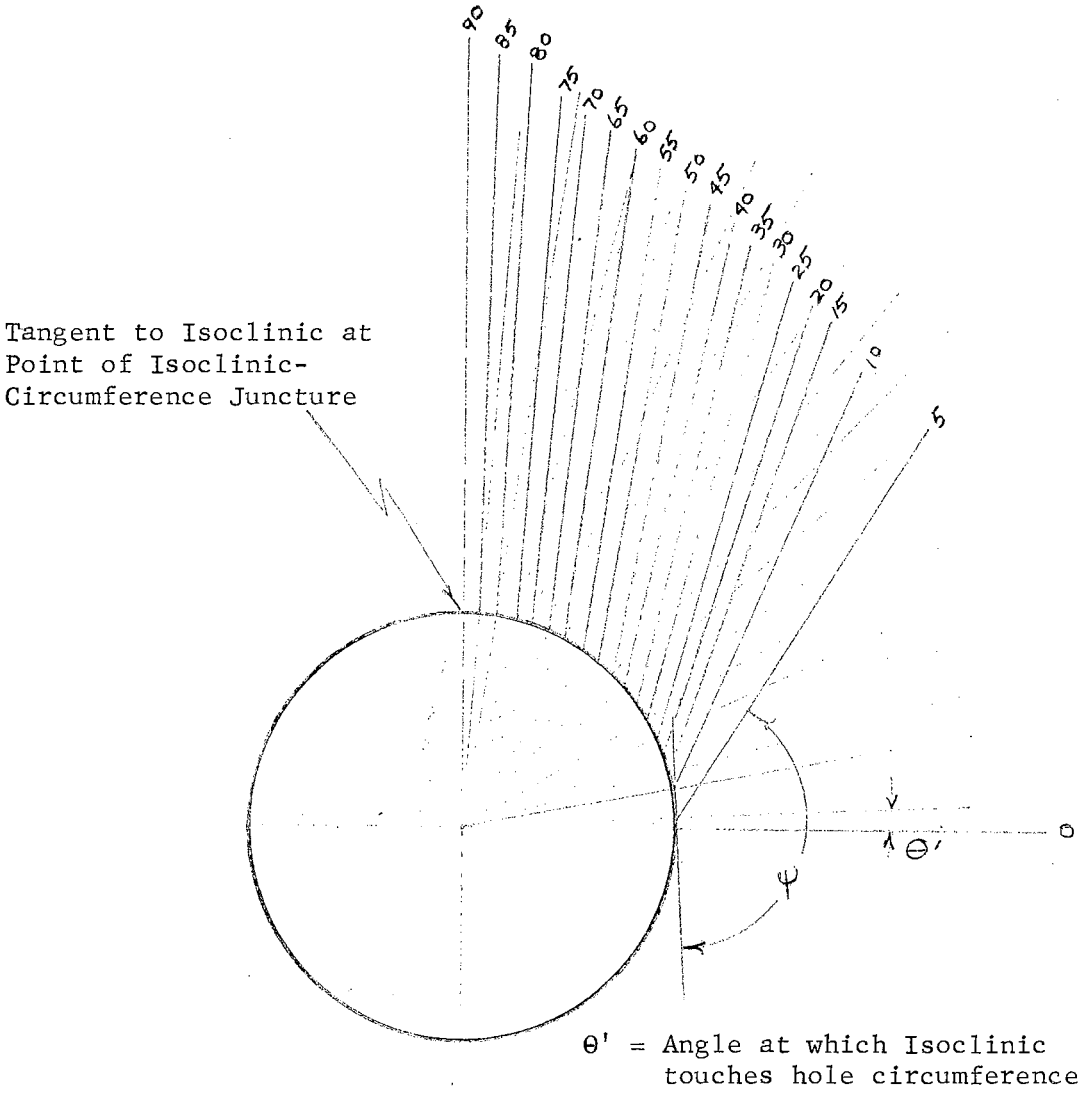

Figure 12. Sketch of the Tangents to the Plate Isoclinics

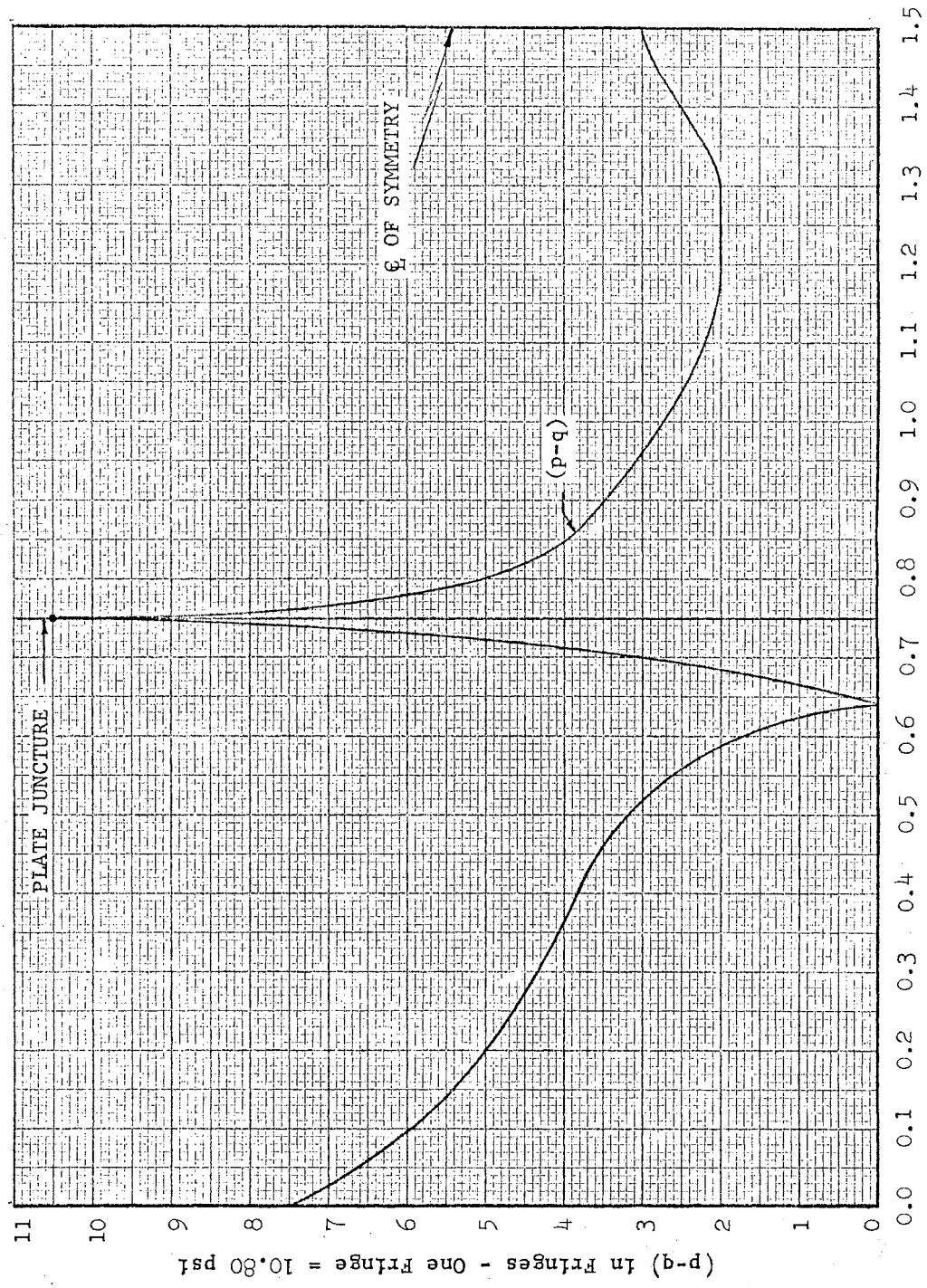

Figure 13. Fringe Distribution Along the Run Two Pin Lower Boundary

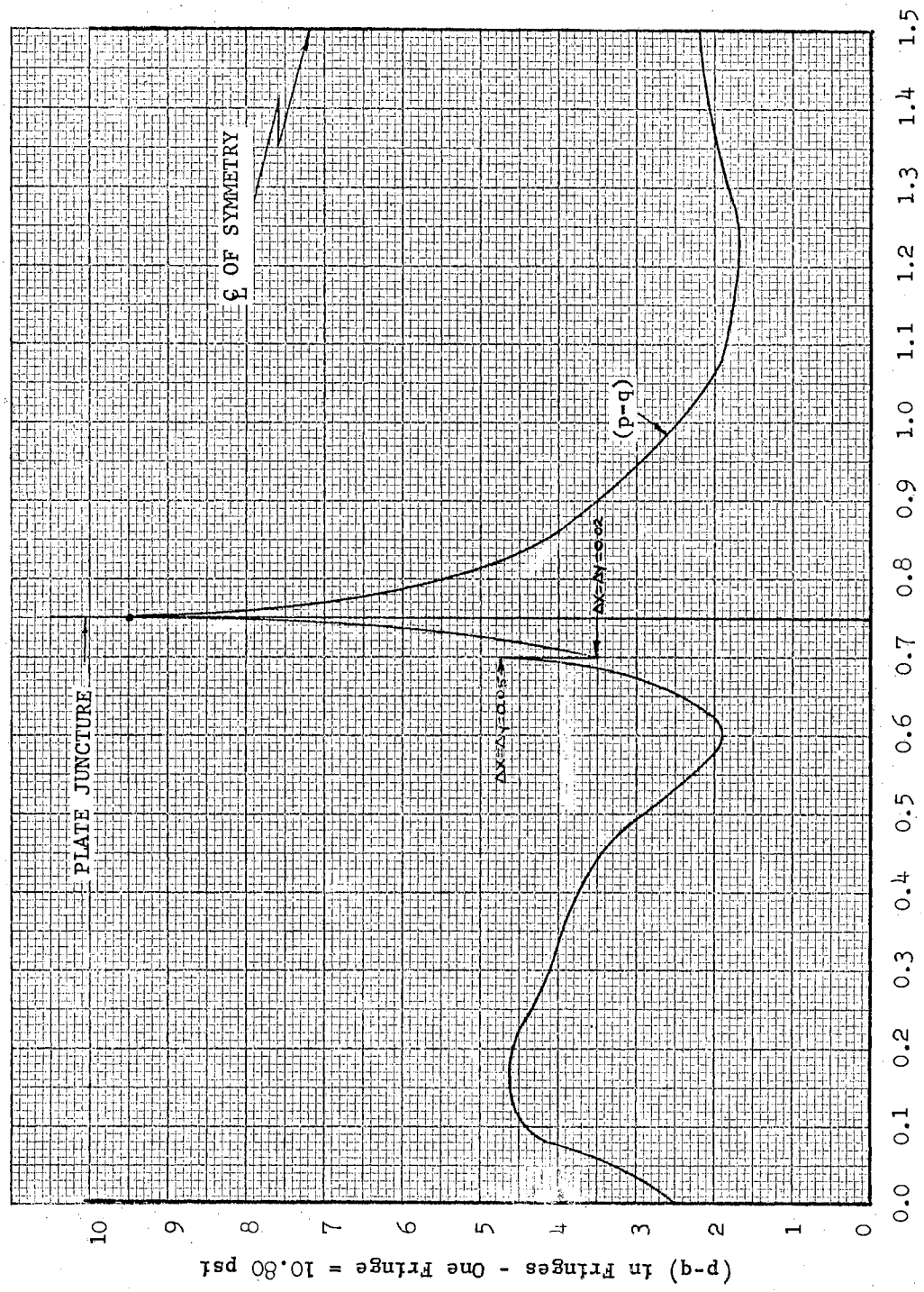

Figure 14. Fringe Distribution Along A - A on the Finite Difference Net for Run Two

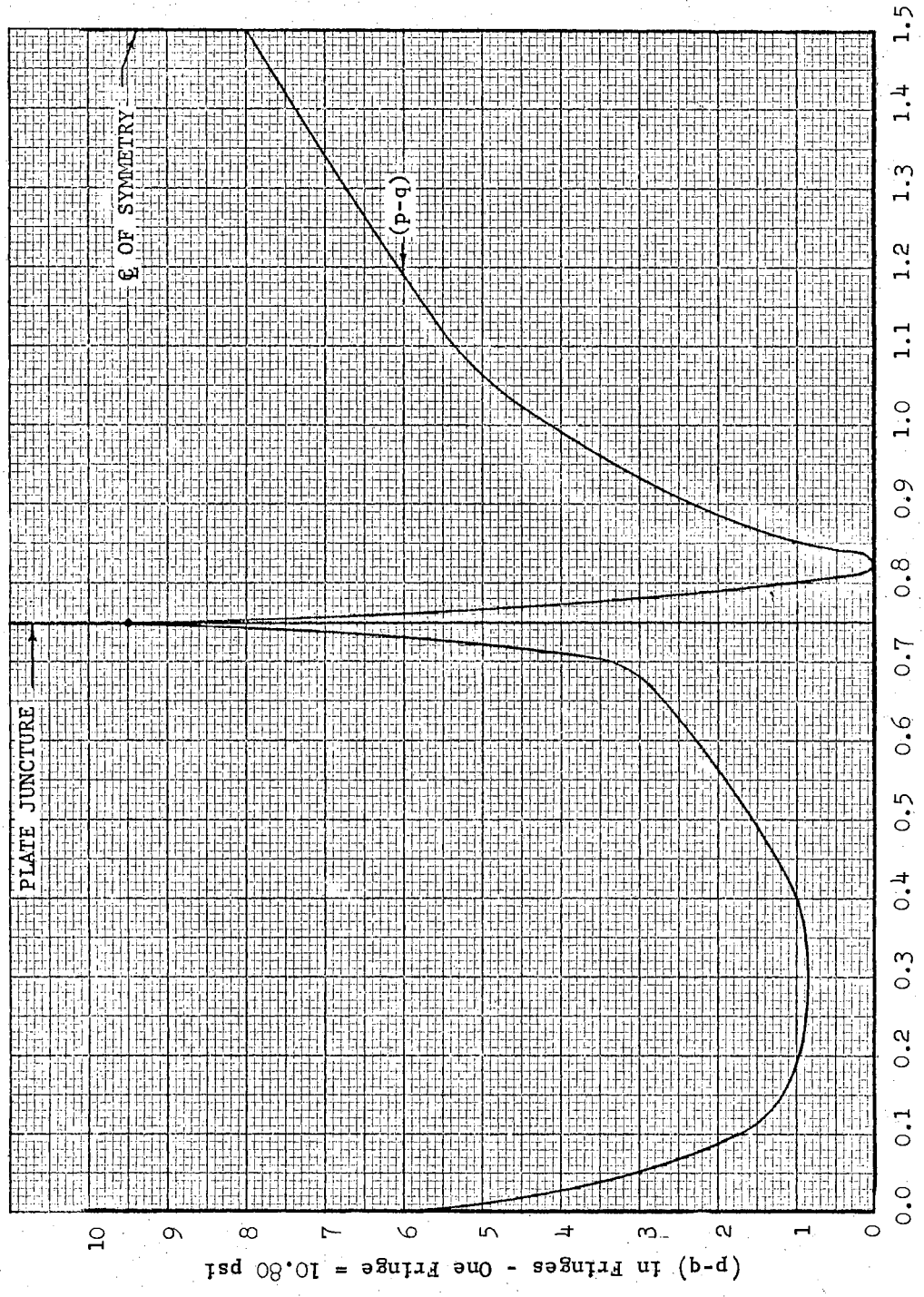

Figure 15. Fringe Distribution Along the Run Two Pin Upper Boundary

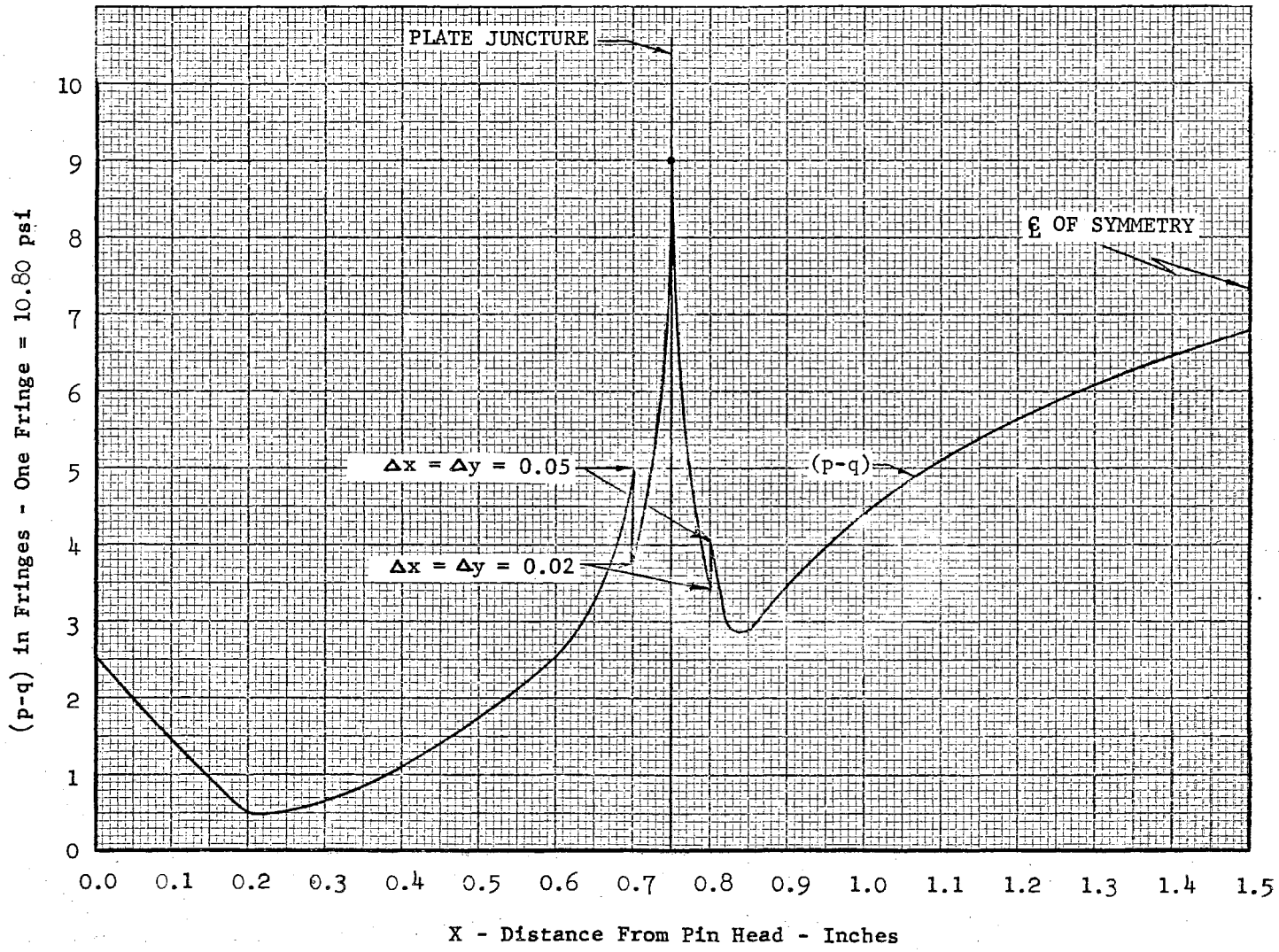

Figure 16. Fringe Distribution Along B - B on the Finite Difference Net for Run Two

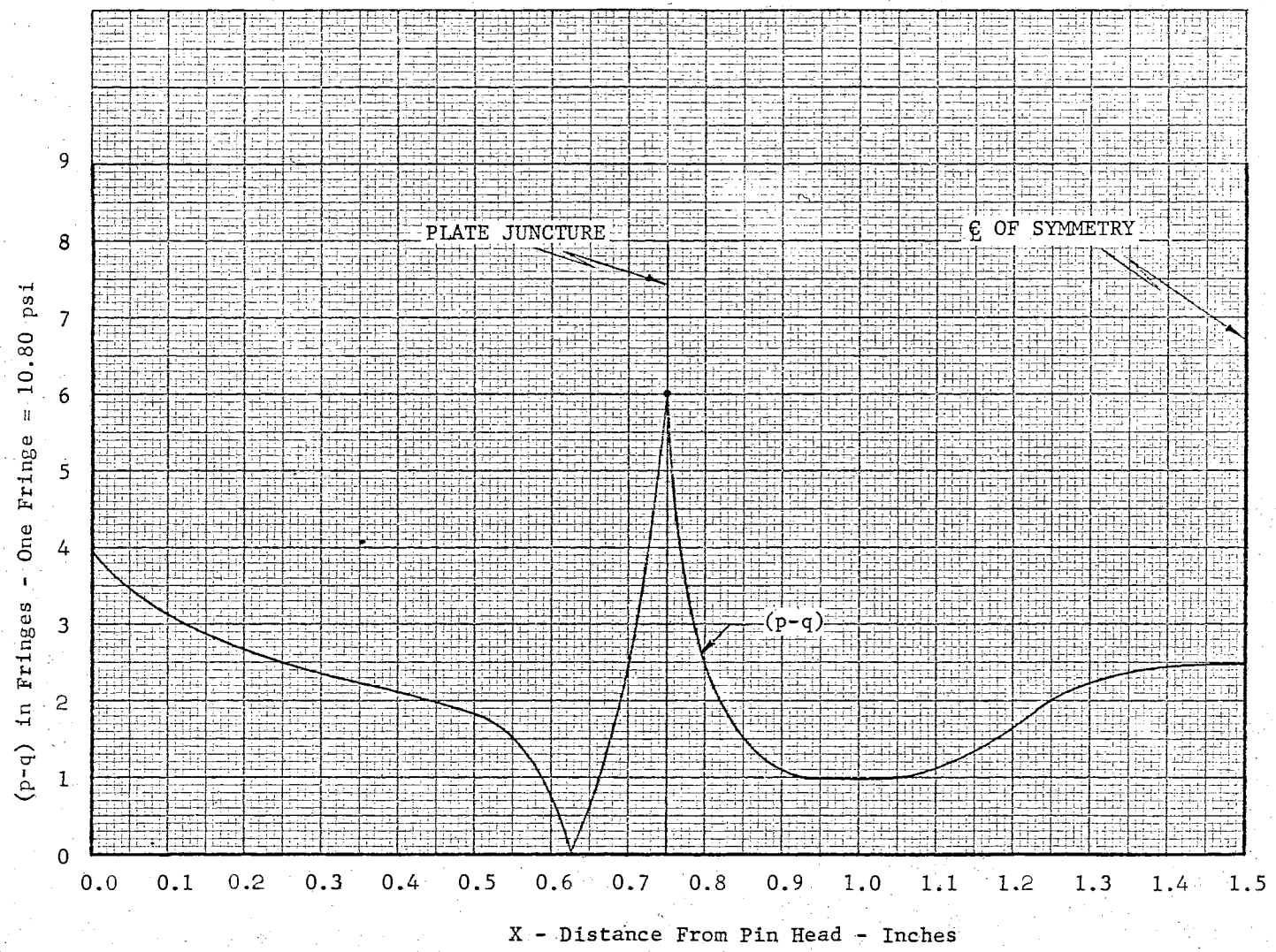

Figure 17. Fringe Distribution Along the Run Three Pin Lower Boundary

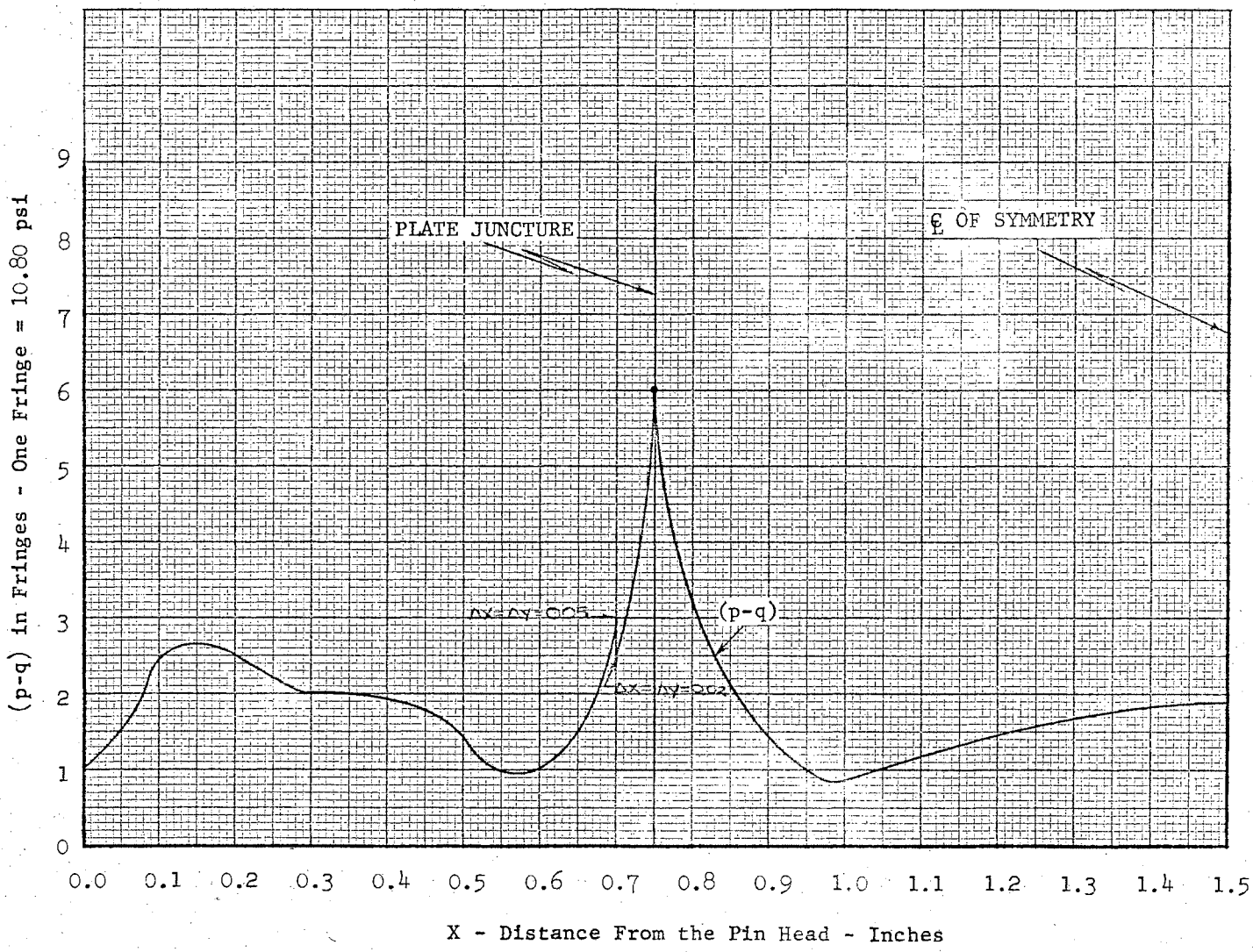

Figure 18. Fringe Distribution Along A - A on the Finite Difference Net for Run Three

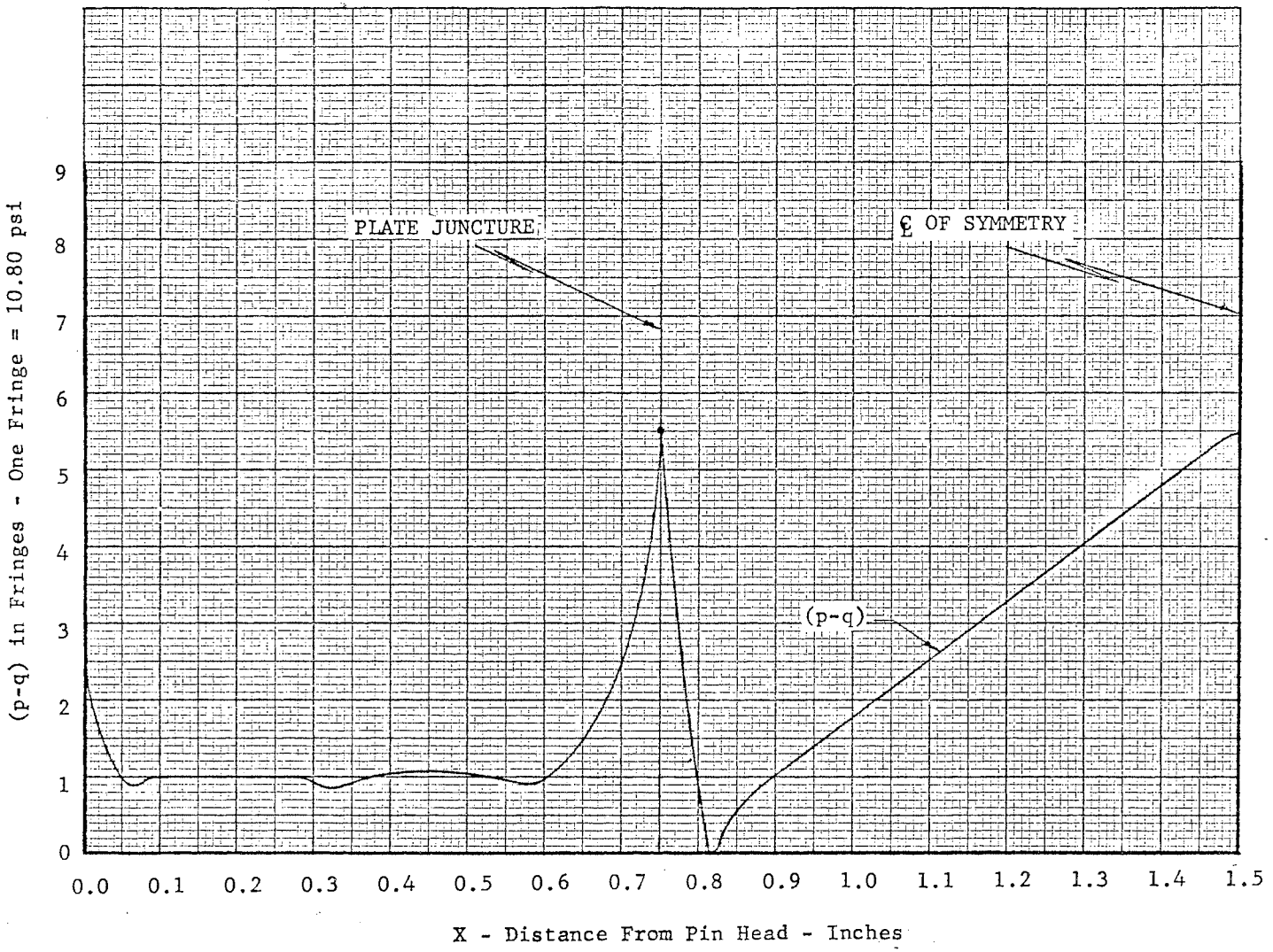

Figure 19. Fringe Distribution Along the Run Three Pin Upper Boundary

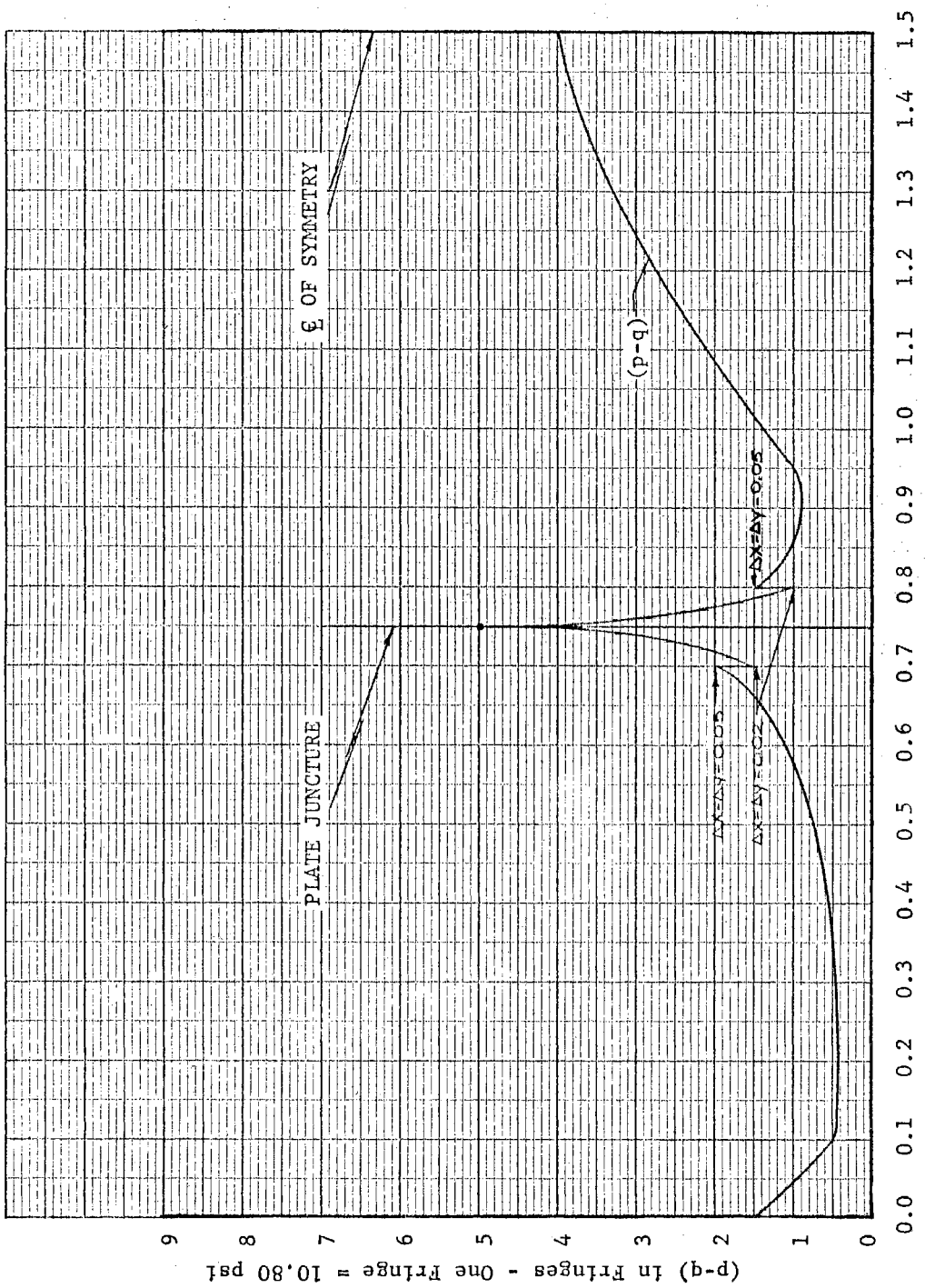

Figure 20. Fringe Distribution Along B - B on the Finite Difference Net for Run Three

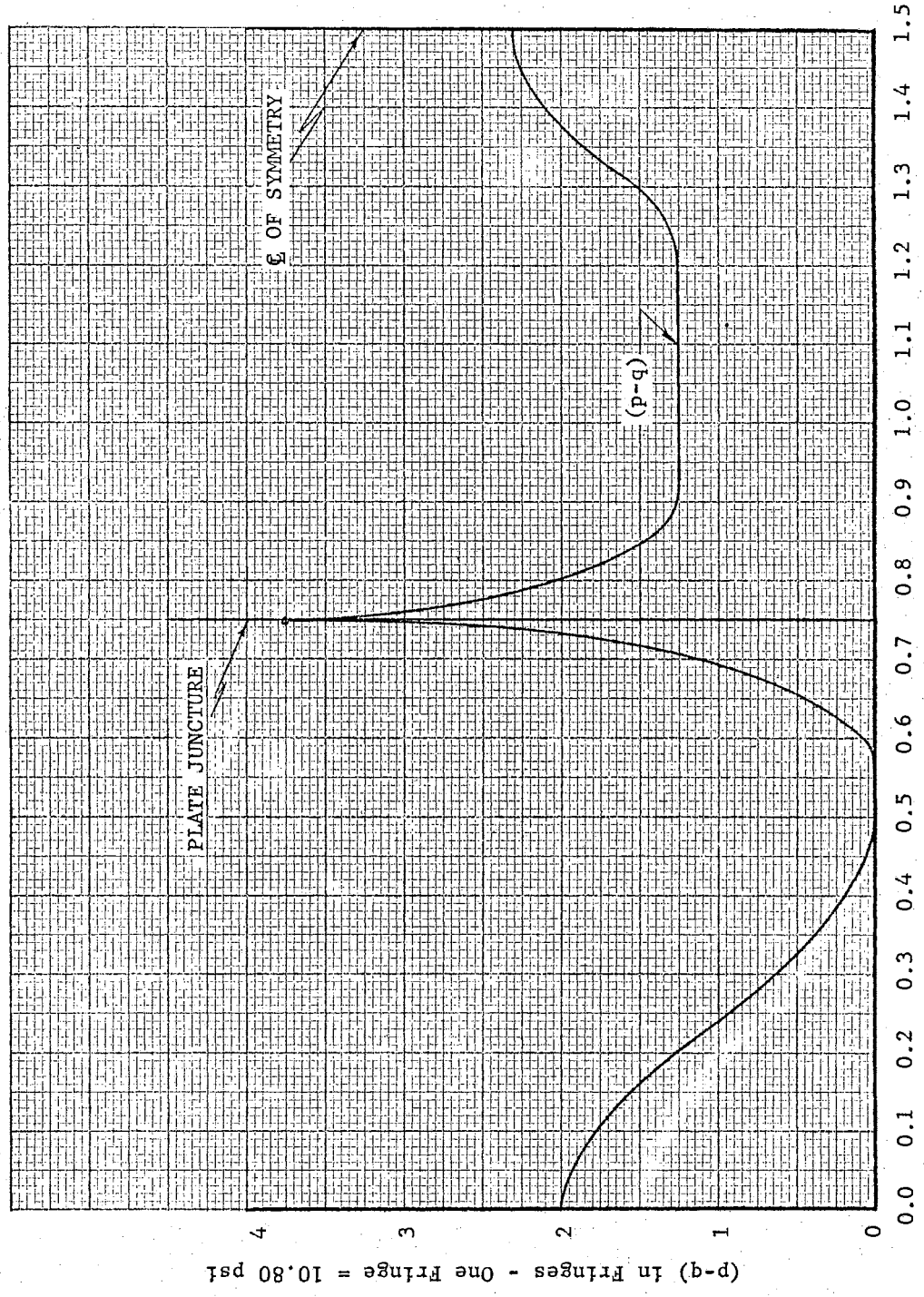

Figure 21. Fringe Distribution Along the Run Four Pin Lower Boundary

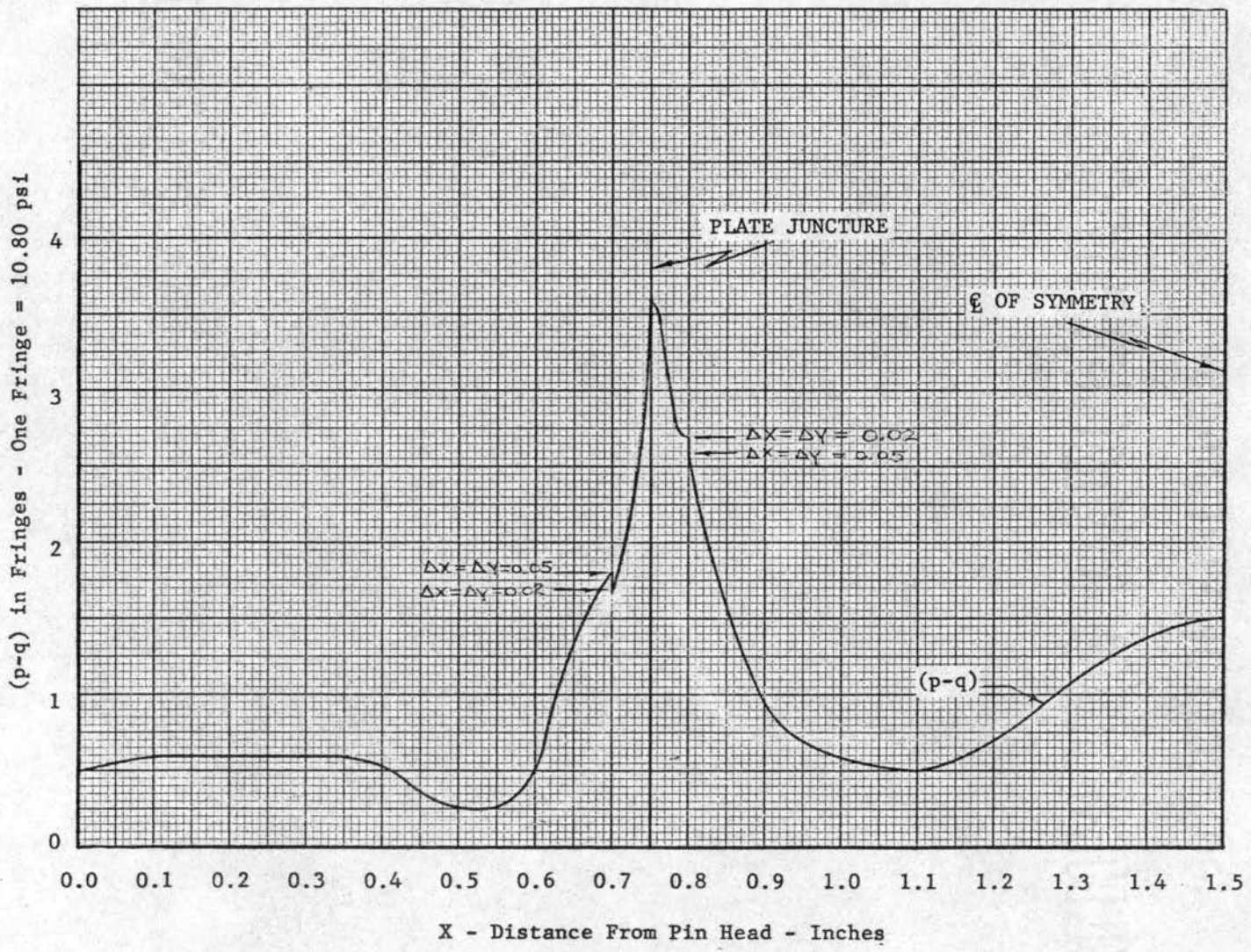

Figure 22. Fringe Distribution Along A - A on the Finite Difference Net for Run Four

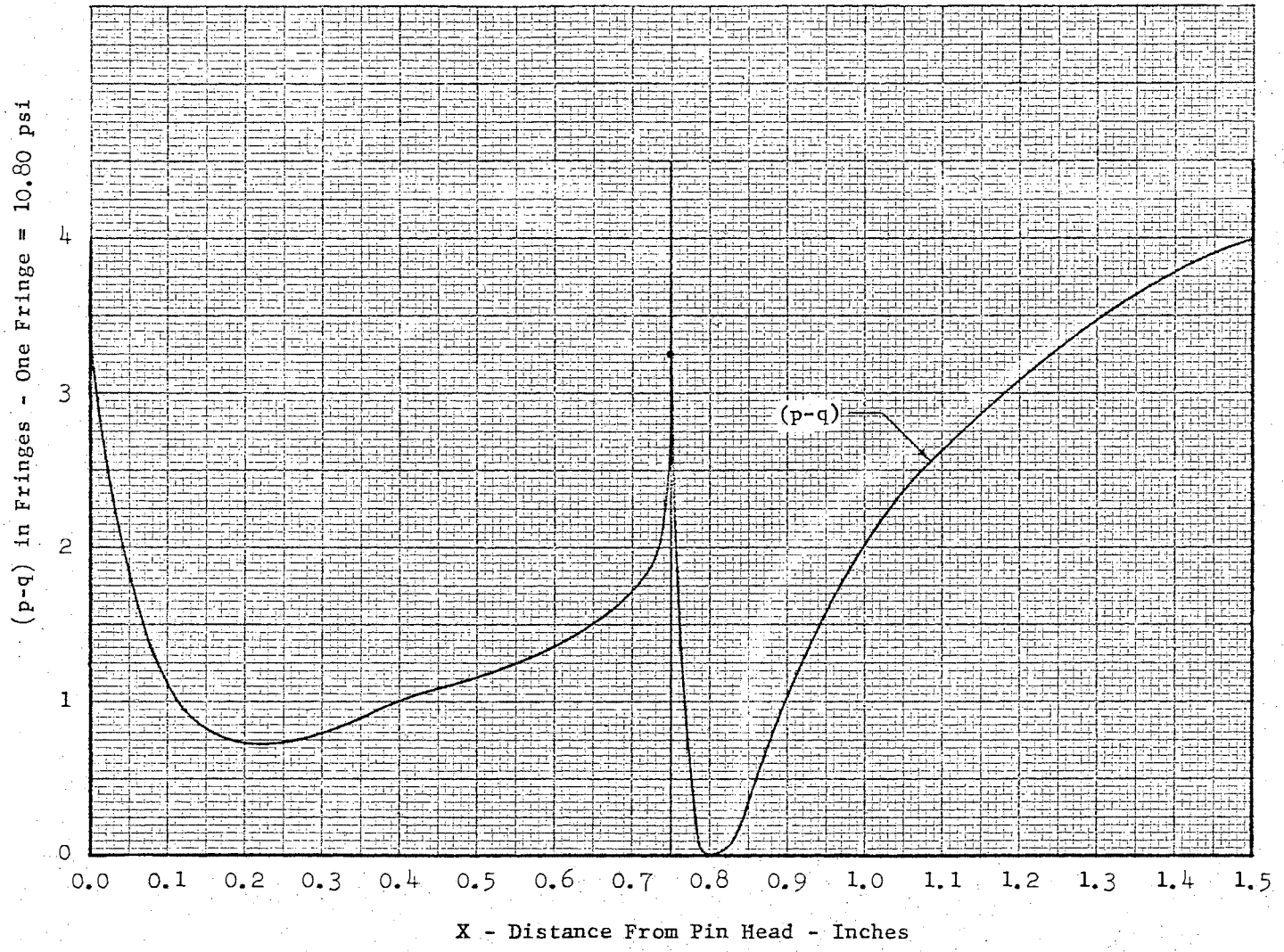

Figure 23. Fringe Distribution Along the Run Four Pin Upper Boundary

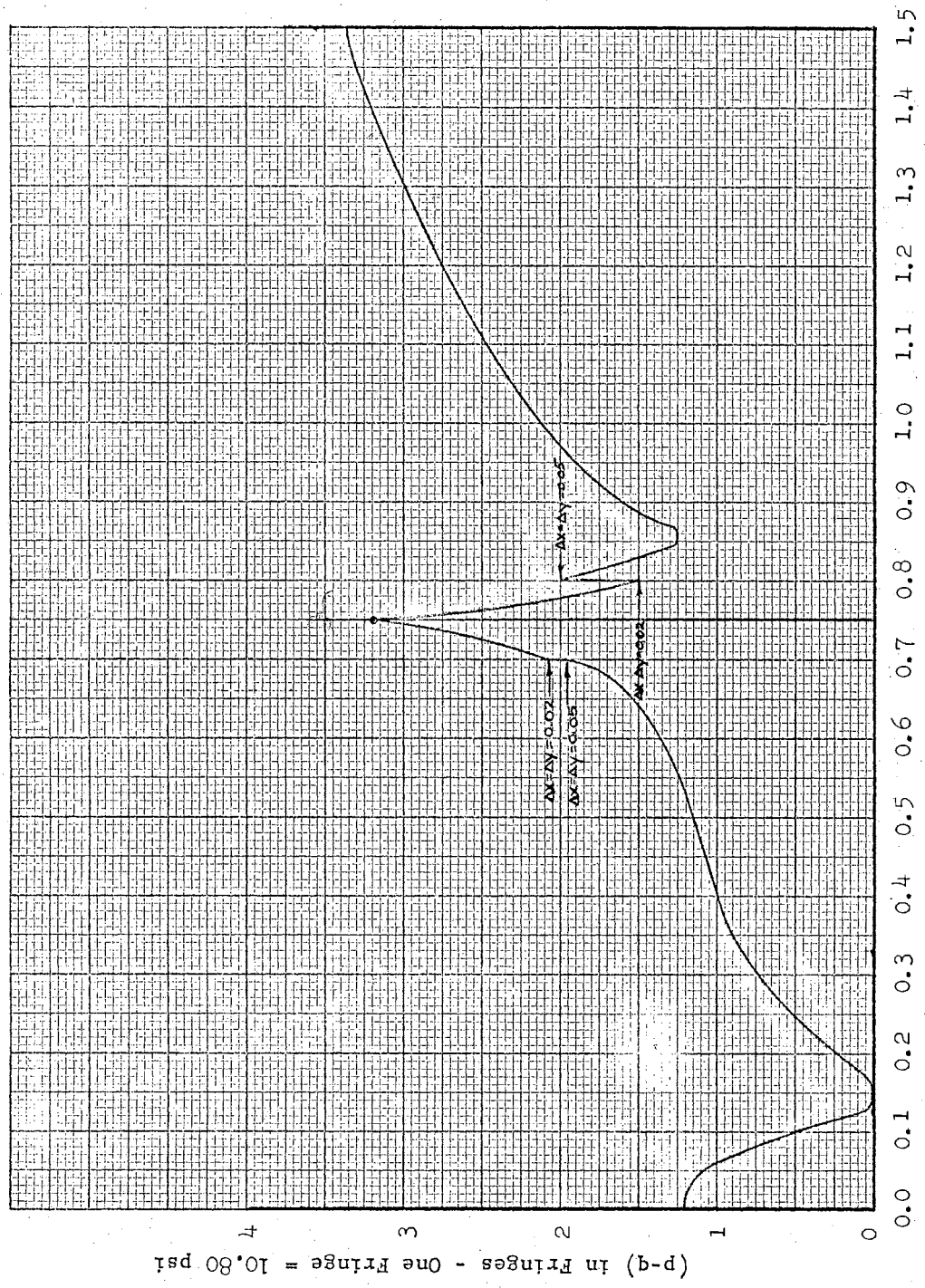

Figure 24. Fringe Distribution Along B - B on the Finite Difference Net for Run Four

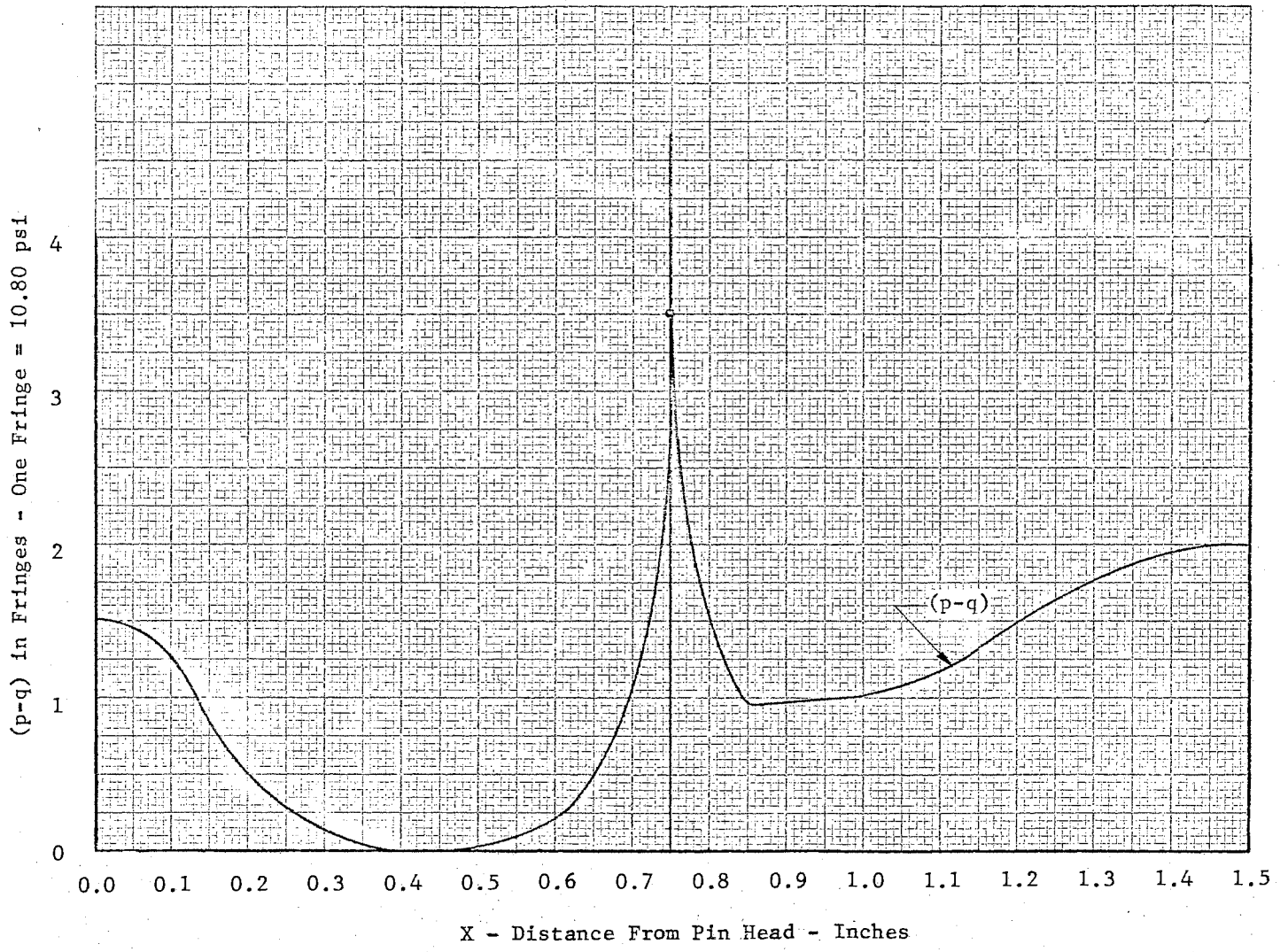

Figure 25. Fringe Distribution Along the Run Five Pin Lower Boundary

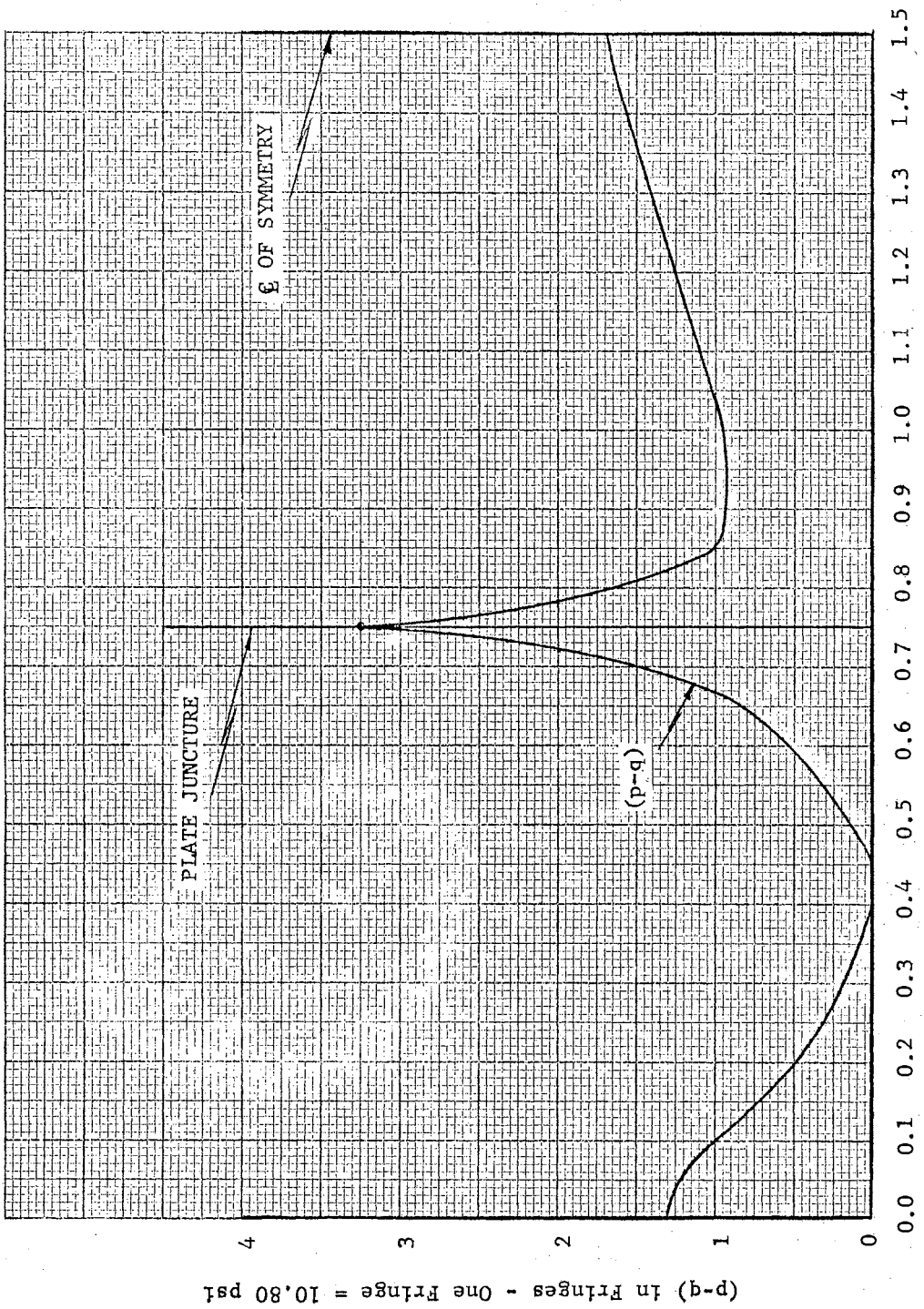

Figure 26. Fringe Distribution Along A - A on the Finite Difference Net for Run Five

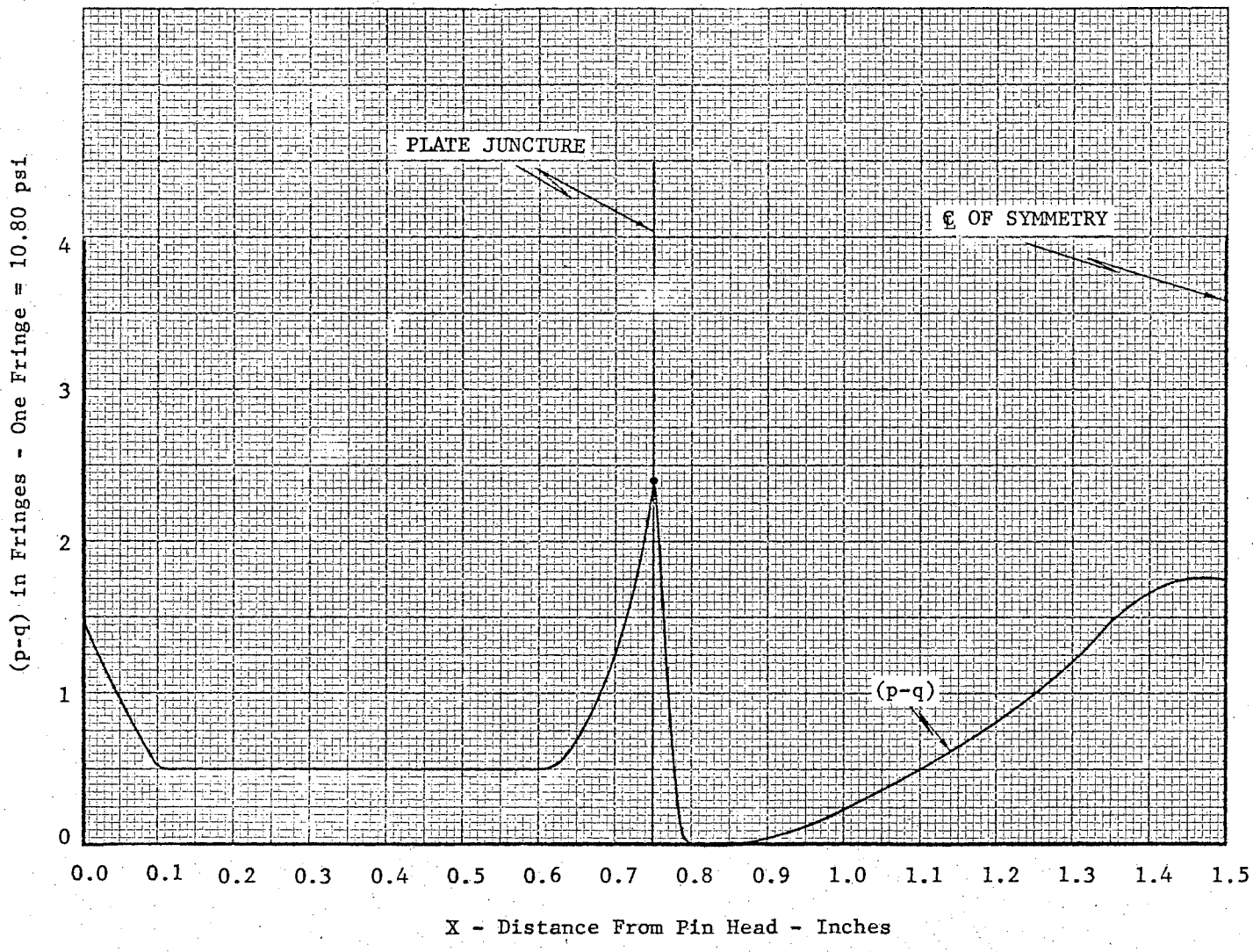

Figure 27. Fringe Distribution Along the Run Five Pin Upper Boundary

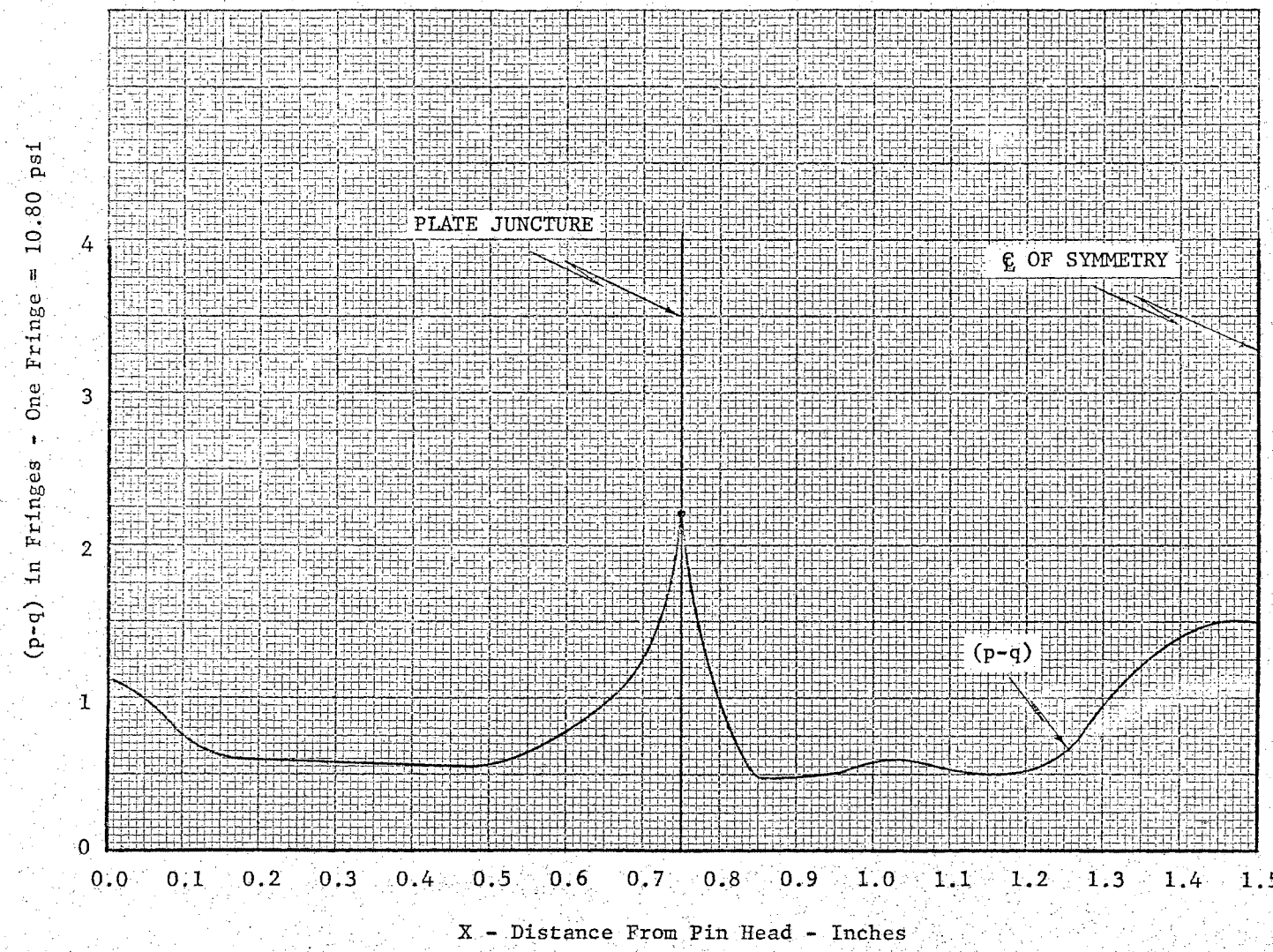

Figure 28. Fringe Distribution Along B - B on the Finite Difference Net for Run Five

CHAPTER VI

ANALYSIS OF RESULTS

The three-dimensional lap joint components are analyzed essentially as if each were composed of several two-dimensional slices. This is the basis for the plate method as has been previously stated. The center longitudinal slice contains a plane of load and geometrical symmetry; therefore, a two-dimensional analysis of it is correct. The use of two-dimensional techniques for the analysis of the other longitudinal slices is questionable however. Therefore, in order to determine the circumferential, as well as the longitudinal stress variations, the lap joint plates are utilized. The compressive stresses which exist on the surface of the pin and on the matching surface of the hole are very nearly equal. (1). The normal compressive stress variation along the portion of the pin lower boundary which mates with the center plate is fairly small, since the compressive stresses are approximately uniform for that portion of the pin boundary. This is illustrated in Figure 34.

The compressive stresses determined from the plate hole are matched correspondingly with the pin compressive stresses to determine the circumferential stress variations over the two quadrants of the pin which are of primary interest. This procedure proved to be quite satisfactory since a static check for equilibrium by summation of radial stresses yielded only 7.6 per cent error. This check is shown in Table X.

Longitudinal Stress Distribution

The calculations of the stresses along the pin lower boundary are given in Tables I, III, V and VII, and the calculations of the stresses along the pin upper boundaries are given in Tables II, IV, VI and VIII. It has been previously stated that the terms lower and upper refer to the orientation of the pin slices in the photographs and in Figure 5. The calculations shown in Tables I-VIII are for the pin center slices and represent the variation of the stresses both normal to the pin surfaces and tangent to the pin surfaces.

The graphical integrations in these two cases are accomplished by using equation (II-14), which is again presented for discussion as

$$(\sigma_x)_i = (\sigma_x)_o - \sum_{o}^{i} \Delta\tau_{xy} \frac{\Delta x}{\Delta y}. \qquad \text{(II-14)}$$

It will be noticed that if the sizes of the increments Δx and Δy are the same, the physical labor of the calculations can be considerably reduced. Therefore, the net utilized for the graphical integration is such that $\Delta x = \Delta y$. This net is illustrated in Figure 29.

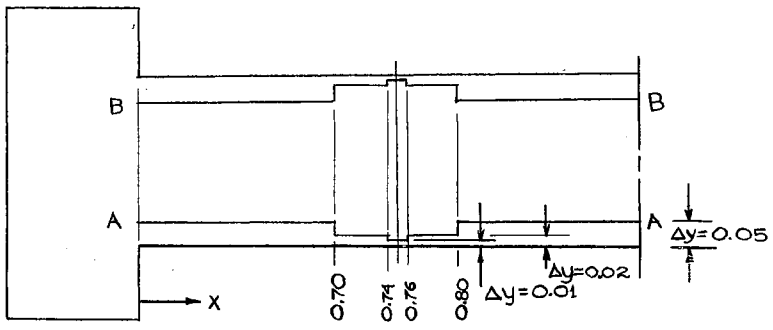

Figure 29. The Finite Difference Net

The starred values in Tables I through VIII refer to values corresponding to points on this net. The variations of fringe order and stresses where x is 0.75 inches are quite large; therefore it was deemed desirable to decrease the incremental sizes in the neighborhood of x equal to 0.75 inches. The starting value $(\sigma_x)_o$ is known where x is 0.75 inches, since at this section a free boundary exists on both the upper and lower pin surfaces. The graphical integration is then carried out for both increasing values of x and decreasing values of x from the starting point x = 0.75 inches. There are two points along the boundaries which serve as check points to determine the accuracy of the calculations. These points are known as singular points and at these points the boundary tangential and normal stresses must be equal to zero. As an example, one of these check points occurs on the run four lower boundary where x is 0.50 inches. The second point occurs on the run four upper boundary where x is 0.80 inches. These points also indicate the points at which the tangential boundary stresses change from tensile to compressive.

Curves of the stress distribution along the pin lower boundaries are shown in Figures 30, 32, 34 and 36, and curves of the stress distribution along the pin upper boundaries are shown in Figures 31, 33, 35 and 37. The summation of the normal stresses σ_y, when summing along both the lower and upper boundaries, should be equal to zero except for a small resistance caused by friction between the pin head and the outside lap joint plate. The actual summations are shown in Figures 38-41.

The longitudinal stress distributions were obtained only from the center slice. The distributions for the other slices are approximately the same as those for the center slice. This can be seen by observing

the fringe order variations in Plates XI and XII. The magnitudes of the fringe orders at similar points are less in the side slices, but the variations are approximately the same.

TABLE I

CALCULATION OF THE STRESSES ALONG THE RUN TWO PIN LOWER BOUNDARY

$$\tau_{xy} = \frac{(p-q)}{2} \sin 2\theta; \quad (\sigma x)_i = (\sigma x)_o - \sum_o^i \Delta\tau_{xy}(\pm 1); \quad \sigma y = \sigma x \pm \sqrt{(p-q)^2 - 4\tau_{xy}^2}$$

X	$\frac{(p-q)}{2}$	θ	τ_{xy}	$\frac{(p-q)}{2}$*	θ*	τ_{xy}*	$\Delta\tau_{xy}$	AVG $-\Delta\tau_{xy}\frac{\Delta x}{\Delta y}$	σx	σy
in.	fringes	degrees	fringes	fringes	degrees	fringes	fringes	fringes	fringes	fringes
0.00	3.75	10	1.28	1.25	10	0.43	-0.85	-0.28	-4.20	-2.86
0.05	3.32	0	0.00	1.63	5	0.28	+0.28	0.33	4.49	-2.15
0.10	3.00	0	0.00	2.20	5	0.38	0.38	0.39	4.16	-1.84
0.15	2.70	0	0.00	2.31	5	0.40	0.40	0.40	3.77	-1.63
0.20	2.50	0	0.00	2.30	5	0.40	0.40	0.39	3.37	-1.63
0.25	2.37	0	0.00	2.17	5	0.38	0.38	0.37	2.98	-1.76
0.30	2.17	0	0.00	2.05	5	0.36	0.36	0.35	2.61	-1.73
0.35	2.03	0	0.00	1.97	5	0.34	0.34	0.30	2.26	-1.80
0.40	1.90	0	0.00	1.87	4	0.26	0.26	0.25	1.96	-1.84
0.45	1.79	0	0.00	1.73	4	0.24	0.24	0.22	1.71	-1.87
0.50	1.60	0	0.00	1.48	4	0.21	0.21	0.20	1.49	-1.71
0.55	1.30	0	0.00	1.15	5	0.20	0.20	0.43	1.29	-1.31
0.60	0.85	0	0.00	0.95	22	0.66	0.66	0.96	+0.86	-0.84
0.65	0.15	90	0.00	1.26	43	1.26	1.26	1.82	-1.06	0.00
$0.70_{(0.05)}$	1.50	90	0.00	2.37	45	2.37	2.37			
$0.70_{(0.02)}$	1.50	90	0.00	1.75	50	1.72	1.72	1.99	-2.88	0.00
0.72	2.50	90	0.00	2.35	52	2.26	2.26	2.83	-4.87	0.00
$0.74_{(0.02)}$	3.85	90	0.00	3.40	45	3.40	3.40			
$0.74_{(0.01)}$	3.85	90	0.00	3.40	70	2.18	2.18	+2.80	-7.70	0.00
0.75	5.25	90	0.00	4.75	67	3.41	3.41		-10.50	0.00
$0.76_{(0.01)}$	3.80	10	1.30	3.95	14	1.85	0.55	-1.98	-12.48	-5.33
$0.76_{(0.02)}$	3.80	10	1.30	3.95	14	1.85	0.55			
0.78	3.00	21	2.00	3.20	20	2.06	+0.06	-0.31	-12.79	-8.32
$0.80_{(0.02)}$	2.50	30	2.16	2.75	25	2.10	-0.06	-0.00	-12.79	-10.26
$0.80_{(0.05)}$	2.50	30	2.16	2.75	20	1.77	-0.39			
0.85	1.95	40	1.92	2.10	31	1.85	-0.07	+0.23	-12.56	-11.89
0.90	1.75	49	1.73	1.75	40	1.72	-0.01	+0.04	-12.52	-12.00
0.95	1.55	59	1.37	1.48	48	1.47	+0.10	-0.05	-12.57	-11.12
1.00	1.37	69	0.92	1.25	58	1.12	0.20	-0.15	-12.72	-10.69
1.05	1.22	78	0.50	1.05	70	0.68	0.18	-0.19	-12.91	-10.68
1.10	1.10	90	0.00	0.90	81	0.28	0.28	-0.23	-13.14	-10.94
1.15	1.03	90	0.00	0.88	85	0.15	0.15	-0.22	-13.36	-11.30
1.20	1.00	90	0.00	0.85	86	0.12	0.12	-0.13	-13.49	-11.49
1.25	1.00	90	0.00	0.85	87	0.09	0.09	-0.10	-13.59	-11.59
1.30	1.00	90	0.00	0.92	88	0.06	0.06	-0.07	-13.66	-11.66
1.35	1.10	90	0.00	0.98	88	0.07	0.07	-0.07	-13.73	-11.53
1.40	1.25	90	0.00	1.04	88	0.07	0.07	-0.07	-13.80	-11.30
1.45	1.40	90	0.00	1.07	88	0.07	0.07	-0.07	-13.87	-11.07
1.50	1.50	90	0.00	1.10	88	0.08	0.08	-0.07	-13.94	-10.94

TABLE II

CALCULATION OF THE STRESSES ALONG THE RUN TWO PIN UPPER BOUNDARY

$$\tau_{xy} = \frac{(p-q)}{2} \sin 2\theta; \quad (\sigma_x)_i = (\sigma_x)_o - \sum_o^i \Delta\tau_{xy}(\pm 1); \quad \sigma_y = \sigma_x \pm \sqrt{(p-q)^2 - 4\tau_{xy}^2}$$

X	$\frac{(p-q)}{2}$	θ	τ_{xy}	$\frac{(p-q)^*}{2}$	θ^*	τ_{xy}^*	$\Delta\tau_{xy}$	AVG $-\Delta\tau_{xy}\frac{\Delta x}{\Delta y}$	σ_x	σ_y
in.	fringes	degrees	fringes	fringes	degrees	fringes	fringes	fringes	fringes	fringes
0.00	3.00	30	2.60	1.25	30	1.08	-1.52	+0.29	-13.35	-10.35
0.05	1.50	90	0.00	1.00	35	0.94	+0.94	-0.65	-13.64	-10.64
0.10	0.87	90	0.00	0.73	75	0.36	0.36	-0.31	-12.99	-11.25
0.15	0.57	90	0.00	0.49	73	0.27	0.27	-0.25	-12.68	-11.54
0.20	0.47	90	0.00	0.26	60	0.23	+0.23	-0.05	-12.43	-11.49
0.25	0.43	60	0.37	0.26	35	0.24	-0.13	+0.07	-12.38	-11.94
0.30	0.41	60	0.36	0.34	48	0.34	-0.02	-0.02	-12.45	-12.07
0.35	0.43	60	0.37	0.44	50	0.43	+0.06	-0.09	-12.43	-11.99
0.40	0.50	60	0.43	0.55	50	0.54	0.11	-0.12	-12.34	-11.83
0.45	0.65	60	0.56	0.70	50	0.69	0.13	-0.15	-12.22	-11.56
0.50	0.79	60	0.68	0.88	50	0.86	0.18	-0.20	-12.07	-11.26
0.55	0.96	60	0.83	1.07	50	1.05	0.22	-0.23	-11.87	-10.91
0.60	1.15	60	1.00	1.26	50	1.24	0.24	-0.33	-11.64	-10.50
0.65	1.35	60	1.17	1.62	50	1.59	0.42	-0.73	-11.31	-9.96
$0.70_{(0.05)}$	1.67	60	1.45	2.50	42	2.48	1.03			
$0.70_{(0.02)}$	1.67	60	1.45	1.87	53	1.80	0.35	-0.37	-10.58	-8.92
0.72	2.50	60	2.17	2.60	50	2.56	0.39	-0.37	-10.21	-7.73
$0.74_{(0.02)}$	3.87	60	3.35	3.75	40	3.69	0.34			
$0.74_{(0.01)}$	3.87	60	3.35	3.75	50	3.69	0.34	-0.34	-9.84	-5.96
0.75	4.75	0	0.00	4.50	40	4.40	4.40		-9.50	0.00
$0.76_{(0.01)}$	3.15	0	0.00	3.15	40	3.10	3.10	+3.75	-5.75	0.00
$0.76_{(0.02)}$	3.15	0	0.00	3.15	40	3.10	3.10			
0.78	1.65	0	0.00	2.25	40	2.20	2.20	2.65	-3.10	0.00
$0.80_{(0.02)}$	0.60	0	0.00	1.73	45	1.73	1.73	1.97	-1.13	0.00
$0.80_{(0.005)}$	0.60	0	0.00	2.00	33	1.83	1.83			
0.85	0.50	0	0.00	1.45	10	0.50	0.50	1.16	+0.83	-0.17
0.90	1.15	0	0.00	1.73	6	0.36	0.36	0.43	1.26	-1.04
0.95	1.65	0	0.00	1.98	5	0.34	0.34	0.35	1.61	-1.69
1.00	2.05	0	0.00	2.20	4	0.31	0.31	0.33	1.94	-2.16
1.05	2.41	0	0.00	2.40	4	0.33	0.33	0.32	2.26	-2.56
1.10	2.67	0	0.00	2.55	3	0.27	0.27	0.30	2.56	-2.78
1.15	2.85	0	0.00	2.70	3	0.28	0.28	0.27	2.83	-2.87
1.20	3.04	0	0.00	2.83	3	0.30	0.30	0.29	3.12	-2.96
1.25	3.20	0	0.00	2.95	3	0.31	0.31	0.30	3.42	-2.98
1.30	3.37	0	0.00	3.05	3	0.32	0.32	0.32	3.74	-3.00
1.35	3.52	0	0.00	3.15	3	0.33	0.33	0.32	4.06	-2.98
1.40	3.67	0	0.00	3.24	3	0.34	0.34	0.33	4.39	-2.95
1.45	3.85	0	0.00	3.33	3	0.35	0.35	0.34	4.73	-2.97
1.50	4.00	0	0.00	3.40	3	0.36	0.36	0.35	5.08	-2.92

TABLE III

CALCULATION OF THE STRESSES ALONG THE RUN THREE PIN LOWER BOUNDARY

$$\tau_{xy} = \frac{(p-q)}{2} \sin 2\theta; \quad (\sigma_x)_i = (\sigma_x)_o - \sum_o^i \Delta\tau_{xy}(\pm 1); \quad \sigma_y = \sigma_x \pm \sqrt{(p-q)^2 - 4\tau_{xy}^2}$$

x	$\frac{(p-q)}{2}$	θ	τ_{xy}	$\frac{(p-q)^*}{2}$	θ^*	τ_{xy}^*	$\Delta\tau_{xy}$	AVG $-\Delta\tau_{xy}\frac{\Delta x}{\Delta y}$	σ_x	σ_y
in.	fringes	degrees	fringes	fringes	degrees	fringes	fringes	fringes	fringes	fringes
0.00	2.00	10	0.68	0.50	10	0.17	-0.51	-0.19	1.92	-1.84
0.05	1.72	0	0.00	0.75	5	0.13	+0.13	+0.17	2.11	-1.33
0.10	1.55	0	0.00	1.25	5	0.22	0.22	0.22	1.94	-1.16
0.15	1.43	0	0.00	1.32	5	0.23	0.23	0.22	1.72	-1.14
0.20	1.34	0	0.00	1.25	5	0.22	0.22	0.20	1.50	-1.18
0.25	1.25	0	0.00	1.10	5	0.19	0.19	0.18	1.30	-1.20
0.30	1.18	0	0.00	1.00	5	0.17	0.17	0.17	1.12	-1.24
0.35	1.12	0	0.00	1.00	5	0.17	0.17	0.17	0.95	-1.29
0.40	1.05	0	0.00	0.96	5	0.17	0.17	0.16	0.78	-1.32
0.45	0.99	0	0.00	0.90	5	0.16	0.16	0.14	0.62	-1.36
0.50	0.90	0	0.00	0.72	5	0.13	0.13	0.11	0.48	-1.32
0.55	0.75	0	0.00	0.50	5	0.09	0.09	0.21	0.37	-0.93
0.60	0.32	0	0.00	0.50	20	0.32	0.32	0.16	0.16	-0.48
0.65	0.30	90	0.00	0.75	50	0.74	0.74	1.07	-0.51	0.00
$0.70_{(0.05)}$	1.24	90	0.00	1.50	55	1.41	1.41			
$0.70_{(0.02)}$	1.24	90	0.00	1.25	70	0.80	0.80	0.96	-1.58	0.00
0.72	1.75	90	0.00	1.75	70	1.12	1.12	1.77	-2.54	0.00
$0.74_{(0.02)}$	2.15	90	0.00	2.45	40	2.42	2.42			
$0.74_{(0.01)}$	2.15	90	0.00	2.45	50	2.42	2.42	+2.69	-4.31	0.00
0.75	3.00	90	0.00	3.00	40	2.96	2.96		-6.00	0.00
$0.76_{(0.01)}$	2.20	21	1.47	2.50	21	1.67	0.20	-1.58	-7.58	-4.32
$0.76_{(0.02)}$	2.20	21	1.47	2.50	20	1.61	0.14			
0.78	1.65	30	1.43	2.00	26	1.57	0.14	-0.14	-7.72	-6.07
$0.80_{(0.02)}$	1.25	32	1.12	1.60	30	1.38	0.26	-0.20	-7.92	-6.80
$0.80_{(0.05)}$	1.25	32	1.12	1.60	25	1.22	0.10			
0.85	0.75	41	0.74	1.05	33	0.96	0.22	-0.16	-8.08	-7.83
0.90	0.55	50	0.54	0.73	40	0.72	0.18	-0.20	-8.28	-7.90
0.95	0.50	57	0.46	0.50	49	0.49	0.03	-0.10	-8.38	-7.97
1.00	0.50	64	0.39	0.42	53	0.40	0.01	-0.02	-8.40	-7.77
1.05	0.50	73	0.28	0.50	62	0.41	0.13	-0.06	-8.46	-7.62
1.10	0.55	85	0.10	0.58	72	0.34	0.24	-0.18	-8.64	-7.56
1.15	0.66	90	0.00	0.65	82	0.18	0.18	-0.21	-8.85	-7.53
1.20	0.82	90	0.00	0.72	85	0.12	0.12	-0.15	-9.00	-7.36
1.25	1.00	90	0.00	0.78	86	0.11	0.11	-0.11	-9.11	-7.11
1.30	1.12	90	0.00	0.85	87	0.09	0.09	-0.10	-9.21	-6.97
1.35	1.18	90	0.00	0.89	88	0.06	0.06	-0.07	-9.28	-6.92
1.40	1.22	90	0.00	0.91	88	0.06	0.06	-0.06	-9.34	-6.90
1.45	1.24	90	0.00	0.94	88	0.07	0.07	-0.06	-9.40	-6.92
1.50	1.24	90	0.00	0.95	88	0.07	0.07	-0.07	-9.47	-6.99

TABLE IV

CALCULATION OF THE STRESSES ALONG THE RUN THREE PIN UPPER BOUNDARY

$$\tau_{xy} = \frac{(p-q)}{2} \sin 2\theta; \quad (\sigma_x)_i = (\sigma_x)_o - \sum_{o}^{i} \Delta\tau_{xy}(\pm 1); \quad \sigma_y = \sigma_x \pm \sqrt{(p-q)^2 - 4\tau_{xy}^2}$$

X	$\frac{(p-q)}{2}$	θ	τ_{xy}	$\frac{(p-q)^*}{2}$	θ^*	τ_{xy}^*	$\Delta\tau_{xy}$	AVG $-\Delta\tau_{xy} \frac{\Delta x}{\Delta y}$	σ_x	σ_y
in.	fringes	degrees	fringes	fringes	degrees	fringes	fringes	fringes	fringes	fringes
0.00	1.25	30	1.08	0.75	60	0.65	-0.43	-0.01	-7.80	-6.54
0.05	0.50	90	0.00	0.47	50	0.46	+0.46	-0.34	-7.79	-6.79
0.10	0.50	90	0.00	0.25	61	0.21	0.21	-0.18	-7.45	-6.45
0.15	0.50	90	0.00	0.22	20	0.14	+0.14	-0.02	-7.27	-6.27
0.20	0.50	70	0.32	0.22	40	0.22	-0.10	+0.09	-7.25	-6.48
0.25	0.50	70	0.32	0.23	49	0.23	-0.09	+0.08	-7.34	-6.57
0.30	0.49	70	0.31	0.24	50	0.24	-0.07	+0.05	-7.42	-6.66
0.35	0.46	70	0.30	0.26	50	0.26	-0.04	+0.04	-7.47	-6.77
0.40	0.51	70	0.33	0.29	50	0.29	-0.04	+0.02	-7.51	-6.73
0.45	0.53	70	0.34	0.33	50	0.33	-0.01	-0.03	-7.53	-6.72
0.50	0.51	70	0.33	0.39	49	0.39	0.06	-0.10	-7.50	-6.72
0.55	0.48	70	0.31	0.45	48	0.45	0.14	-0.19	-7.40	-6.67
0.60	0.49	70	0.31	0.55	46	0.55	0.24	-0.28	-7.21	-6.45
0.65	0.75	70	0.48	0.70	41	0.69	0.21	-0.20	-6.98	-5.83
$0.70_{(0.05)}$	1.25	70	0.80	1.00	40	0.98	+0.18			
$0.70_{(0.02)}$	1.25	70	0.80	0.76	49	0.75	-0.05	+0.01	-6.78	-4.86
0.72	1.60	70	1.03	1.05	45	1.05	+0.02	-0.11	-6.79	-4.34
$0.74_{(0.02)}$	2.10	70	1.35	1.55	42	1.55	0.20			
$0.74_{(0.01)}$	2.10	70	1.35	1.55	46	1.54	0.19	-1.18	-6.68	-3.46
0.75	2.75	0	0.00	2.50	30	2.16	2.16		-5.50	0.00
$0.76_{(0.01)}$	2.25	0	0.00	1.45	30	1.25	1.25	+1.71	-3.79	0.00
$0.76_{(0.02)}$	2.25	0	0.00	1.45	30	1.25	1.25			
0.78	1.30	0	0.00	0.85	25	0.65	0.65	0.95	-2.84	0.00
$0.80_{(0.02)}$	0.50	0	0.00	0.50	15	0.25	0.25	0.45	-2.39	0.00
$0.80_{(0.05)}$	0.50	0	0.00	0.75	20	0.48	0.48			
0.85	0.26	0	0.00	0.51	10	0.17	0.17	0.32	+0.32	-0.20
0.90	0.50	0	0.00	0.44	5	0.08	0.08	0.12	0.44	-0.56
0.95	0.69	0	0.00	0.50	5	0.09	0.09	0.08	0.52	-0.86
1.00	0.87	0	0.00	0.70	5	0.12	0.12	0.11	0.63	-1.11
1.05	1.05	0	0.00	0.88	5	0.15	0.15	0.14	0.77	-1.33
1.10	1.25	0	0.00	1.05	5	0.13	0.18	0.17	0.94	-1.56
1.15	1.45	0	0.00	1.21	5	0.21	0.21	0.19	1.13	-1.77
1.20	1.62	0	0.00	1.37	5	0.24	0.24	0.23	1.36	-1.88
1.25	1.80	0	0.00	1.51	5	0.26	0.26	0.25	1.61	-1.99
1.30	2.00	0	0.00	1.65	5	0.29	0.29	0.28	1.89	-2.11
1.35	2.20	0	0.00	1.75	5	0.30	0.30	0.29	2.18	-2.22
1.40	2.39	0	0.00	1.85	5	0.32	0.32	0.31	2.49	-2.29
1.45	2.57	0	0.00	1.93	5	0.33	0.33	0.32	2.81	-2.33
1.50	2.75	0	0.00	2.00	5	0.35	0.35	0.34	3.15	-2.35

TABLE V

CALCULATION OF THE STRESSES ALONG THE RUN FOUR PIN LOWER BOUNDARY

$$\tau_{xy} = \frac{(p-q)}{2} \sin 2\theta; \quad (\sigma x)_i = (\sigma x)_o - \sum_{o}^{i} \Delta\tau xy(\pm 1); \quad \sigma y = \sigma x \pm \sqrt{(p-q)^2 - 4\tau_{xy}^2}$$

X	$\frac{(p-q)}{2}$	θ	τ_{xy}	$\frac{(p-q)^*}{2}$	θ^*	τ_{xy}	$\Delta\tau_{xy}$	AVG $\frac{\Delta x}{\Delta y}\Delta\tau_{xy}$	σ_x	σ_y
in.	fringes	degrees	fringes	fringes	degrees	fringes	fringes	fringes	fringes	fringes
0.00	1.00	10	0.34	0.25	21	0.17	-0.17	-0.04	0.75	-1.13
0.05	0.98	0	0.00	0.27	10	0.09	+0.09	+0.09	0.79	-1.17
0.10	0.88	0	0.00	0.30	9	0.09	0.09	0.09	0.70	-1.06
0.15	0.77	0	0.00	0.30	9	0.09	0.09	0.09	0.61	-0.93
0.20	0.62	0	0.00	0.30	9	0.09	0.09	0.09	0.52	-0.72
0.25	0.47	0	0.00	0.30	9	0.09	0.09	0.09	0.43	-0.51
0.30	0.32	0	0.00	0.30	9	0.09	0.09	0.09	0.34	-0.30
0.35	0.20	0	0.00	0.30	9	0.09	0.09	0.09	0.25	-0.15
0.40	0.10	0	0.00	0.27	10	0.09	0.09	0.07	0.16	-0.04
0.45	0.05	0	0.00	0.17	11	0.06	0.06	0.09	0.09	-0.01
0.50	0.00	90	0.00	0.13	50	0.13	0.13	0.11	(0)	0.00
0.55	0.00	90	0.00	0.13	67	0.09	0.09	0.13	-0.00	0.00
0.60	0.07	90	0.00	0.25	69	0.17	0.17	0.30	-0.13	0.00
0.65	0.22	90	0.00	0.63	68	0.44	0.44	0.58	-0.43	0.00
0.70(0.05)	0.50	90	0.00	0.90	63	0.73	0.73			
0.70(0.02)	0.50	90	0.00	0.85	75	0.43	0.43	0.55	-1.01	0.00
0.72	0.75	90	0.00	1.05	70	0.67	0.67	0.93	-1.56	0.00
0.74(0.02)	1.25	90	0.00	1.50	64	1.18	1.18			
0.74(0.01)	1.25	90	0.00	1.50	70	0.96	0.96	+1.26	-2.49	0.00
0.75	1.88	90	0.00	1.80	60	1.56	1.56		-3.75	0.00
0.76(0.01)	1.59	46	1.58	1.75	40	1.72	0.14	-0.85	-4.60	-4.28
0.76(0.02)	1.59	46	1.58	1.75	39	1.71	0.13			
0.78	1.25	48	1.24	1.40	44	1.40	0.16	-0.15	-4.75	-4.44
0.80(0.02)	1.04	53	1.00	1.35	50	1.33	0.33	-0.25	-5.00	-4.43
0.80(0.05)	1.04	53	1.00	1.30	42	1.29	0.29			
0.85	0.72	65	0.55	0.80	54	0.76	0.21	-0.25	-5.25	-4.32
0.90	0.64	73	0.36	0.50	62	0.41	0.05	-0.13	-5.38	-4.32
0.95	0.63	90	0.00	0.35	72	0.21	0.21	-0.13	-5.51	-4.25
1.00	0.63	90	0.00	0.29	80	0.10	0.10	-0.15	-5.66	-4.40
1.05	0.63	90	0.00	0.26	82	0.07	0.07	-0.08	-5.74	-4.48
1.10	0.63	90	0.00	0.25	84	0.05	0.05	-0.06	-5.80	-4.54
1.15	0.63	90	0.00	0.27	86	0.04	0.04	-0.04	-5.84	-4.58
1.20	0.63	90	0.00	0.35	87	0.04	0.04	-0.04	-5.88	-4.62
1.25	0.65	90	0.00	0.43	88	0.03	0.03	-0.03	-5.91	-4.61
1.30	0.75	90	0.00	0.54	88	0.04	0.04	-0.03	-5.94	-4.44
1.35	0.92	90	0.00	0.61	88	0.04	0.04	-0.04	-5.98	-4.14
1.40	1.05	90	0.00	0.69	88	0.05	0.05	-0.05	-6.02	-3.92
1.45	1.13	90	0.00	0.73	88	0.05	0.05	-0.05	-6.07	-3.81
1.50	1.15	90	0.00	0.75	88	0.05	0.05	-0.05	-6.12	-3.82

TABLE VI

CALCULATION OF THE STRESSES ALONG THE RUN FOUR PIN UPPER BOUNDARY

$$\tau_{xy} = \frac{(p-q)}{2} \sin 2\theta; \quad (\sigma_x)_i = (\sigma_x)_o - \sum_o^i \Delta\tau_{xy}(\pm 1); \quad \sigma_y = \sigma_x \pm \sqrt{(p-q)^2 - 4\tau_{xy}^2}$$

X	$\frac{(p-q)}{2}$	θ	τ_{xy}	$\frac{(p-q)^*}{2}$	θ^*	τ_{xy}^*	$\Delta\tau_{xy}$	AVG $-\Delta\tau_{xy}$	$\frac{\Delta x}{\Delta y}$	σ_x	σ_y
in.	fringes	degrees	fringes	fringes	degrees	fringes	fringes	fringes		fringes	fringes
0.00	1.63	30	1.41	0.60	70	0.39	-1.02	+0.27		-4.76	-3.13
0.05	0.88	90	0.00	0.55	30	0.48	+0.48	-0.36		-5.03	-3.27
0.10	0.55	90	0.00	0.25	57	0.23	+0.23	-0.11		-4.67	-3.51
0.15	0.42	90	0.00	0.00	48	0.00	+0.00	+0.10		-4.56	-3.72
0.20	0.37	60	0.32	0.13	30	0.11	-0.21	+0.12		-4.66	-4.29
0.25	0.36	60	0.31	0.27	40	0.27	-0.04	0.00		-4.78	-4.41
0.30	0.39	60	0.34	0.38	41	0.38	+0.04	-0.05		-4.78	-4.39
0.35	0.44	60	0.38	0.45	43	0.45	+0.07	-0.07		-4.73	-4.29
0.40	0.50	60	0.43	0.50	43	0.50	+0.07	-0.07		-4.66	-4.15
0.45	0.54	60	0.47	0.54	42	0.54	+0.07	-0.07		-4.59	-4.05
0.50	0.58	60	0.50	0.58	41	0.57	+0.07	-0.07		-4.52	-3.93
0.55	0.63	60	0.55	0.63	40	0.62	+0.07	-0.07		-4.45	-3.83
0.60	0.68	60	0.59	0.69	39	0.67	+0.08	-0.09		-4.38	-3.70
0.65	0.75	60	0.65	0.77	38	0.75	+0.10	-0.13		-4.29	-3.54
$0.70_{(0.05)}$	0.85	60	0.74	0.96	35	0.90	+0.16				
$0.70_{(0.02)}$	0.85	60	0.74	1.04	45	1.04	+0.30	-0.30		-4.16	-3.33
0.72	0.90	50	0.89	1.20	43	1.20	+0.31	-0.30		-3.86	-3.58
$0.74_{(0.02)}$	1.13	50	1.11	1.43	40	1.41	+0.30				
$0.74_{(0.01)}$	1.13	50	1.11	1.43	48	1.42	+0.31	-0.31		-3.56	-3.12
0.75	1.63	0	0.00	1.60	45	1.60	+1.60			-3.25	0.00
$0.76_{(0.01)}$	0.88	0	0.00	1.37	42	1.36	+1.36	+1.48		-1.77	0.00
$0.76_{(0.02)}$	0.88	0	0.00	1.37	36	1.30	+1.30				
0.78	0.31	0	0.00	1.00	30	0.87	+0.87	1.09		-0.68	0.00
$0.80_{(0.02)}$	0.00	0	0.00	0.75	20	0.48	+0.48	0.67		(0)	0.00
$0.80_{(0.05)}$	0.00	0	0.00	1.00	26	0.79	+0.79				
0.85	0.35	0	0.00	0.63	20	0.41	+0.41	0.60		+0.60	-0.10
0.90	0.55	0	0.00	0.80	7	0.19	+0.19	0.30		0.90	-0.20
0.95	0.79	0	0.00	0.95	5	0.16	0.16	0.18		1.08	-0.50
1.00	1.00	0	0.00	1.07	4	0.15	0.15	0.15		1.23	-0.77
1.05	1.17	0	0.00	1.15	3	0.12	0.12	0.13		1.36	-0.98
1.10	1.31	0	0.00	1.24	3	0.13	0.13	0.13		1.49	-1.13
1.15	1.43	0	0.00	1.31	3	0.14	0.14	0.13		1.62	-1.24
1.20	1.55	0	0.00	1.38	3	0.14	0.14	0.14		1.76	-1.34
1.25	1.64	0	0.00	1.44	3	0.15	0.15	0.14		1.90	-1.38
1.30	1.75	0	0.00	1.50	3	0.16	0.16	0.15		2.05	-1.45
1.35	1.83	0	0.00	1.55	3	0.16	0.16	0.16		2.21	-1.45
1.40	1.89	0	0.00	1.60	3	0.17	0.17	0.16		2.37	-1.41
1.45	1.95	0	0.00	1.65	3	0.17	0.17	0.17		2.54	-1.36
1.50	2.00	0	0.00	1.68	3	0.18	0.18	0.18		2.72	-1.28

TABLE VII

CALCULATION OF THE STRESSES ALONG THE RUN FIVE PIN LOWER BOUNDARY

$$\tau_{xy} = \frac{(p-q)}{2} \sin 2\theta; \quad (\sigma x)_i = (\sigma x)_o - \sum_{o}^{i} \Delta\tau_{xy} \ (\pm 1); \quad \sigma y = \sigma x \pm \sqrt{(p-q)^2 - 4\tau_{xy}^2}$$

X	$\frac{(p-q)}{2}$	θ	τ_{xy}	$\frac{(p-q)^*}{2}$	θ^*	τ_{xy}^*	$\Delta\tau_{xy}$	AVG $-\Delta\tau_{xy}\frac{\Delta x}{\Delta y}$	σ_x	σ_y
in.	fringes	degrees	fringes	fringes	degrees	fringes	fringes	fringes	fringes	fringes
0.00	0.75	10	0.26	0.66	10	0.23	-0.03	0.09	0.94	-0.47
0.05	0.72	0	0.00	0.62	10	0.21	+0.21	0.23	0.85	-0.59
0.10	0.60	0	0.00	0.50	15	0.25	0.25	0.22	0.62	-0.58
0.15	0.42	0	0.00	0.37	15	0.18	0.18	0.16	0.40	-0.44
0.20	0.25	0	0.00	0.25	15	0.13	0.13	0.11	0.24	-0.26
0.25	0.15	0	0.00	0.18	15	0.09	0.09	0.07	0.13	-0.17
0.30	0.09	0	0.00	0.10	15	0.05	0.05	0.04	0.06	-0.12
0.35	0.04	0	0.00	0.05	15	0.03	0.03	0.02	0.02	-0.06
0.40	0.00	0	0.00	0.00	15	0.00	0.00	0.00	0.00	0.00
0.45	0.00	0	0.00	0.00	20	0.00	0.00	0.04	(0.00)	0.00
0.50	0.01	90	0.00	0.08	60	0.07	0.07	0.10	-0.12	0.00
0.55	0.05	90	0.00	0.18	70	0.12	0.12	0.13	-0.22	0.00
0.60	0.10	90	0.00	0.28	75	0.14	0.14	0.21	-0.35	0.00
0.65	0.25	90	0.00	0.43	70	0.28	0.28	0.49	-0.56	0.00
$0.70_{(0.05)}$	0.53	90	0.00	0.73	55	0.69	0.69			
$0.70_{(0.02)}$	0.53	90	0.00	0.73	75	0.36	0.36	0.45	-1.05	0.00
0.72	0.75	90	0.00	0.98	73	0.55	0.55	0.60	-1.50	0.00
$0.74_{(0.02)}$	1.05	90	0.00	1.31	75	0.65	0.65			
$0.74_{(0.01)}$	1.05	90	0.00	1.31	57	1.20	1.20	+1.40	-2.10	0.00
0.75	1.75	90	0.00	1.62	40	1.60	1.60		-3.50	0.00
$0.76_{(0.01)}$	1.25	46	1.25	1.37	43	1.37	0.12	-0.12	-3.62	-3.30
$0.76_{(0.02)}$	1.25	46	1.25	1.37	41	1.36	0.11			
0.78	0.95	50	0.93	1.02	45	1.02	0.09	-0.10	-3.72	-3.33
$0.80_{(0.02)}$	0.75	52	0.73	0.82	50	0.81	0.08	-0.08	-3.80	-3.41
$0.80_{(0.05)}$	0.75	52	0.73	0.82	40	0.81	0.08			
0.85	0.48	62	0.40	0.50	58	0.45	0.05	-0.06	-3.86	-3.33
0.90	0.48	70	0.31	0.47	65	0.36	0.05	-0.05	-3.91	-3.18
0.95	0.49	80	0.17	0.47	70	0.30	0.13	-0.09	-4.00	-3.08
1.00	0.50	90	0.00	0.48	80	0.16	0.16	-0.15	-4.15	-3.15
1.05	0.52	90	0.00	0.52	82	0.14	0.14	-0.15	-4.30	-3.26
1.10	0.57	90	0.00	0.55	84	0.11	0.11	-0.12	-4.42	-3.28
1.15	0.65	90	0.00	0.58	86	0.08	0.08	-0.09	-4.51	-3.21
1.20	0.75	90	0.00	0.63	87	0.07	0.07	-0.08	-4.59	-3.09
1.25	0.82	90	0.00	0.67	88	0.05	0.05	-0.06	-4.65	-3.01
1.30	0.88	90	0.00	0.70	88	0.05	0.05	-0.05	-4.70	-2.94
1.35	0.93	90	0.00	0.74	88	0.05	0.05	-0.05	-4.75	-2.89
1.40	0.97	90	0.00	0.78	88	0.05	0.05	-0.05	-4.80	-2.86
1.45	1.00	90	0.00	0.82	88	0.06	0.06	-0.05	-4.85	-2.85
1.50	1.00	90	0.00	0.85	88	0.06	0.06	-0.06	-4.91	-2.91

TABLE VIII

CALCULATION OF THE STRESSES ALONG THE RUN FIVE PIN UPPER BOUNDARY

$$\tau_{xy} = \frac{(p-q)}{2} \sin 2\theta; \quad (\sigma_x)_i = (\sigma_x)_o - \sum_o^i \Delta\tau_{xy}(\pm 1); \quad \sigma_y = \sigma_x \pm \sqrt{(p-q)^2 - 4\tau_{xy}^2}$$

X	$\frac{(p-q)}{2}$	θ	τ_{xy}	$\frac{(p-q)^*}{2}$	θ^*	τ_{xy}	$\Delta\tau_{xy}$	AVG $-\Delta\tau_{xy}\frac{\Delta x}{\Delta y}$	σ_x	σ_y
in.	fringes	degrees	fringes	fringes	degrees	fringes	fringes	fringes	fringes	fringes
0.00	0.75	20	0.48	0.56	45	0.56	0.08	-0.12	-3.94	-2.79
0.05	0.48	90	0.00	0.50	80	0.17	0.17	-0.26	-3.82	-2.86
0.10	0.26	90	0.00	0.37	40	0.36	0.36	-0.20	-3.56	-3.04
0.15	0.25	60	0.22	0.31	30	0.27	0.05	-0.06	-3.36	-3.11
0.20	0.25	60	0.22	0.30	47	0.29	0.07	-0.07	-3.30	-3.05
0.25	0.25	60	0.22	0.29	50	0.29	0.07	-0.07	-3.23	-2.98
0.30	0.25	60	0.22	0.29	50	0.29	0.07	-0.07	-3.16	-2.91
0.35	0.25	60	0.22	0.29	50	0.29	0.07	-0.06	-3.09	-2.84
0.40	0.25	60	0.22	0.28	50	0.28	0.06	-0.06	-3.03	-2.78
0.45	0.25	60	0.22	0.28	50	0.28	0.06	-0.06	-2.97	-2.72
0.50	0.25	60	0.22	0.29	50	0.29	0.07	-0.08	-2.91	-2.66
0.55	0.25	60	0.22	0.32	50	0.31	0.09	-0.12	-2.83	-2.58
0.60	0.25	60	0.22	0.39	50	0.38	0.16	-0.16	-2.71	-2.46
0.65	0.35	60	0.30	0.48	50	0.47	0.17	-0.12	-2.55	-2.19
$0.70_{(0.05)}$	0.63	60	0.55	0.62	44	0.62	0.07			
$0.70_{(0.02)}$	0.63	60	0.55	0.62	50	0.61	0.06	-0.03	-2.43	-1.81
0.72	0.80	55	0.75	0.75	47	0.75	0.00	-0.00	-2.40	-1.84
$0.74_{(0.02)}$	1.07	60	0.92	0.92	45	0.92	0.00			
$0.74_{(0.01)}$	1.07	60	0.92	0.92	47	0.92	0.00	0.00	-2.40	-1.35
0.75	1.20	0	0.00	1.10	45	1.10	1.10		-2.40	0.00
$0.76_{(0.01)}$	0.80	0	0.00	0.90	44	0.90	0.90	+1.00	-1.40	0.00
$0.76_{(0.02)}$	0.80	0	0.00	0.90	40	0.89	0.89			
0.78	0.25	0	0.00	0.65	38	0.63	0.63	0.76	-0.64	0.00
$0.80_{(0.02)}$	0.00	0	0.00	0.50	30	0.43	0.43	0.53	-0.11	0.00
$0.80_{(0.05)}$	0.00	0	0.00	0.50	22	0.35	0.35			
0.85	0.00	0	0.00	0.25	5	0.04	0.04	0.20	(0.00)	0.00
0.90	0.03	0	0.00	0.24	5	0.04	0.04	0.04	+0.04	-0.02
0.95	0.06	0	0.00	0.25	5	0.04	0.04	0.04	0.08	-0.04
1.00	0.12	0	0.00	0.29	5	0.05	0.05	0.05	0.13	-0.11
1.05	0.18	0	0.00	0.29	5	0.05	0.05	0.05	0.18	-0.18
1.10	0.25	0	0.00	0.27	5	0.05	0.05	0.05	0.23	-0.27
1.15	0.33	0	0.00	0.25	5	0.04	0.04	0.05	0.28	-0.38
1.20	0.40	0	0.00	0.26	5	0.05	0.05	0.05	0.33	-0.47
1.25	0.50	0	0.00	0.32	5	0.06	0.06	0.06	0.39	-0.61
1.30	0.60	0	0.00	0.47	5	0.08	0.08	0.07	0.46	-0.74
1.35	0.75	0	0.00	0.62	5	0.11	0.11	0.10	0.56	-0.94
1.40	0.83	0	0.00	0.70	5	0.12	0.12	0.12	0.68	-0.98
1.45	0.87	0	0.00	0.75	5	0.13	0.13	0.13	0.81	-0.93
1.50	0.87	0	0.00	0.75	5	0.13	0.13	0.13	0.94	-0.80

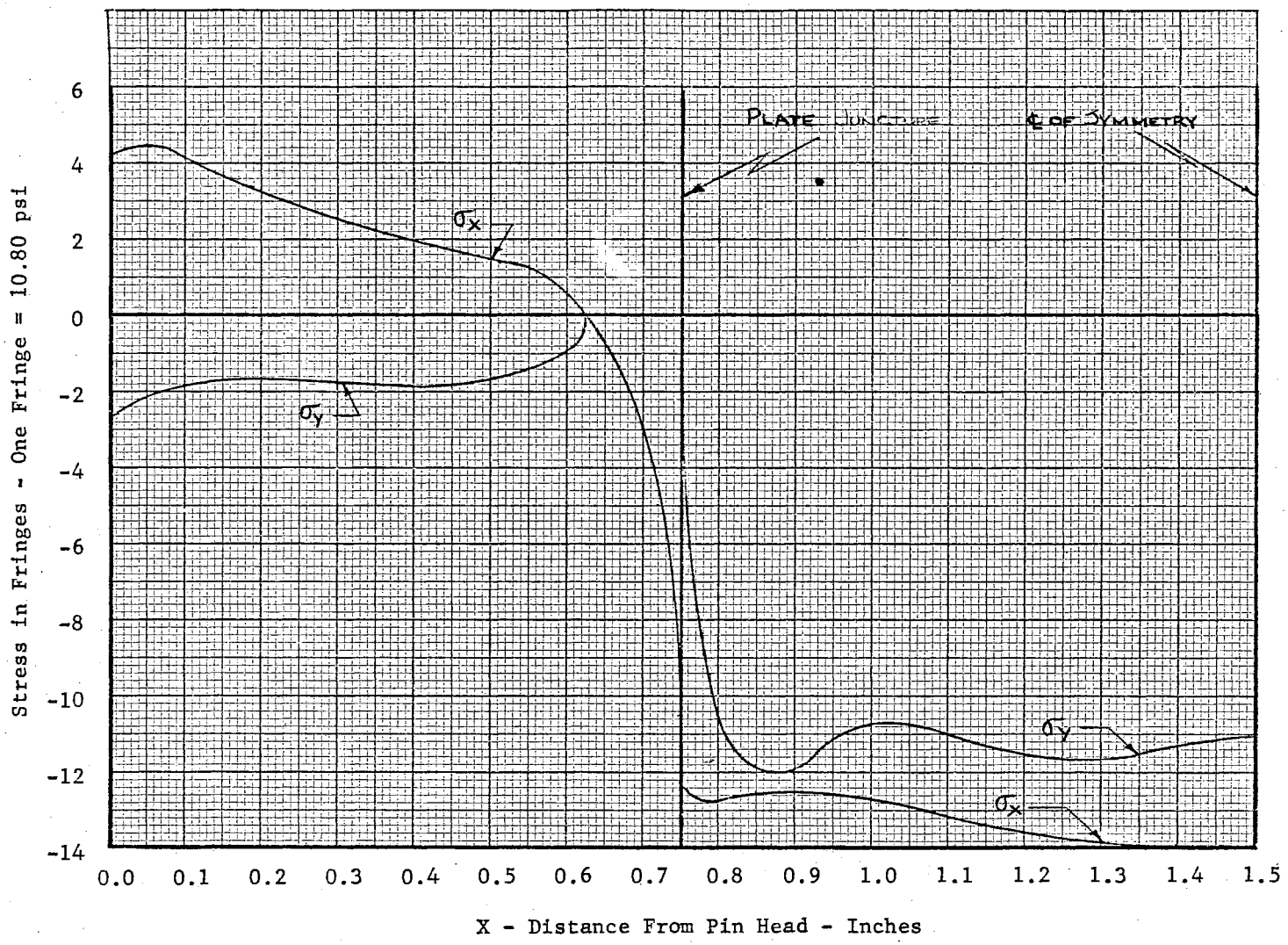

Figure 30. Stress Distribution Along the Run Two Pin Lower Boundary

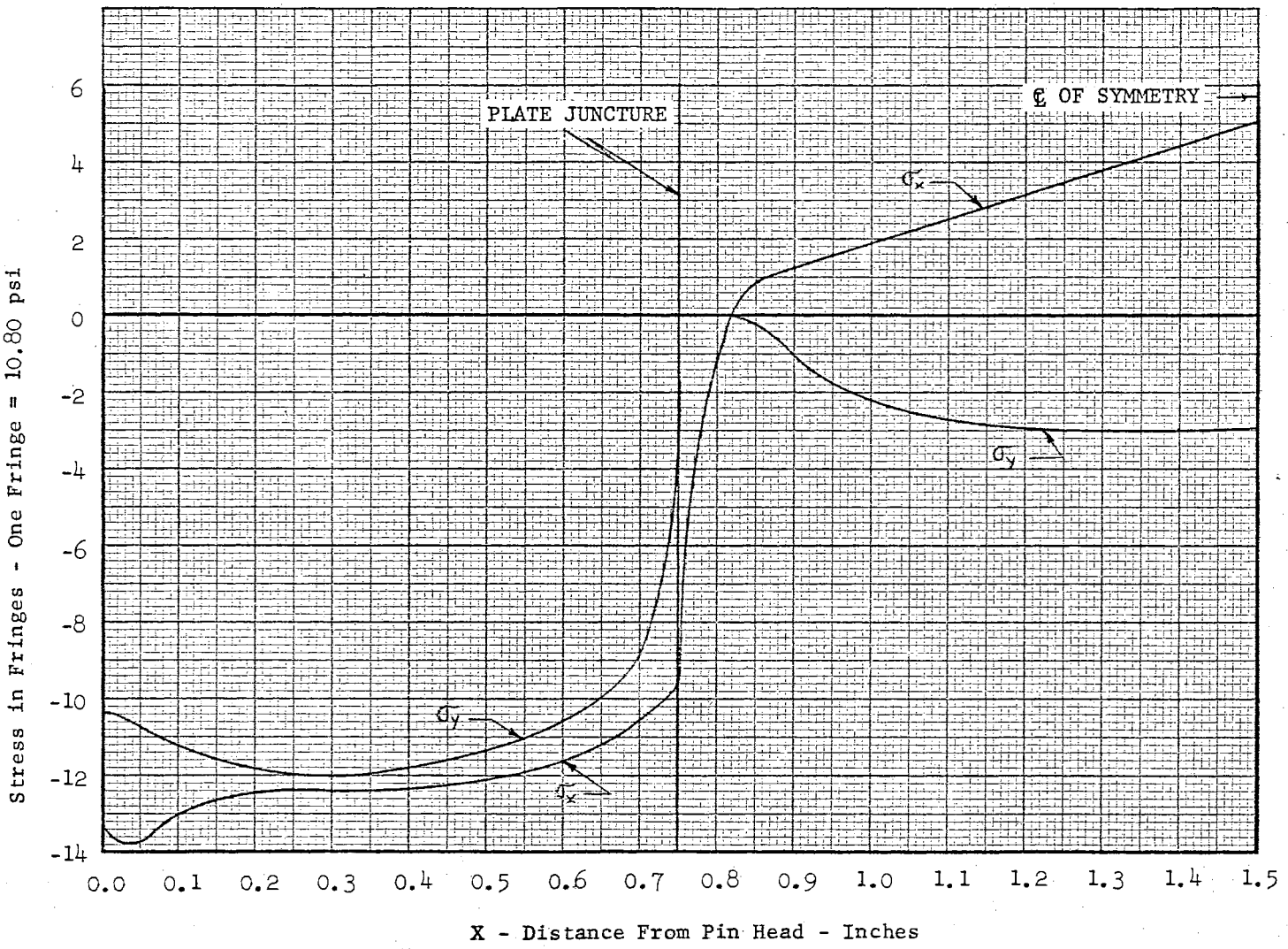

Figure 31. Stress Distribution Along the Run Two Pin Upper Boundary

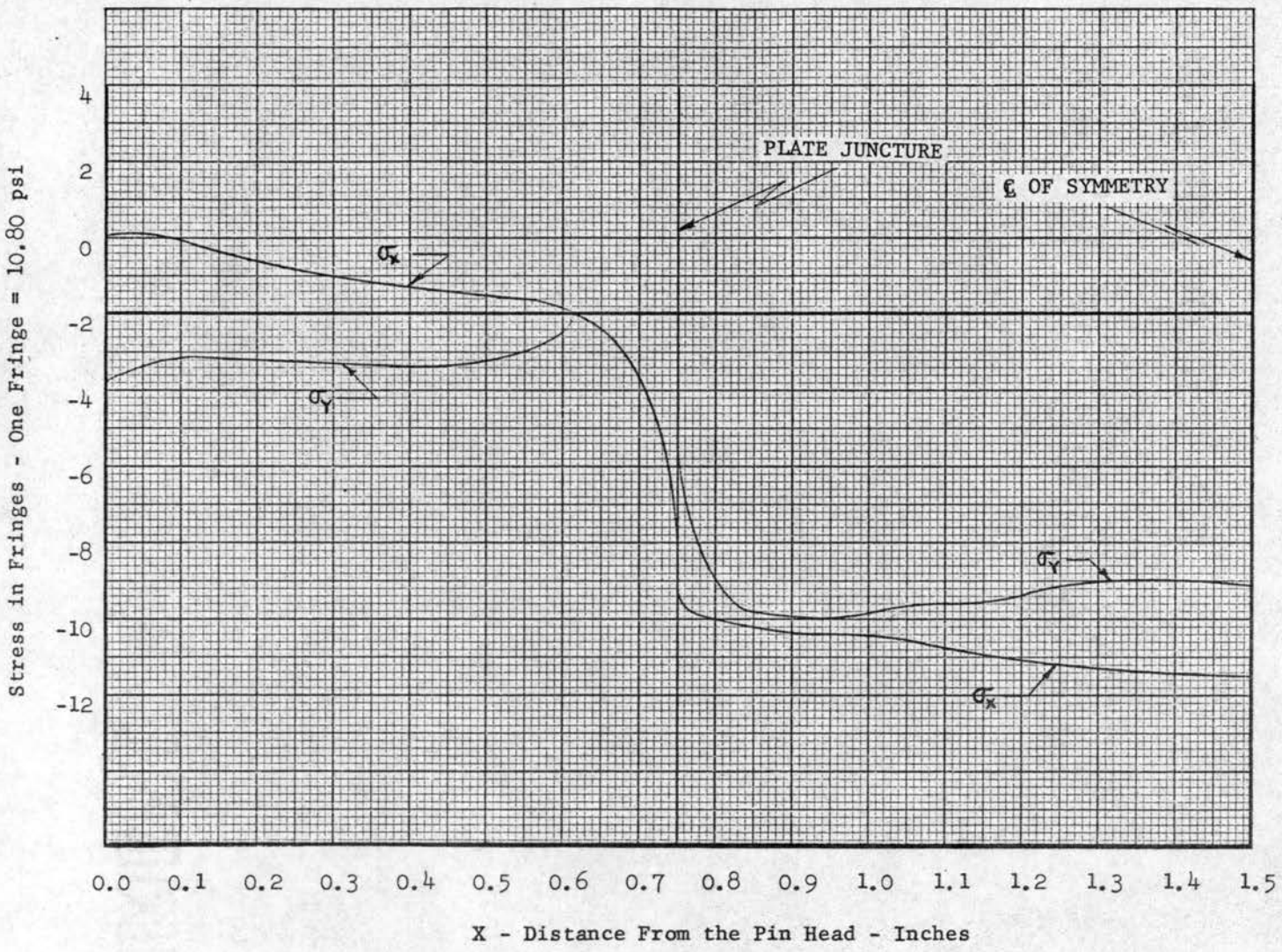

Figure 32. Stress Distribution Along the Run Three Pin Lower Boundary

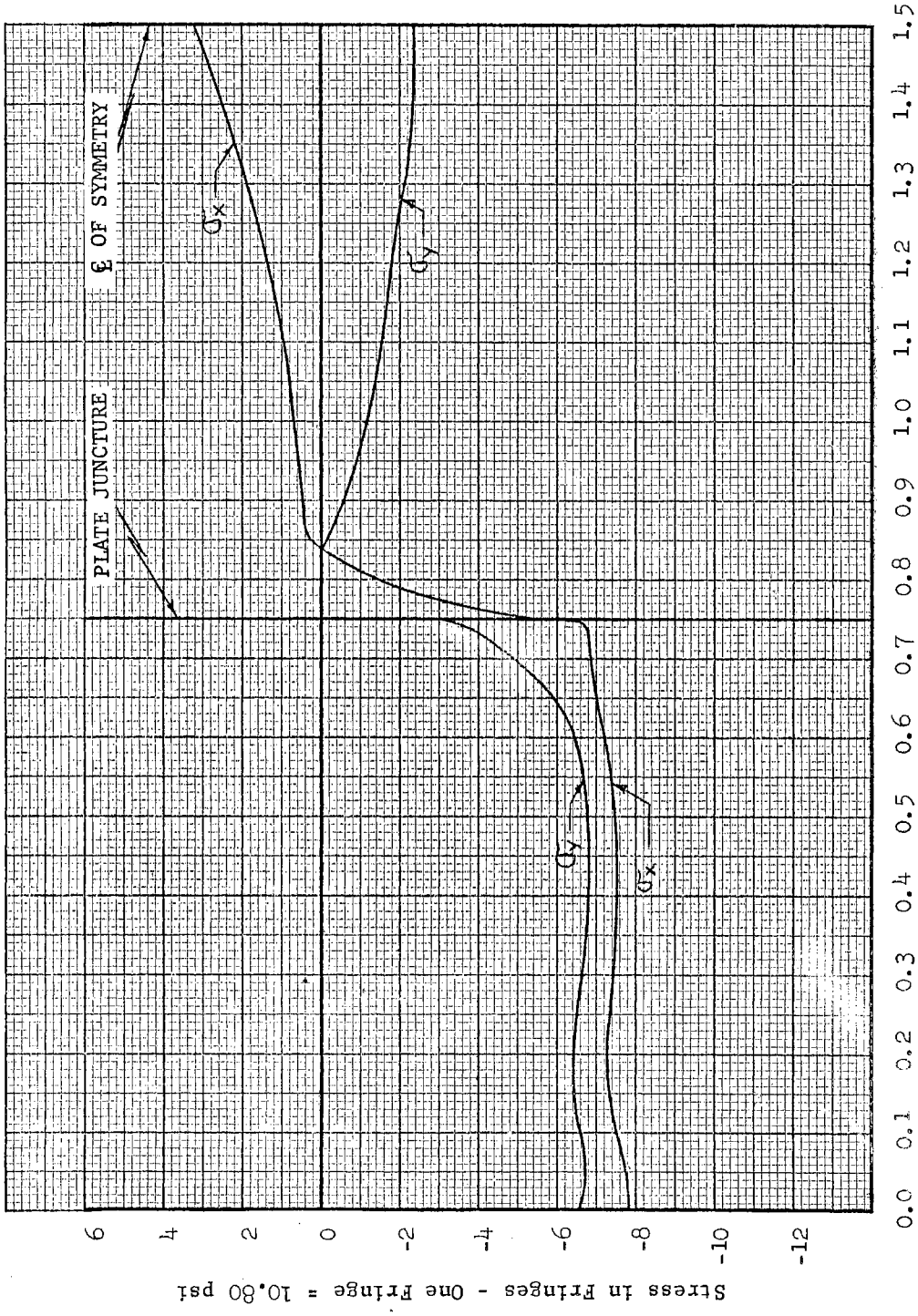

Figure 33. Stress Distribution Along the Run Three Pin Upper Boundary

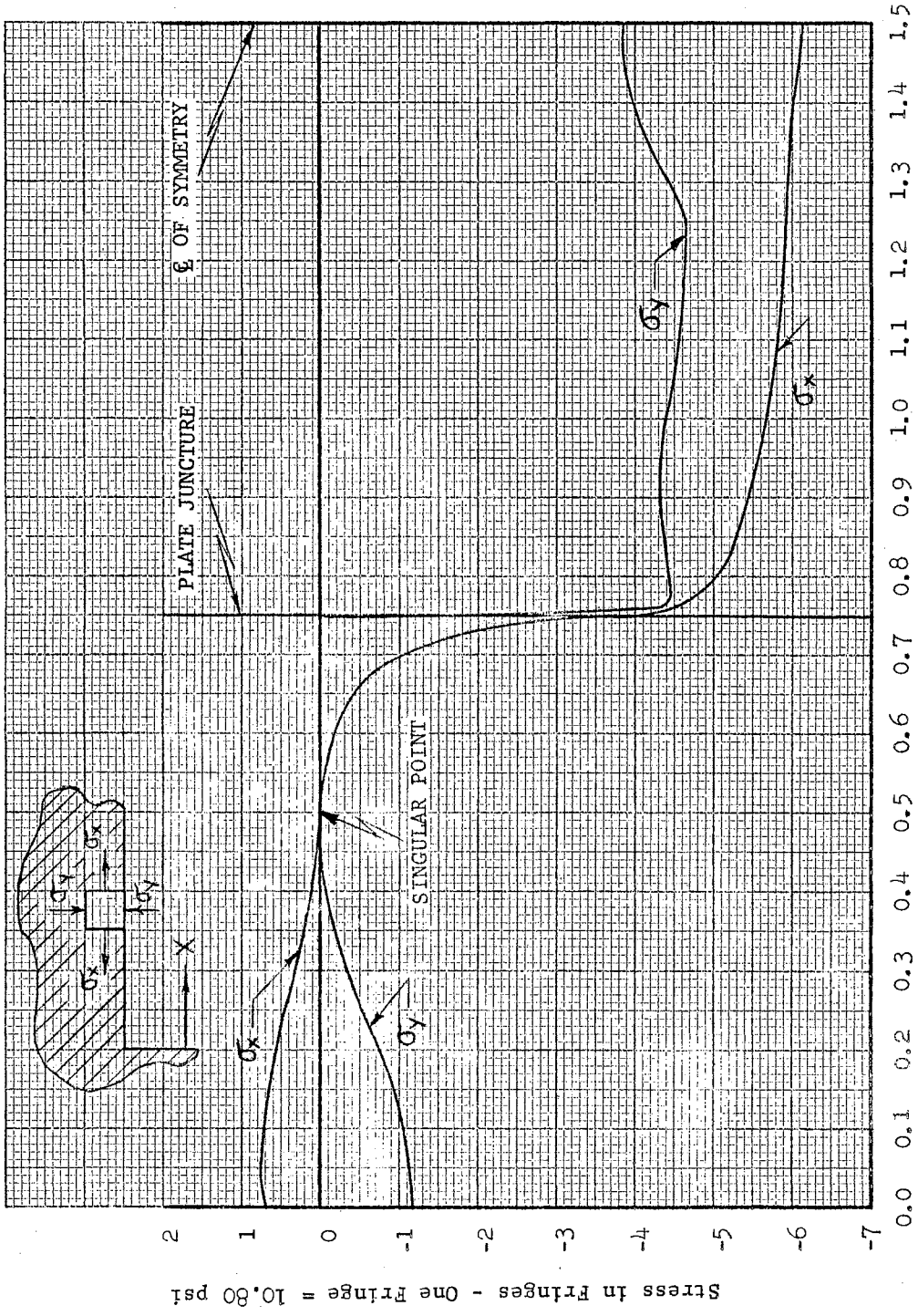

Figure 34. Stress Distribution Along the Run Four Pin Lower Boundary

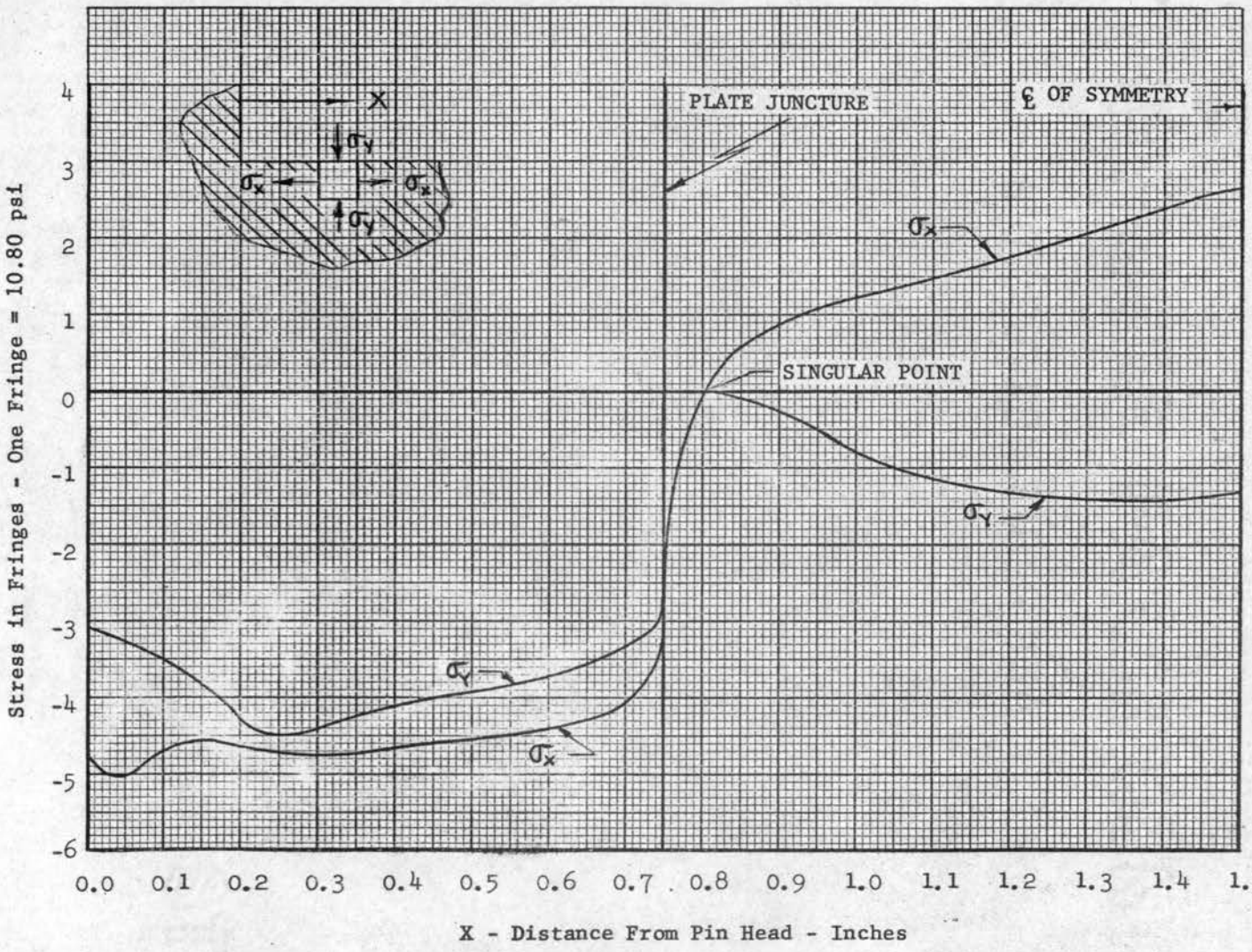

Figure 35. **Stress Distribution Along the Run Four Pin Upper Boundary**

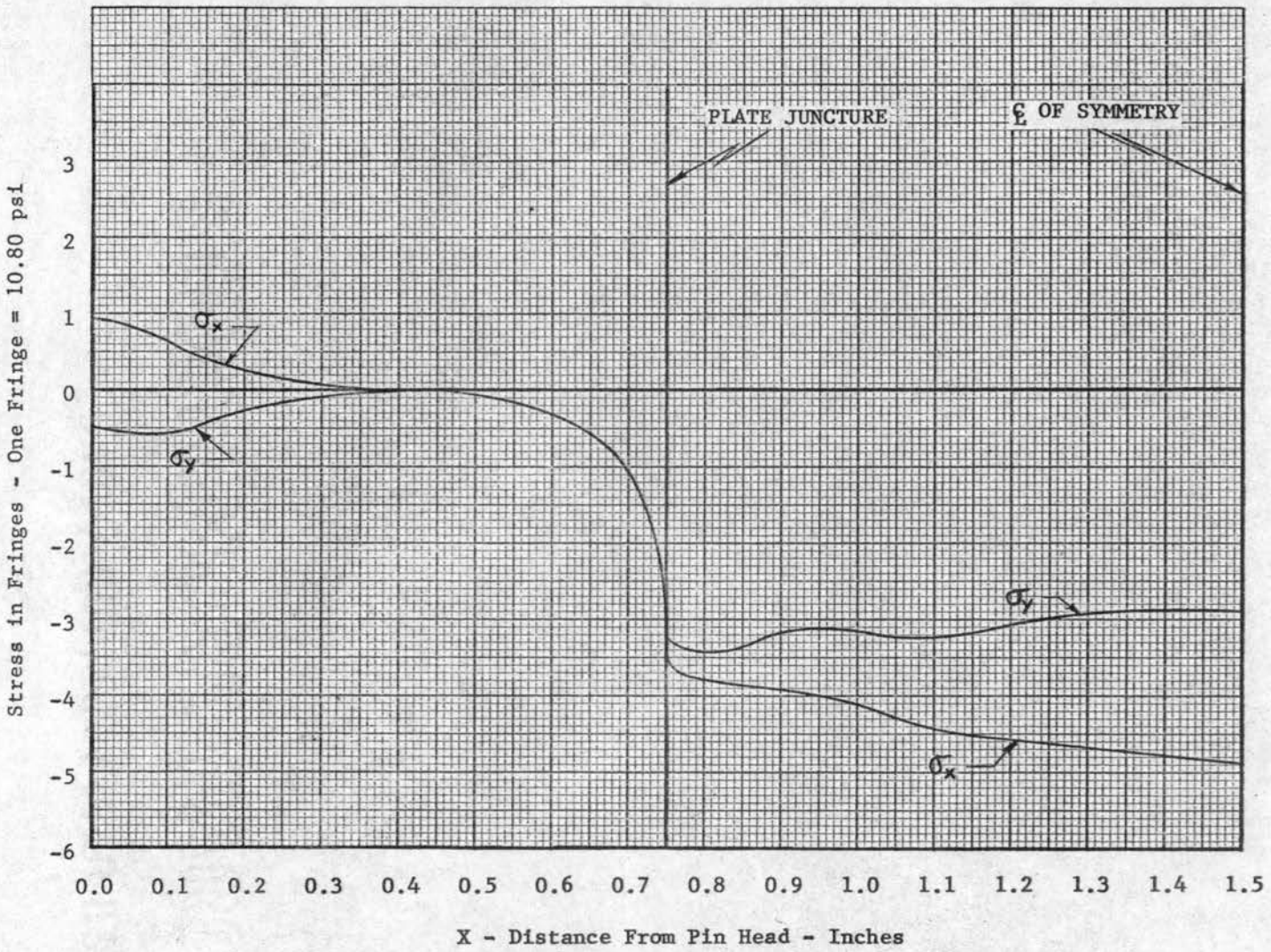

Figure 36. Stress Distribution Along the Run Five Pin Lower Boundary

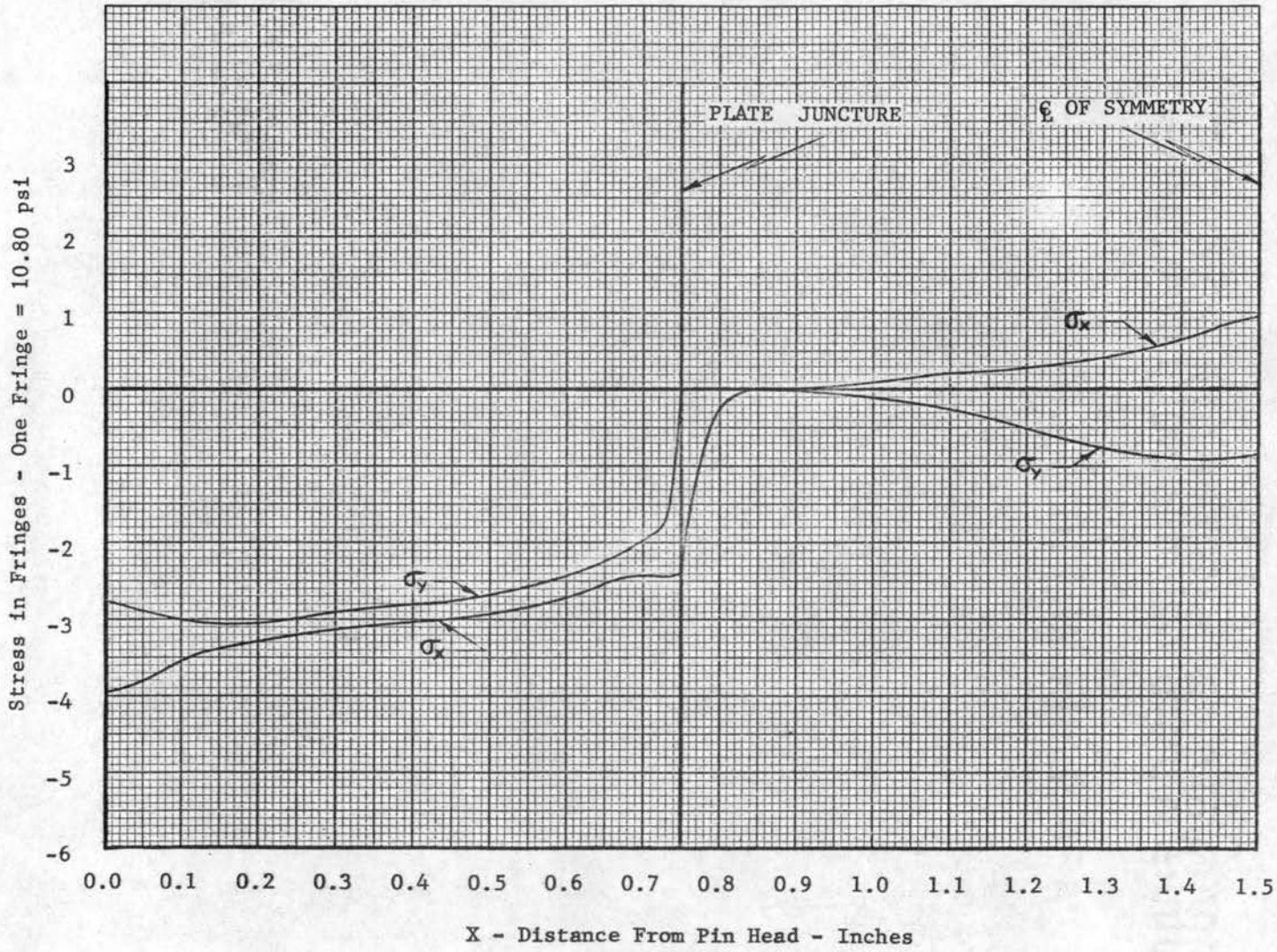

Figure 37. Stress Distribution Along the Run Five Pin Upper Boundary

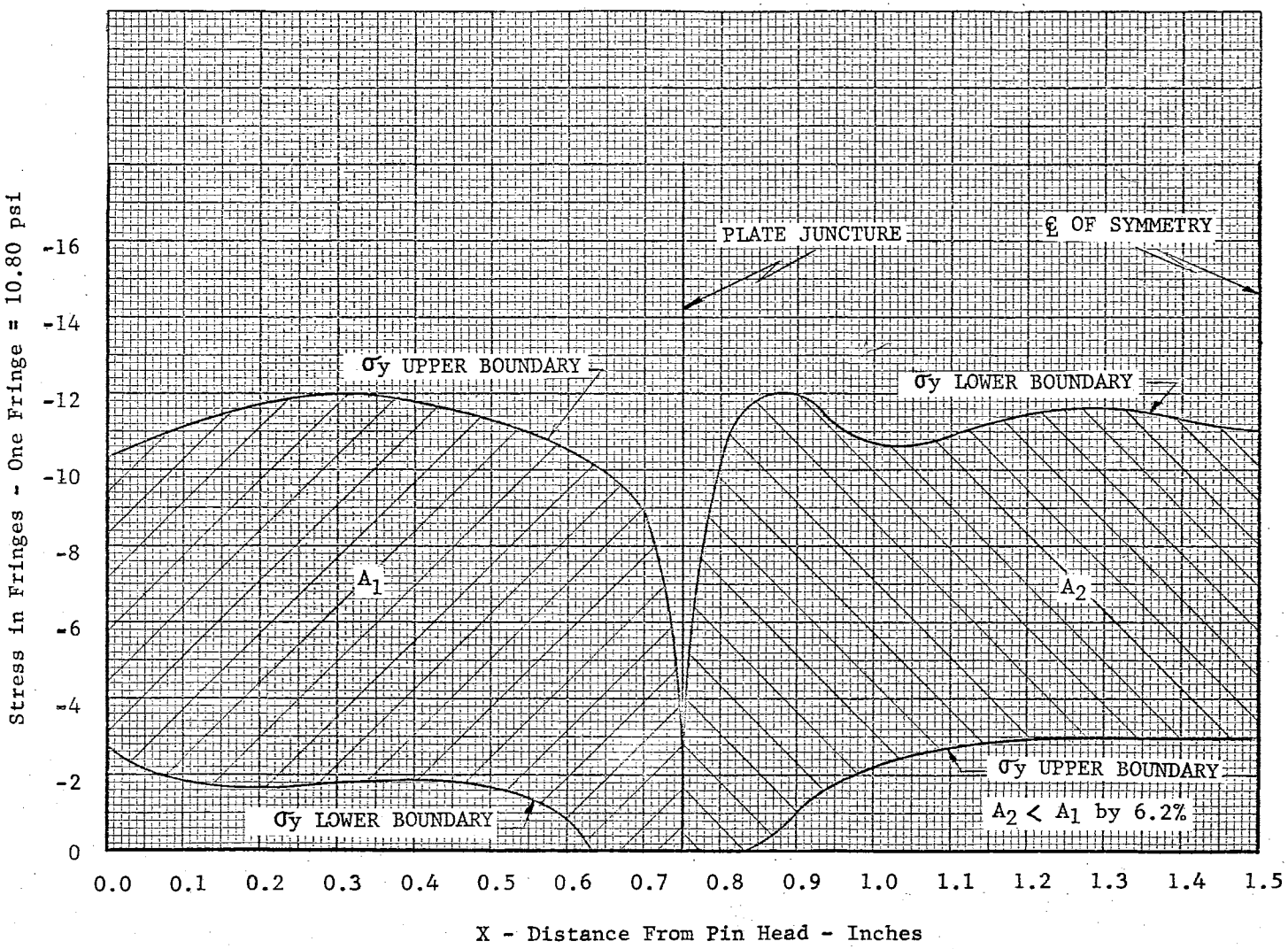

Figure 38. Static Equilibrium Check of Run Two by Summation of Normal Stresses

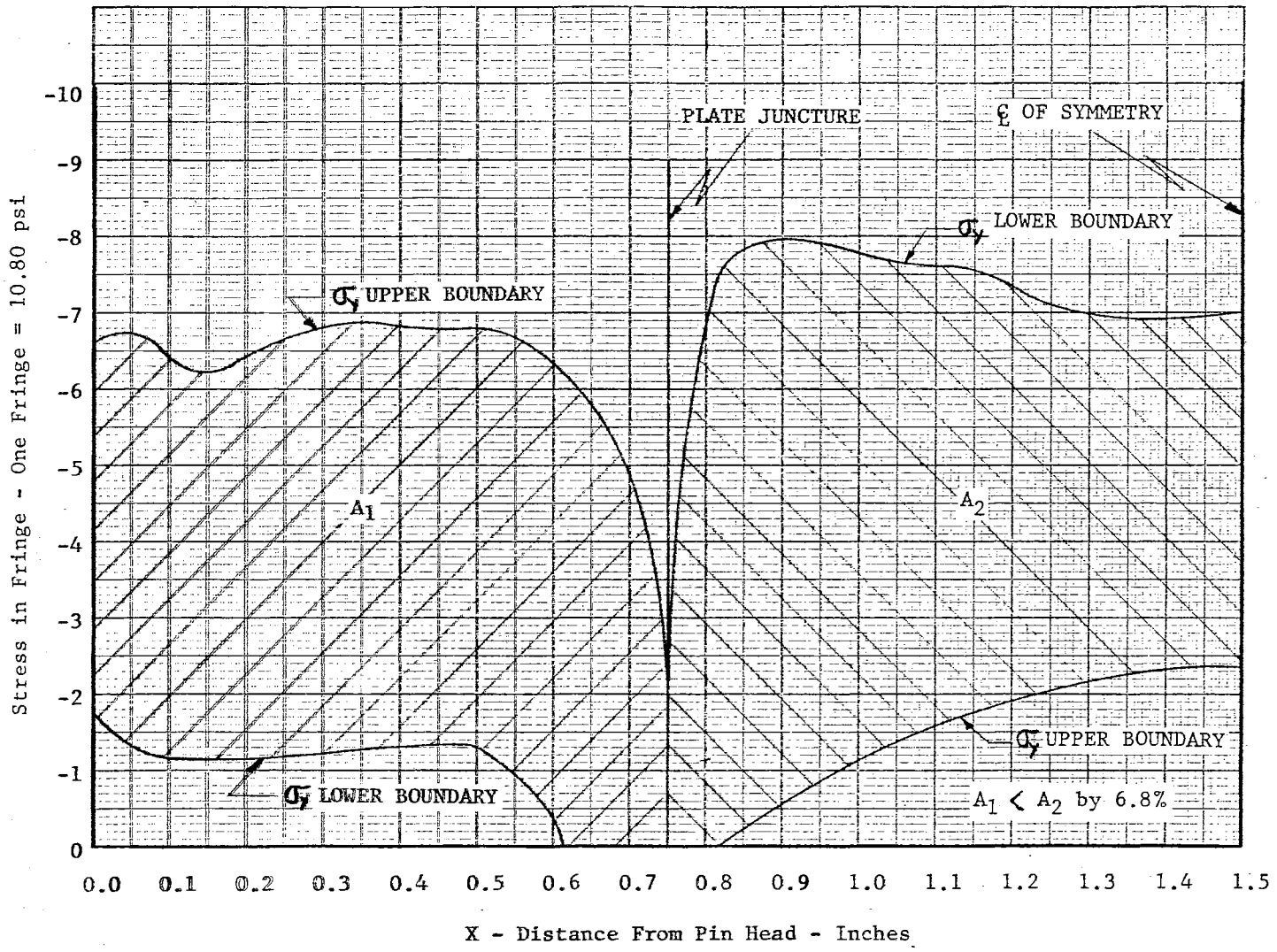

Figure 39. Static Equilibrium Check of Run Three by Summation of Normal Stresses

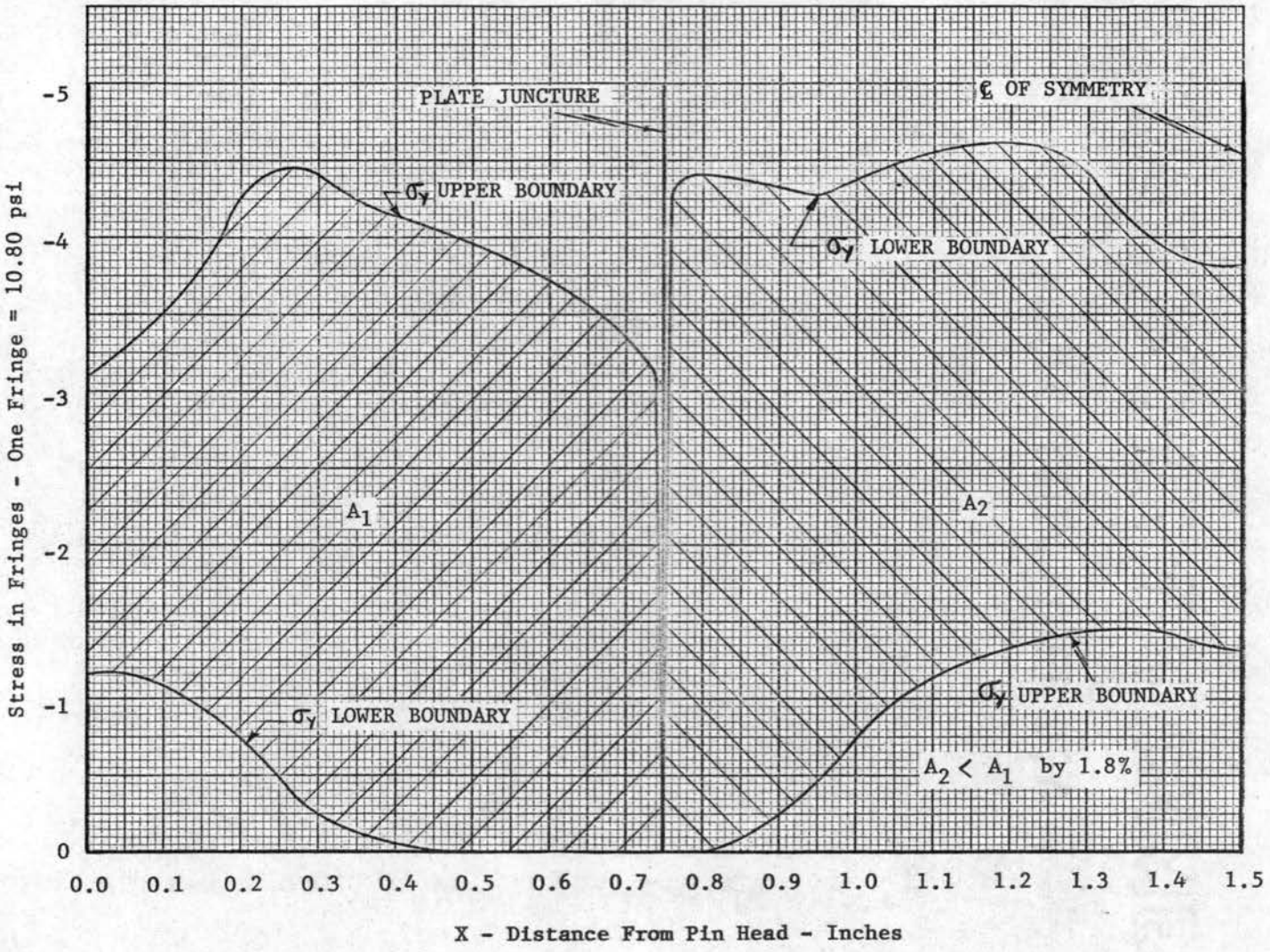

Figure 40. Static Equilibrium Check of Run Four by Summation of Normal Stresses

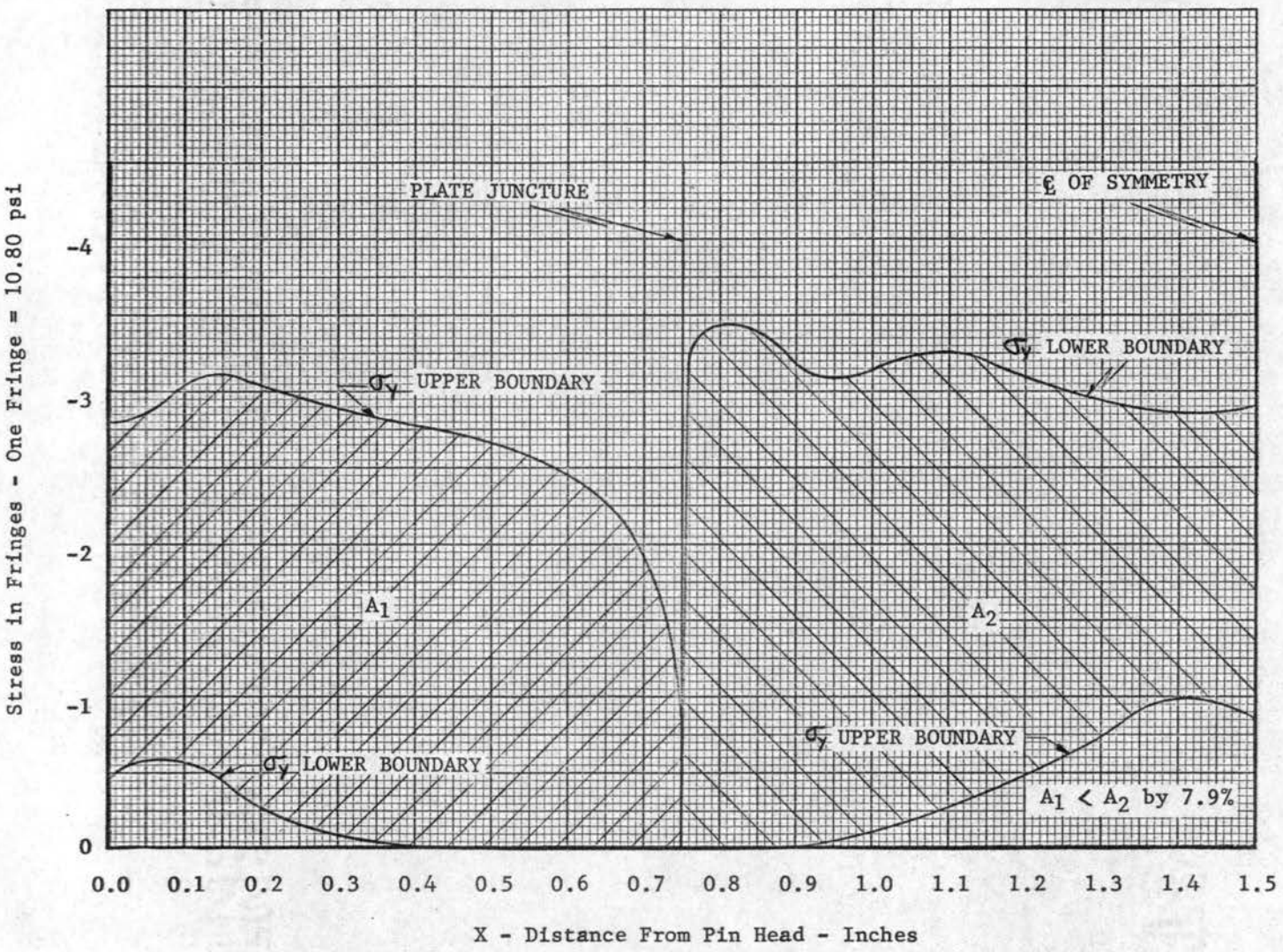

Figure 41. Static Equilibrium Check of Run Five by Summation of Normal Stresses

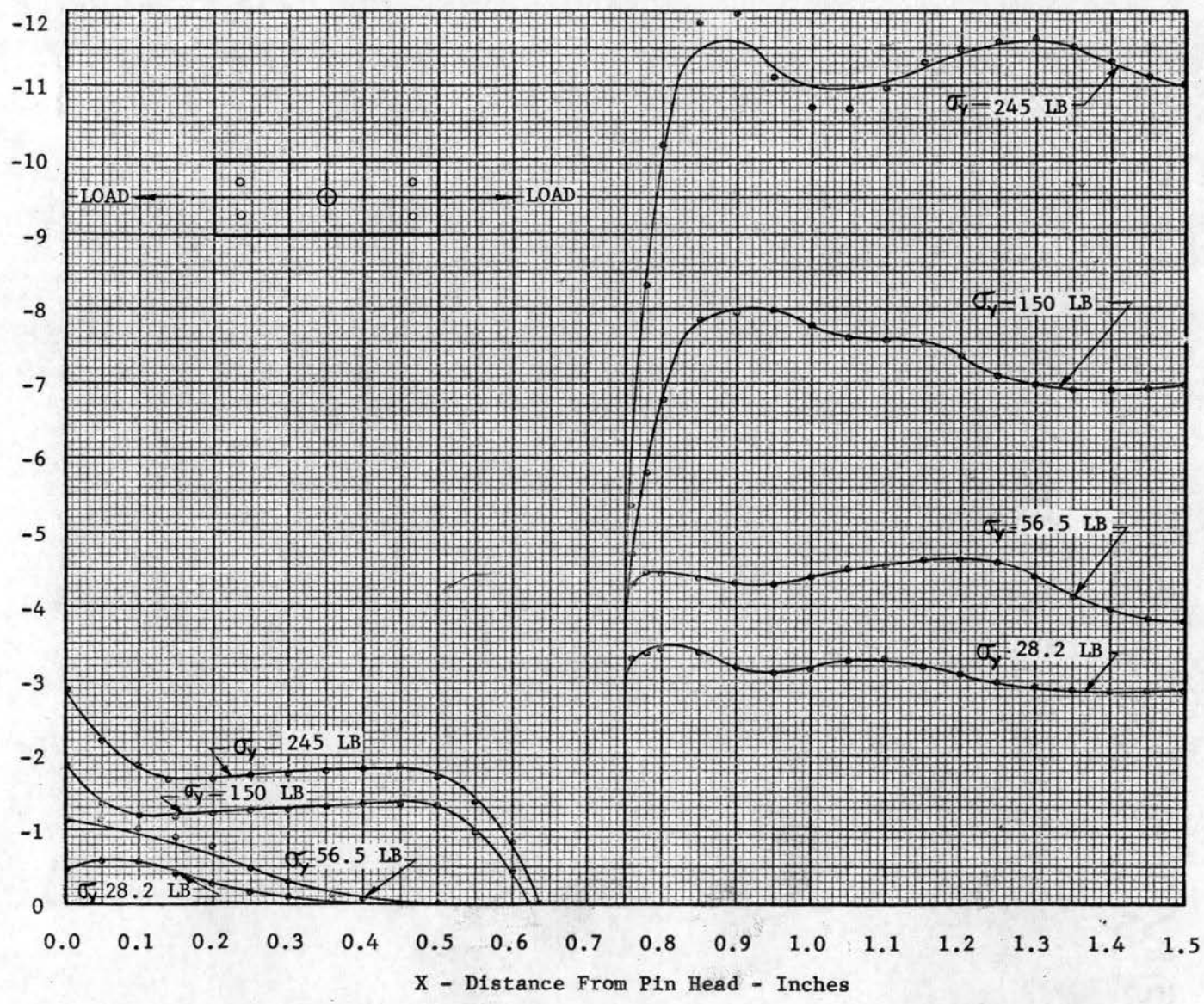

Figure 42. Composite Graph of the Normal Stresses Along the Pin Lower Boundary

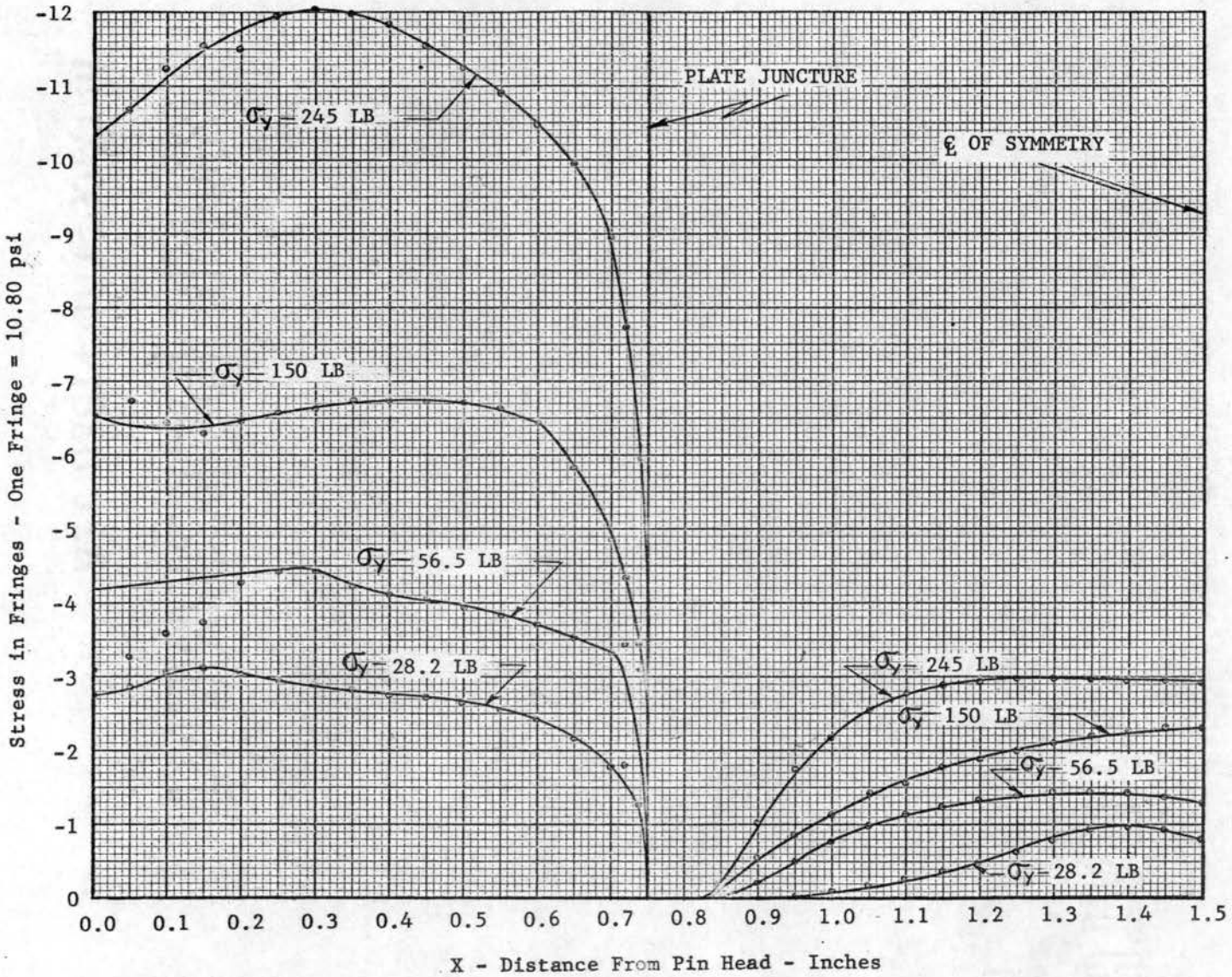

Figure 43. Composite Graph of the Normal Stresses Along the Pin Upper Boundary

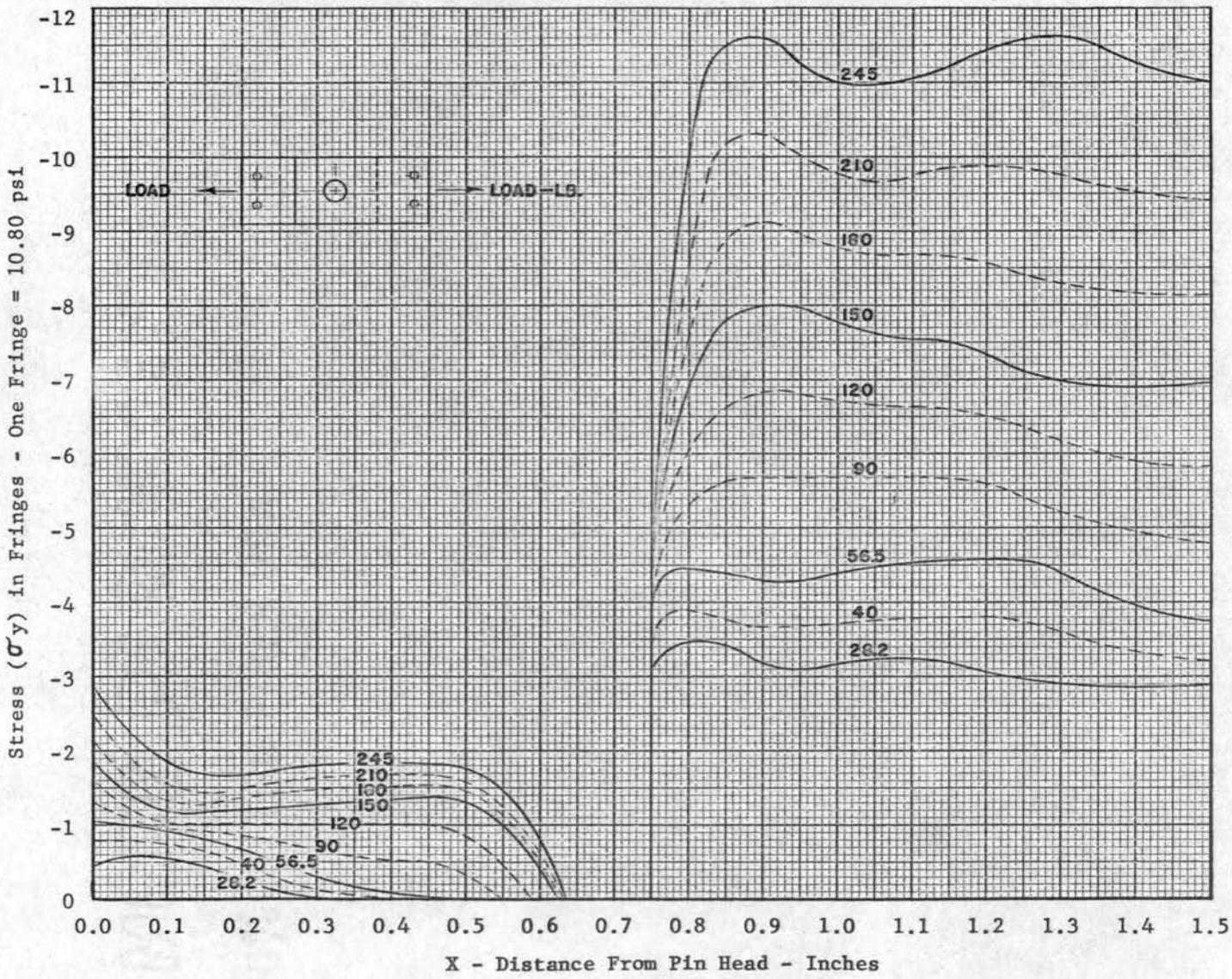

Figure 44. Stress Prediction Chart for the Pin Lower Boundary

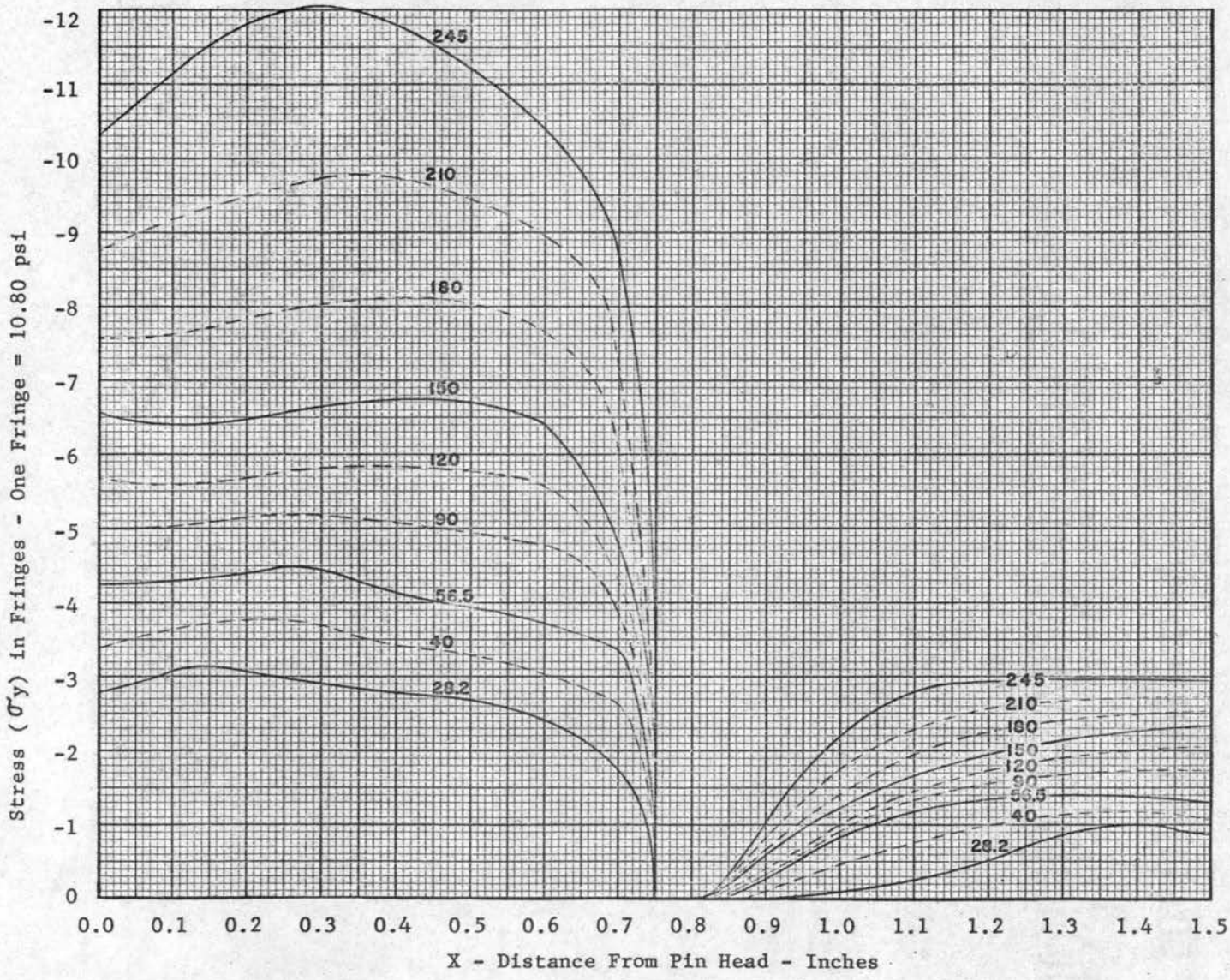

Figure 45. Stress Prediction Chart for the Pin Upper Boundary

Circumferential Stress Distribution

The actual calculation to determine the stresses around the circumference of the run four hole is given in Table IX. The general equation for graphical integration is equation (II-9). The starting principal stress p_o is known at the point where θ is zero degrees. The boundary where θ is zero is a free boundary, and since the remaining principal stress is tensile, the (p-q) value obtained from Figure 11 reduces to p and the magnitude and direction are immediately determined. The graphical integration is carried out with θ increments of five degrees. The increment is positive in all cases since the incremental variation occurs in a counter-clockwise sense which agrees with the positive sense shown in Figure 1. The angle at which the isoclinic touches the hole circumference, θ', is nearly equal to the parameter of the isoclinic in every case. This means that the hole boundary is a stress trajectory and that the principal stresses are perpendicular and tangent to the hole boundary. The variation from this condition is on the same order of magnitude as the difference between θ and θ'.

The variables in Table IX have all been defined and illustrated in Chapter II. The integration is made for only one quadrant since the two quadrants of interest are symmetrically loaded. Column (8) in Table IX gives the value of the function $(p-q)\cot\psi$ at the center of each element of integration. The values of q are the normal radial stresses directly since the hole boundary is a stress trajectory. A graph illustrating the variation of q is shown in Figure 46. In this graph the ordinates have been matched to agree with the longitudinal stress at corresponding points.

TABLE IX

CALCULATION OF THE STRESSES AROUND THE HOLE CIRCUMFERENCE

$$p_i = p_o + \sum_{o}^{i} [(p-q)\cot\Psi]\,\Delta\theta \qquad \Delta\theta = 5^\circ = 0.0873$$

(1)	(2)	(3)	(4)	(5)	(6)	(7)	(8)	(9)	(10)	(11)
Point	θ	θ'	$(p-q)$	Ψ	$\cot\Psi$	$(p-q)\cot\Psi$	Mean $(p-q)\cot\Psi$	Mean $[(p-q)\cot\Psi]\Delta\theta$	p	q
	Degrees	Degrees	Fringes	Degrees		Fringes	Fringes	Fringes	Fringes	Fringes
(1)	0	0.0	22.5	90.0	0.000	0.00			22.5	0.00
							-16.1	-1.41		
(2)	5	3.0	23.0	144.5	-1.402	-32.20			21.09	-1.91
							-33.7	-2.94		
(3)	10	10.5	24.0	145.5	-1.455	-34.95			18.15	-5.85
							-35.5	-3.10		
(4)	15	15.0	24.5	145.5	-1.455	-35.60			15.05	-9.40
							-35.0	-3.06		
(5)	20	20.0	25.5	142.5	-1.302	-33.20			11.99	-13.51
							-32.0	-2.80		
(6)	25	25.0	25.0	138.25	-1.120	-29.98			9.19	-15.81
							-27.0	-2.36		
(7)	30	30.5	24.75	134.5	-0.983	-24.37			6.83	-17.92
							-22.0	-1.92		
(8)	35	35.75	23.0	130.5	-0.854	-19.64			4.91	-18.09
							-17.2	-1.50		
(9)	40	41.0	21.0	125.5	-0.713	-14.97			3.41	-17.59
							-13.7	-1.20		
(10)	45	46.0	19.5	122.5	-0.637	-12.42			2.21	-17.29
							-11.0	-0.96		
(11)	50	51.0	18.0	118.5	-0.542	- 9.76			1.25	-16.75
							- 8.5	-0.74		
(12)	55	56.0	17.0	114.75	-0.461	- 7.84			0.51	-16.49
							- 6.2	-0.54		
(13)	60	62.0	15.0	109.5	-0.354	- 5.31			-0.03	-15.03
							- 4.5	-0.39		
(14)	65	66.5	14.0	106.5	-0.296	- 4.14			-0.42	-14.42
							- 3.3	-0.29		
(15)	70	71.5	13.0	102.5	-0.222	- 2.89			-0.71	-13.71
							- 2.3	-0.20		
(16)	75	75.75	13.0	99.5	-0.167	- 2.16			-0.91	-13.91
							- 1.5	-0.13		
(17)	80	81.25	14.0	95.25	-0.092	- 1.29			-1.04	-15.04
							- 1.0	-0.09		
(18)	85	85.75	16.0	93.0	-0.053	- 0.85			-1.13	-17.13
							- 0.4	-0.03		
(19)	90	90.0	16.5	90.0	0.000	0.00			-1.16	-17.66

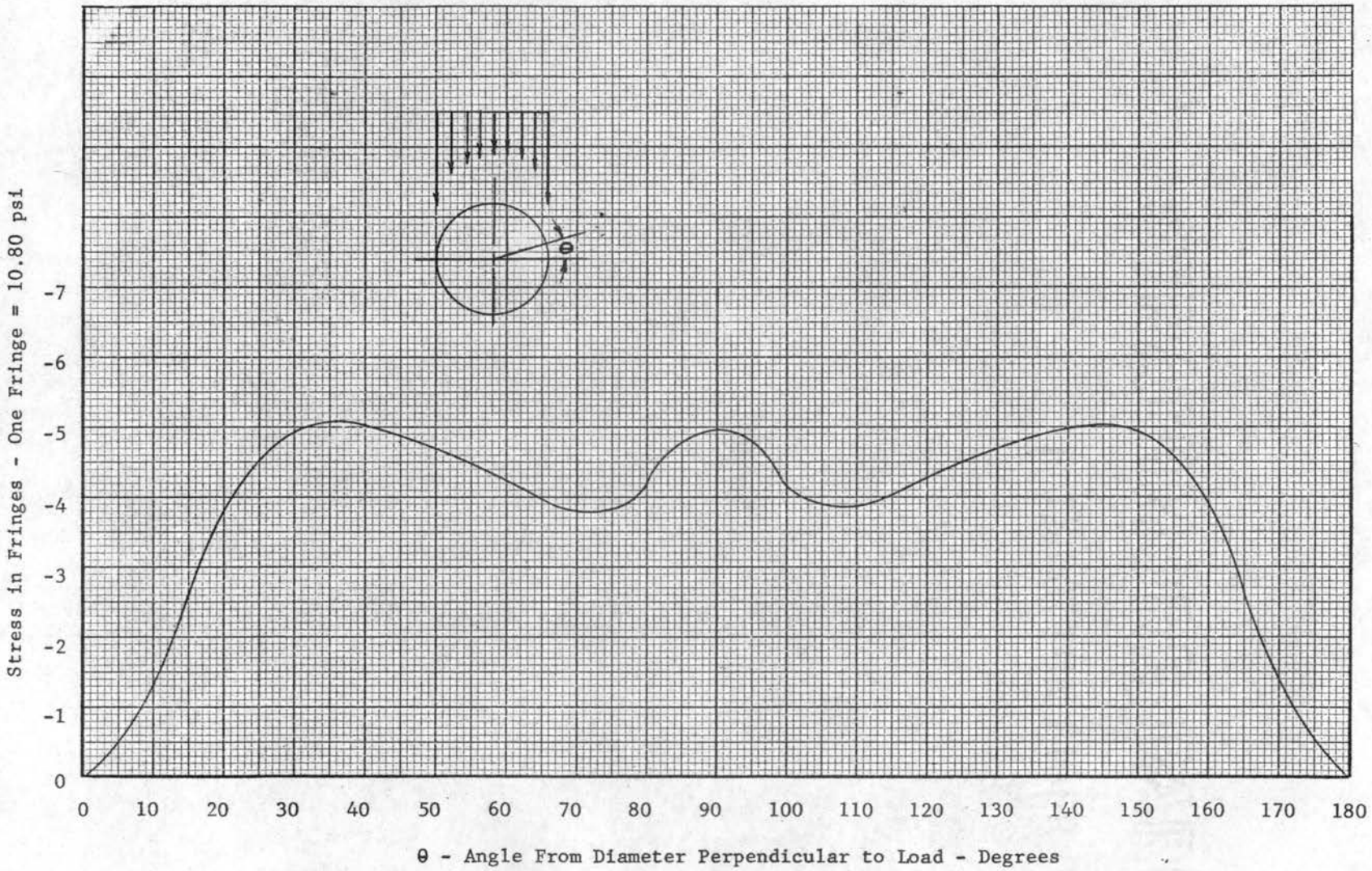

Figure 46. Circumferential Stress Distribution Along the Pin Surface

TABLE X

STATIC CHECK FOR EQUILIBRIUM BY SUMMATION OF RADIAL STRESSES

Radius r = 0.375 in.; Thickness t = 1.50 in;
Load P = 56.5 lb.
$\Delta\theta$ = 0.0873 radian

(1) θ Degrees	(2) sin θ	(3) q psi	(4) q·sin θ psi	(5) mean q·sin θ psi	(6) q·sin θ·r·$\Delta\theta$·t lb
90	1.000	52.98	52.98		
85	0.996	51.39	51.18	52.8	2.59
80	0.985	45.12	44.44	48.4	2.38
75	0.966	41.73	40.31	41.8	2.05
70	0.940	41.13	38.66	39.6	1.94
65	0.906	43.26	39.19	38.9	1.91
60	0.866	45.09	39.05	39.1	1.92
55	0.819	49.47	40.52	39.8	1.95
50	0.766	50.25	38.49	39.6	1.94
45	0.707	51.87	36.67	37.8	1.86
40	0.643	52.77	33.93	35.4	1.74
35	0.574	54.27	31.15	32.8	1.61
30	0.500	53.76	26.88	29.0	1.42
25	0.423	47.43	20.06	23.4	1.15
20	0.342	40.53	13.86	16.8	0.82
15	0.259	28.20	7.30	10.2	0.50
10	0.174	17.55	3.05	5.0	0.24
5	0.087	5.73	0.50	1.6	0.08
0	0.000	0.00	0.00	0.2	0.00
				Total =	26.10

26.10 x 2 = 52.2 lb against actual load of 56.5 lb.
Error = 7.6 per cent.

CHAPTER VII

CONCLUSIONS AND RECOMMENDATIONS

The purpose of this thesis was to make a three-dimensional photoelastic analysis of the surface stress distribution in the pin of a lap joint. The objectives were twofold. One of these objectives was to present a technique which could be used experimentally to solve problems similar to the one investigated in this thesis. The other objective was to present the stress distributions which were present in the models of investigation. Those conclusions concerning experimental technique are:

1. Three-dimensional photoelasticity is a satisfactory experimental method for the determination of the surface stress distribution in the pin of a lap joint.

2. The design and construction of the "stress freezing" oven and the lap joint loading frame were satisfactory.

3. Satisfactory isoclinic and fringe patterns were obtained. These patterns are shown in Plates VI through XIII and Figures 8 through 12.

For a lap joint with a pin diameter to plate thickness ratio of one to one and for the load range analyzed it was determined that:

1. The variation in magnitudes of the tangential stresses (σ_x) and the normal stresses (σ_y) follows the curves illustrated in

Figures 30 through 37.

2. The typical circumferential stress distribution is illustrated in Figure 46.

3. The stress system at any point in the pin surface can be determined approximately by utilizing Figures 30 through 37 in conjunction with the circumferential distribution illustrated in Figure 46.

4. The normal stress (σ_y) increases with increasing loads. Composite graphs illustrating this are shown in Figures 42 and 43. The tangential stress also increases with increasing loads.

5. The variation in the normal stress (σ_y) for various loads can be predicted from the curves shown in Figures 44 and 45.

6. As the load increases more of the pin surface acts to resist the applied load. This is illustrated in Figures 42 and 43 where the singular points each move toward the plate juncture with an increase in load.

In view of the above conclusions it is believed that the pin surface stress distribution for any configuration of lap joint and for any set of loads can be determined photoelastically by following the recommendations listed below.

1. Various lap joint configurations should be investigated. These configurations should include a wide range of pin diameters and a wide range of lap joint plate width ratios.

2. The effect of clearance between the pin and plate holes should be determined by investigating a wide range of clearances.

3. The effect of various pin torques impressed upon a wide range of lap joint loads would be of value.

4. Investigations of multipinned lap joints would be quite useful. These should include various patterns and spacings of pins.

5. The effect of a pin made of one material mating with plates of a different material would provide valuable information.

6. Investigations which would more clearly define three-dimensional photoelastic phenomena would be of value.

   a. Experiments to determine the effect of a range of cooling rates used in stress freezing.

   b. Experiments to determine the effect of departing from the recommended critical temperature.

In summary it may be said that the manner in which the lap joint components transfer the applied load is imperfectly understood. The stress distributions determined from this thesis have a direct appli-tion only for lap joint systems similar to the ones investigated in this thesis.

SELECTED BIBLIOGRAPHY

(1) Frocht, M. M., Photoelasticity, (John Wiley and Sons: New York, 1949), I.

(2) Hetenyi, M., Handbook of Experimental Stress Analysis, (John Wiley and Sons: New York, 1950).

(3) Peery, D. M., Aircraft Structures, (McGraw-Hill: New York, 1950).

(4) Levosky, J. M., "Two Dimensional Photoelastic Analysis of the Surface Stresses of a Bolt in Double Shear." Master of Science Thesis, Oklahoma State University, 1959.

(5) Houghton Laboratories Inc., "Technical Data for Hysol 6000-OP." Olean, New York, (1958).

(6) Hetenyi, M., "Fundamentals of Three-Dimensional Photoelasticity," Journal of Applied Mechanics, 5, A149, (1938).

(7) Franz, W. F., "A Three-Dimensional Photoelastic Stress Analysis of a Thread Drill Pipe Joint," Proceedings of the Society for Experimental Stress Analysis, Vol. IX no. 2, (1952).

(8) Weller, R., "Letter to the Editor," Journal of Applied Physics, 10, 266, (1939).

(9) Weller, R., and Bussey, J. K., "Photoelastic Analysis of Three-Dimensional Stress Systems Using Scattered Light," N.A.C.A. Technical Note, no. 737, Washington, (November, 1939).

(10) Drucker, D. C., and Mindlin, R. D., "Stress Analysis by Three-Dimensional Photoelastic Methods," Journal of Applied Physics, 11, 724-732, (November, 1940).

(11) Rosenberg, P. R., "Study of a Shrink-Fit Model by the Scattered Light Method," Proceedings of the Thirteenth Semi-Annual Eastern Photoelasticity Conference, Mass. Inst. of Tech., (June, 1941).

(12) Johnson, R. C., "Three-Dimensional Photoelastic Analysis of Shafts in Pure Torsion and a Comparison with Results from Relaxation," Proceedings of the Society for Experimental Stress Analysis, Vol. XIII, no. 2, (1956).

(13) Rao, K. K., "Stress Concentration at a Circular Groove in a Shaft Subjected to pure Torsion," Master of Science Report, Oklahoma State University, 1960.

(14) Frocht, M. M., Photoelasticity, (John Wiley and Sons: New York, 1948), II.

(15) Frocht, M. M., "On the Removal of Time Stresses in Three-Dimensional Photoelasticity," Proceedings of the Society for Experimental Stress Analysis, Vol. V, no. 2, (1948).

APPENDIX A

PROPERTIES OF HYSOL 6000-OP (5)

TABLE XI

PHOTOELASTIC PROPERTIES OF HYSOL 6000-OP

Annealing Temperature	280 °F
Stress Freezing or Critical Temperature	270 °F
Annealing Cooling Rate	no greater than 2 °F/hr
Fringe Value at 77 °F (tensile)	.57 psi/fr/in.
Fringe Value at 270 °F (tensile)	1.35 psi/fr/in.
Poisson's Ratio	0.500
Figure of Merit at 77 °F (Q = Eeff/feff)*	7250
Figure of Merit at 270 °F	1620

*Eeff = Modulus of Elasticity
feff = Fringe value in frozen stress test

TABLE XII

MECHANICAL PROPERTIES OF HYSOL 6000-OP

	77 °F	270 °F
Tensile Strength, psi	12,000	3,540
Modulus of Elasticity, psi	480,000	2,190
Compressive Strength, psi	18,000	
Flexural Strength, psi	18,500	
Refractive Index	1.605	
Thermal Coefficient of Expansion, Linear/°C	4.7×10^{-5}	8.2×10^{-5}

APPENDIX B

PHOTOGRAPHIC TECHNIQUE

The camera set-up is shown in Plate V. This camera is a bellows type portrait camera with a Wollensak Betax 2 lens. After much experimentation it was found that a good sharp contrast negative could be obtained by using an f stop of 32 with an exposure time of 6 ~~minutes.~~ This was obtained using Kodak Super Panchro-Press, type B, 4 x 5 inch film. The developer used was Kodak D-11. The developing time varied from 3 to 4 minutes depending upon the room temperature. A cold water stop bath was used with a rinsing time of 8 seconds. The fixer used was Ansco Acid Fixer with Hardener and the fixing time was 10 minutes.

The actual procedure was to support the test specimen in the general loading frame shown in Plate IV. The quarter wave plates were inserted into the system and the camera was focused on the specimen using the monochromatic light source. It was found to be much easier to focus the lens with an f stop of 6.3 although the actual exposure was made with an f stop of 32. During the focusing and actual exposing of the film the room was completely dark except for the monochromatic light source.

After each negative was exposed it was immediately taken to the photography laboratory and developed. This was to insure that a good

negative had been made of each test specimen. Since the photography laboratory was very convenient to the photoelastic laboratory this presented no problem and was in keeping with recommended practice. (1). The negative film was handled in total darkness until fixed.

It was thought to be desirable to make prints of the negatives in order that the thesis layout and preliminary study would be more clear. The chemicals used to make the prints were the same as were used for the negatives. The prints were made using a contact printer actuated by a Lektra Laboratories Inc., model TM-8, Timer which was set on 0.3 seconds. The developing time was approximately 45 seconds with the stop bath and fixer bath times remaining the same as for the negatives. The prints can be made using a safe-light so that the developing time can be visually adjusted. Glossy prints can be obtained by rolling the wet prints onto ferrotype tins.

APPENDIX C

OVEN COOLING RATE CONTROL

TABLE XIII

OVEN VARIAC SETTINGS

Oven Temperature (°F)	Variac Settings (volts)
270	26.5
270-265	24.0
265-255	22.0
255-245	20.0
245-230	18.0
230-210	16.0
210-190	14.0
190-170	12.0
170-150	10.0
150-room temperature	Off

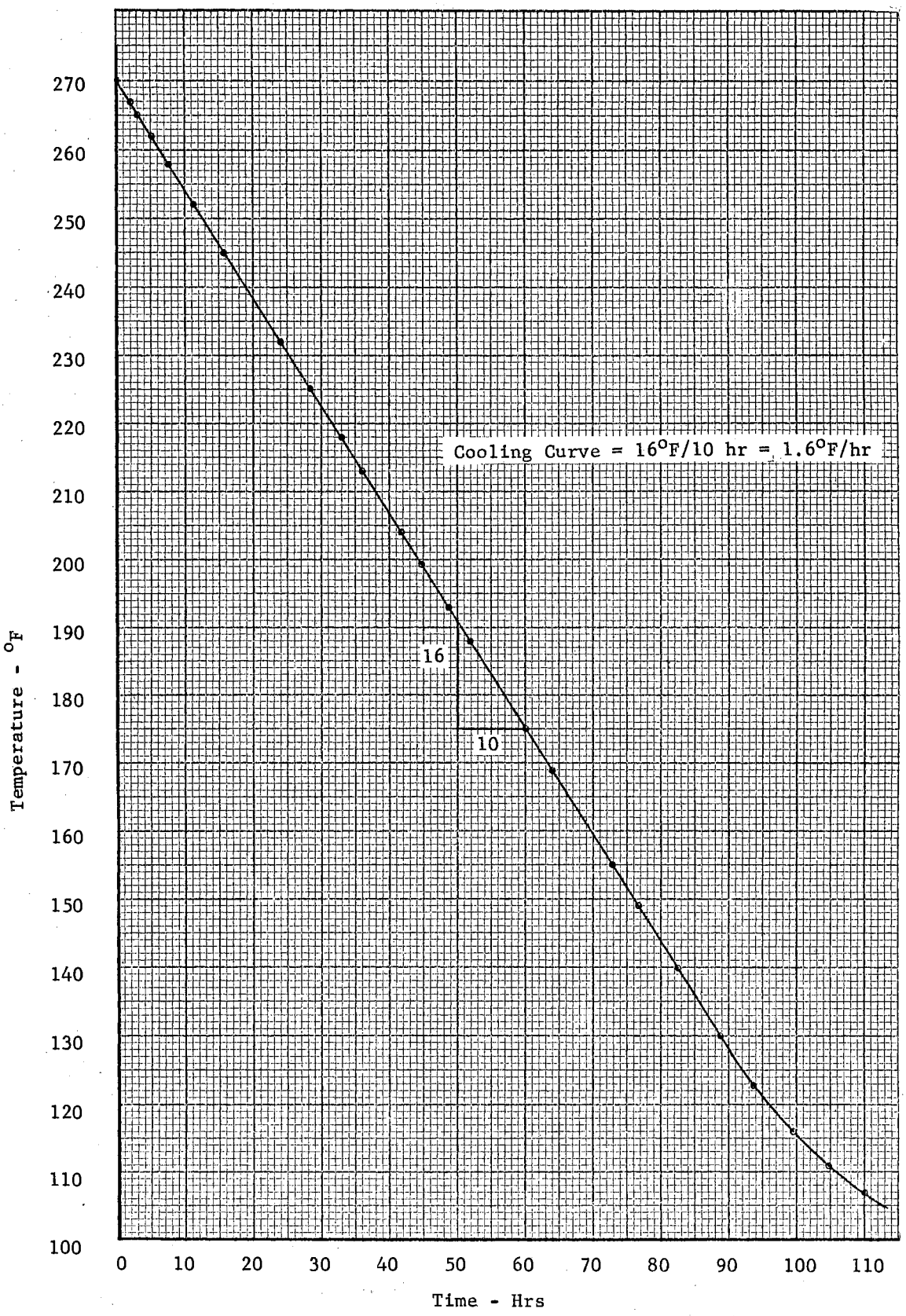

Figure 47. Oven Cooling Curve

APPENDIX D

PIN SLICING PROCEDURE

The pins were sliced as shown in Figures 5 and 6. It is difficult to support a complex shape such as the pin without inducing extraneous stresses into the pin. This difficulty was overcome by casting the pin into a block of cerro-bend. Cerro-bend has a melting temperature of approximately 120 °F and can be readily cast to any shape desired. Since this melting temperature is so low, no reheating effects were present in the pins. The pins were aligned in the casting box so that the direction and angle of slicing could be determined after the cast blocks containing the pins were removed. This is shown on the following page in Plate XIV.

The actual slicing was done on a milling machine and the part is shown being sliced longitudinally in Plates XIV and XV. Transverse slicing is shown in Plate XV. The rate of table feed was ½ inch per minute and the cutting speed was 190 revolutions per minute. These procedures were quite satisfactory and no effects of slicing could be detected in any of the specimens.

PIATE XIV

PIN CASTING AND SLICING

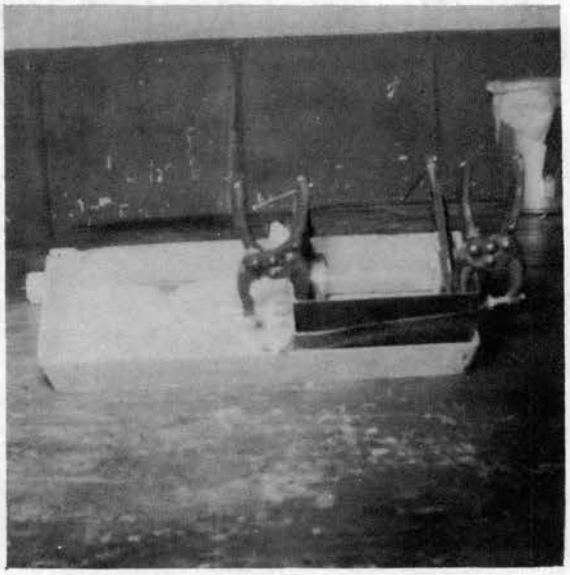

1. Casting Box

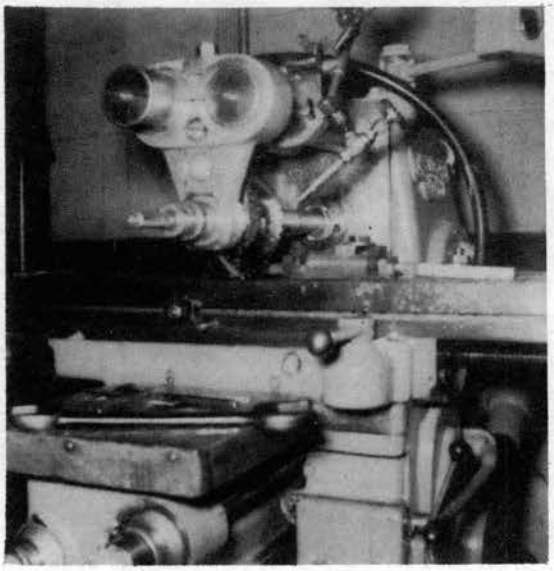

2. Longitudinal Slicing

PLATE XV

TRANSVERSE AND LONGITUDINAL PIN SLICING

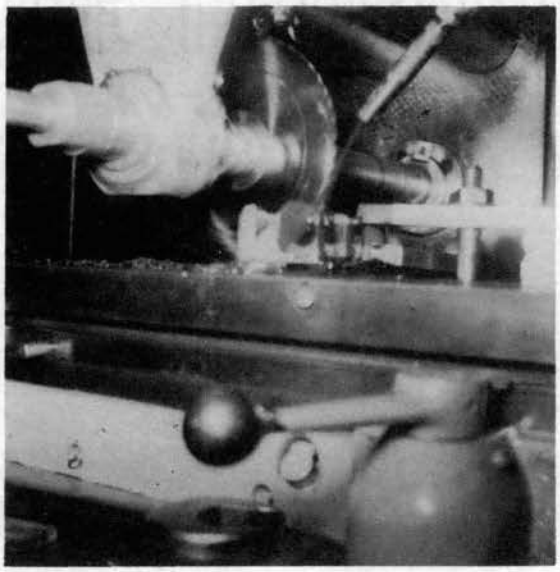

1. Transverse Slicing

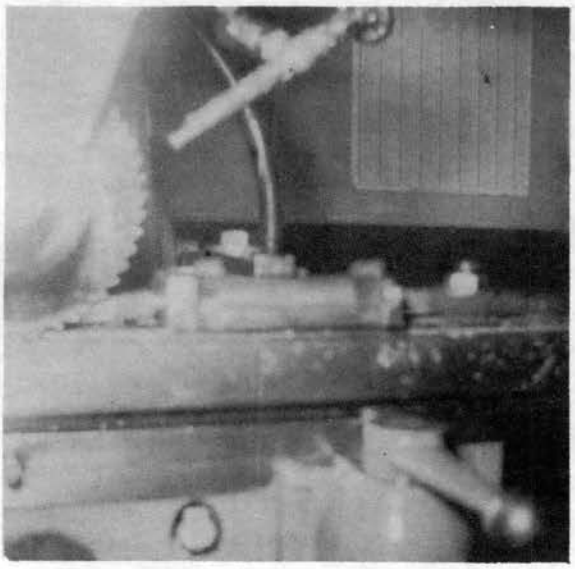

2. Longitudinal Slicing

APPENDIX E

DETAILS OF LOADING FRAME COMPONENTS

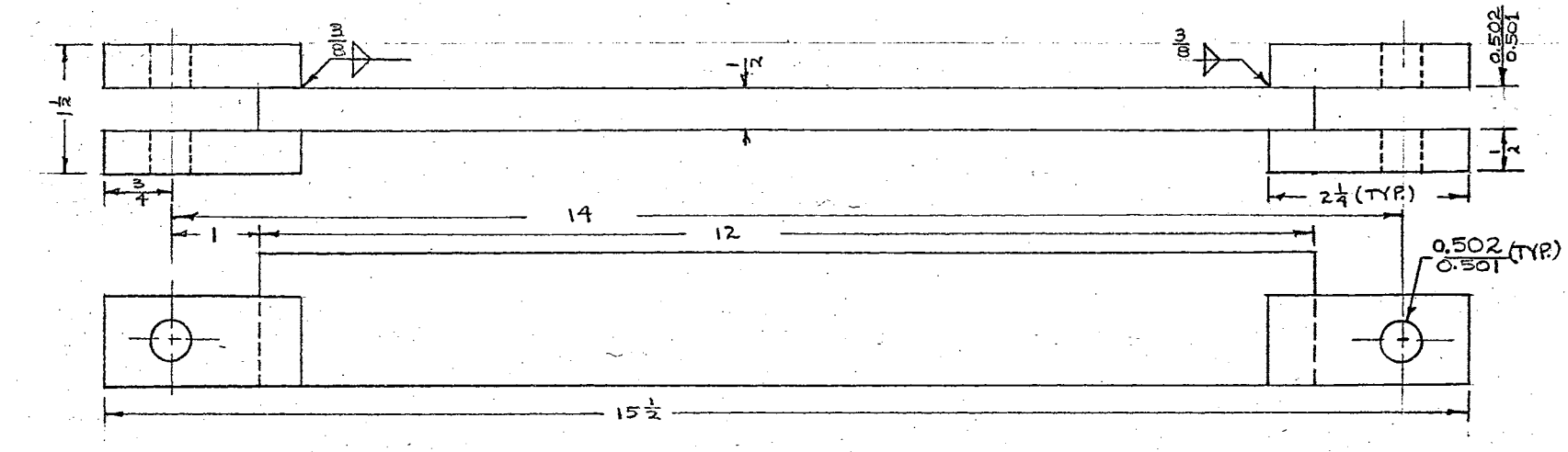

TOP BAR - 1 REQUIRED - MILD STEEL - SCALE 1/2 : 1

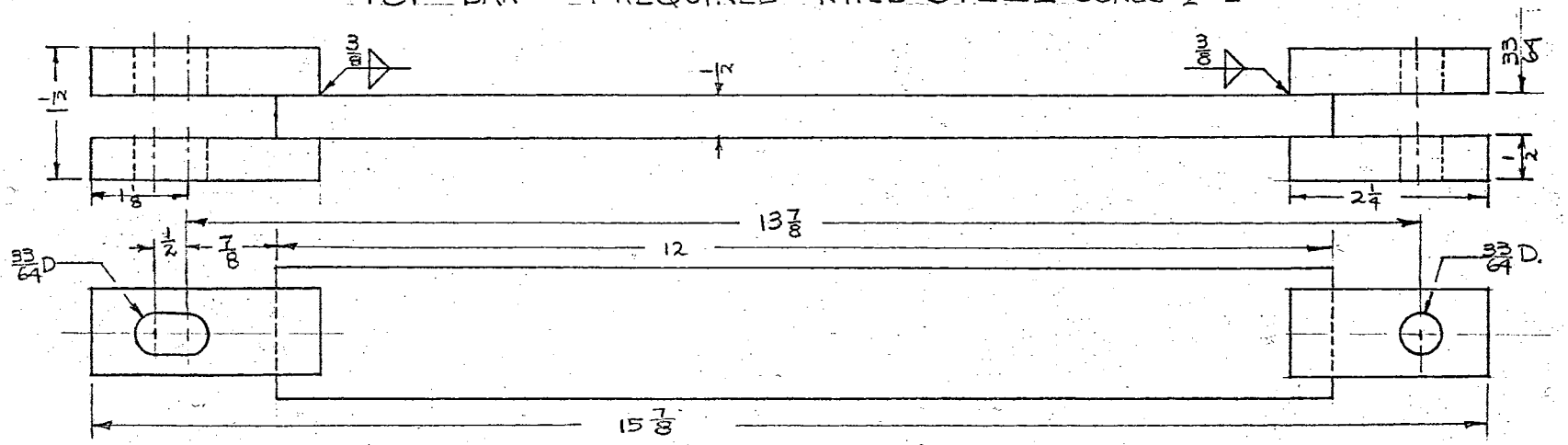

SAFETY BAR - 1 REQUIRED - MILD STEEL - SCALE 1/2 : 1

Figure 48 (a). Details of Loading Frame Components - Sheet 1

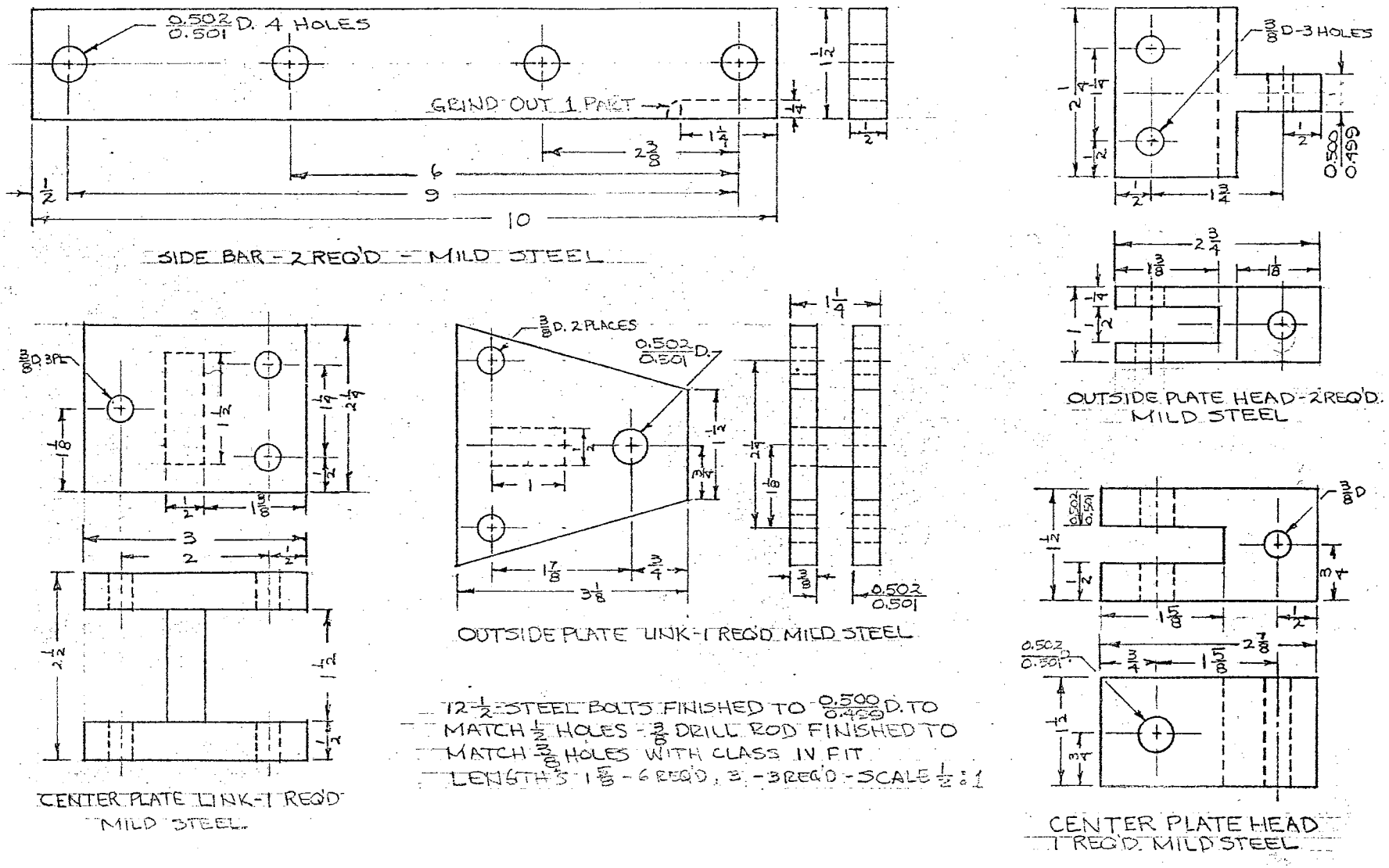

Figure 48 (b). Details of Loading Frame Components - Sheet 2

APPENDIX F

SYMBOLS

A	Area, in^2.
C	Stress-optic coefficient.
E	Modulus of elasticity, psi.
f	Material fringe value, psi/fringe/in.
F	Model fringe value, psi/fringe.
I	Isotropic point or isoclinic.
n	Fringe order.
p	Algebraic maximum stress, psi or pressure, psi.
q	Algebraic minimum stress, psi.
Q	Figure of merit.
R	Retardation, wave lengths.
S	Stress trajectory.
t	Thickness, in.
T	Tangent to a curve.
x	Distance from the pin head in the direction of the pin axis, in.
y	Distance from the pin boundary, in.
α	An angle defined by Figure 2, degrees.
θ	An angle defined by Figure 1, degrees.
λ	Wave length.
ρ	Radius of curvature, in.

σ Normal stress, psi.

τ Shear stress, psi.

Ψ An angle defined by Figure 1, degrees.

Subscripts

i General point.

o Known reference point.

m Model.

c Compensator.

VITA

Max Marlin Spencer

Candidate for the Degree of

Doctor of Philosophy

Thesis: THREE-DIMENSIONAL PHOTOELASTIC ANALYSIS OF THE SURFACE STRESS DISTRIBUTION IN THE PIN OF A LAP JOINT

Major Field: Mechanical Engineering

Biographical:

Personal Data: The writer was born in Rocky Ford, Colorado, January 10, 1935.

Undergraduate Study: He graduated from Clover Park High School, Tacoma, Washington, with honors, in May, 1952. In September, 1952, he entered Oklahoma State University and in June, 1956, received the Bachelor of Science Degree in Mechanical Engineering.

Graduate Study: The writer entered the Graduate School of Oklahoma State University in June, 1956, and received the Master of Science Degree in Mechanical Engineering from that institution in June, 1957. He commenced study toward the Doctor of Philosophy Degree in September, 1957, and completed the requirements for the Doctor of Philosophy Degree in May, 1960.

Experience: The writer was employed as an associate engineer in the Stress Group of Boeing Airplane Company for seventeen weeks during the summer of 1957. He also was employed as a faculty associate in the Advanced Design Group of Boeing Airplane Company for sixteen weeks during the summer of 1958. While working on the Master of Science Degree in Mechanical Engineering and while working on the Doctor of Philosophy Degree he served as a graduate teaching assistant, teaching one-half time. He taught courses in Aircraft Structures, Machine Drawing and Design, and Mechanical Drawing. He also served as a teaching assistant for courses in Aircraft Structures, Machine Design and Kinematics.